

Doctorate Dissertation

2022

Modeling and Simulation of  
Airframe Design Optimization and  
Impulsive Load by Emergency  
Landing for a Flying Car

MIHARA, Yusuke

(Student ID Number : 81952076)

Supervisor Yoshiki YAMAGATA

March 2022

Graduate School of System Design and Management,

Keio University

Major in System Engineering

## SUMMARY OF DOCTORAL'S DISSERTATION

Student Identification Number	81952075	Name	三原裕介 (MIHARA, Yusuke)
Title :  Modeling and Simulation of Airframe Design Optimization and Impulsive Load by Emergency Landing for a Flying Car			

Flying Cars (FCs) are envisioned not only as air taxis but also as air ambulances. An FC which is also called urban air mobility has the potential to relieve seriously congested ground traffic in cities via direct point-to-point air movements. While most of the conventional research is limited to vehicle design, infrastructure design, or business analysis. A different use case can highlight different issues. In this study, the implementation of a new use case of FC using the system approach, requires the analysis of an FC system, with a focus on the vehicle and the Take-Off and Landing Area (TOLA). In fact, the purpose of this research is to evaluate an FC vehicle and TOLA design using system approach. This study is divided into five chapters.

In Chapter 1, the author conducts an exhaustive literature review about FCs. Reviewing conventional studies, the author shows the originality of this research and its purposes.

In Chapter 2, the author proposes a method overview of this research including the analysis of vehicle and TOLA designs. Firstly, the author presents a requirement analysis of the Helicopter Emergency Medical Services (HEMS) in Japan and propose an optimization-based simulation model for an FC vehicle design. To evaluate the FC vehicle design simulation, four objective functions are considered: the energy required for a round trip, the generated noise, the downwash, and the landing area size. The details of this method are explained in

Chapter 3. Secondly, the author develops an impulsive load simulation method for an FC in the air taxi service in Tokyo to evaluate its impact on the passengers, the vehicle, and the TOLA. The details of this method are explained in Chapter 4.

In Chapter 3, the author conducts an optimization-based simulation to evaluate the airframe design of three different FC types in terms of societal and economic factors. The purpose of this chapter is to verify the technical applicability of an FC for medical emergencies use. To date, conventional research, in which the airframe of an FC is optimized in the context of medical emergencies, did not identify a sustainable solution. The used method is a weighted sum method. It is used to optimize the design of multi-rotor, vectored-thrust (tiltrotor), and lift+cruise types of FC. A simulation scenario, which considers cruising speed and flight height, is conducted based on analysis of stakeholder interviews with a pilot, an in-flight doctor, and an operating company. To optimize the parameters of an FC airframe, four objective functions are considered: the required amount of energy for a round trip, the rotors' noise value, and downwash speed, and the landing area size. The objective functions are based on the requirement analysis to be significant for the FC system sustainability. The results reveal that the required battery energy density for all three types of FC is estimated to exceed the existing lithium-ion battery capacities. Therefore, an upgrade in battery capacity is critical to the realization of an FC. Although the noise level is found to be less than that of a conventional helicopter, the development of a rotor to decrease noise levels

for environmental reasons is necessary. Finally, both the downwash speed and the landing area of an FC are estimated to be less than those of a conventional helicopter, making it possible to land in narrow spaces.

In Chapter 4, the impulsive load simulation based on the equation of motion of an FC with or without a parachute is conducted to evaluate the dynamic effects of the impulsive load to a vertiport, a vehicle body, the fuselage, and passengers. The purpose of this chapter is to verify the safety of passengers, the vehicle body, and the TOLA. And to calculate the design strength requirement of a vertiport by simulating the impulsive load on emergent landing. At this point, the spring-damper mechanism is introduced to evaluate the force and acceleration of the fuselage. Simulation results show that a conventional heliport and an emergency TOLA in Tokyo have enough strength against the impulsive load of a landing FC. Moreover, the crushable of a fuselage, and a seat, and an airbag need to absorb most of the impulsive load to protect passengers. A destruction probability against a vertiport by the impulsive load of a repeated landing is calculated using the Poisson process based on the operational frequency.

In Chapter 5, the author summarizes the overall discussion and conclusion with remaining research issues which the author should solve in the future. The airframe design optimization model shows that the most feasible vehicle type is a vectored thrust in a medical emergency application, especially from the viewpoint of a battery deployment. Impulsive load simulation shows that its effects on a

passenger inside a vehicle with a mushroom parachute are under safety criteria when a vehicle takes off. However, the analysis is limited to first-order analysis because a vehicle design is not detailed. A more detailed vehicle design in the use case of a medical emergency FC can be the subject for a further work.

Keyword

Flying Car, eVTOL, System Design, Airframe Optimization, Impulsive Load

Copyright 2022 Yusuke Mihara

# Index

Index .....	viii
List of Figures.....	xi
List of Tables .....	xiv
Nomenclature.....	16
Chapter 1 Introduction.....	24
1.1 Background.....	25
1.1.1 Why is a Flying Car (FC) Emerging?.....	25
1.1.2 Applications.....	27
1.1.3 Vehicle Types .....	30
1.1.4 Infrastructure .....	32
1.2 Conventional Research .....	34
1.2.1 Airframe analysis for a medical emergency for a normal flight in the medical e mergency use case .....	37
1.2.2 Safety analysis by a impulsive load simulation for emergency landing.....	40
1.3 Purpose .....	45
1.4 Overview of This Paper .....	46
1.5 Conclusion .....	48
Chapter 2 Research Methods .....	49

2.1 Method Overview .....	50
2.2 Airframe Design Optimization Model.....	52
2.3 Impulsive Load Model for Designing a Safety TOLA.....	55
2.4 Conclusion .....	58
Chapter 3            Vehicle Design Analysis.....	59
3.1 Problem Definition .....	60
3.2 Method.....	63
3.2.1 Method Overview .....	63
3.2.2 Requirement Analysis for a Medical Emergency.....	65
3.2.3 Vehicle Model .....	66
3.2.4 Optimization Model.....	68
3.2.5 Determining the Weighting .....	87
3.3 Result and Discussion.....	88
3.3.1 Requirement Analysis Result and Mission Profile.....	88
3.3.2 Weighting for Optimization.....	91
3.3.3 Optimization Result.....	93
3.3.4 Parameter Study.....	101
3.4 Conclusion .....	106
Chapter 4            TOLA Design Analysis .....	109
4.1 Problem Definition .....	110
4.2 Method.....	113
4.2.1 Method Overview .....	113
4.2.2 Impulsive Load Model.....	116

4.2.2.1 TOLA Floor Strength .....	116
4.2.2.2 Impulsive Load on a TOLA of a FC.....	118
4.2.2.3 Mechanical Model of a FC's Body.....	122
4.2.3 Fracture Probability Model.....	125
4.3 Numerical Results and Discussion .....	127
4.3.1 Weight and Impulsive Load .....	127
4.3.2 Comparison with exist TOLA Design Criteria.....	129
4.3.3 Effect of Impulsive Load on Passengers .....	133
4.3.4 Probability of the TOLA Destruction by a FC .....	139
4.3.5 Model Verification .....	141
4.4 Conclusion.....	142
Chapter 5      Discussion and Conclusion.....	145
Acknowledgments .....	148
Appendix A Cost Analysis of a FC Configuration Design for Medical Emergencies [76][77 ].....	153
Appendix B Demand Estimation in the USA.....	174
References .....	186

# List of Figures

Figure 1 Map of Conventional Research and This research .....	34
Figure 2 Overview of Main FC's Issues.....	36
Figure 3 Two Stages Parachute for Emergency Landing [33].....	41
Figure 4 Emergency Landing with a Mushroom Type Parachute in the Phase of Hove ring.....	43
Figure 5 Overview of This Paper .....	46
Figure 6 Method Overview.....	50
Figure 7 Research Flow in an Airframe Design Optimization Model.....	52
Figure 8 Conceptional Diagram of Impulsive Load Simulation.....	56
Figure 9 Research method process .....	64
Figure 10 Three FC configurations.....	67
Figure 11 Equilibrium of the forces exerted on a multi-rotor aircraft during cruising. 7 4	
Figure 12 Equilibrium of the forces exerted on a vectored-thrust aircraft during cruise ng.....	76

Figure 13 Equilibrium of the forces exerted on a lift + cruise aircraft during cruising	7
Figure 14 Positional relationship of the rotors and the observer during hovering.....	82
Figure 15 Landing area model of the multi-rotor type .....	85
Figure 16 Landing area model of the vectored-thrust type.....	85
Figure 17 Landing area model of the lift + cruise type.....	86
Figure 18 Comparison between the NEDO Battery Roadmap and the Results [65]	105
Figure 19 Conceptional Diagram of Impulsive Load Simulation.....	115
Figure 20 Functional Flow of a Ballistic Parachute System.....	118
Figure 21 Mechanical Model of an Airframe and a Parachute .....	119
Figure 22 Springer Damper Model of One-Mass System .....	122
Figure 23 Time Series Variation of Impulsive Load at $\Delta t=0.15$ , $m=1000$ .....	127
Figure 24 Total Weight and Impulsive Load by $\Delta t$ .....	128
Figure 25 Impulsive Load by Altitude with and Without a Parachute .....	129
Figure 26 Impulsive Load by Total Weight.....	131
Figure 27 Impulsive Load by the Size of a Parachute .....	132
Figure 28 Acceleration of a Fuselage in Spring Damper System by time .....	133

Figure 29 Vertical Velocity Transition .....	137
Figure 30 Maximum Acceleration by Initial Altitude .....	138
Figure 31 Cost per Unit [94].....	166
Figure 32 Component-cost breakdown [94] .....	167
Figure 33 Cost breakdown of direct operating cost [94] .....	169

## List of Tables

Table 1 Classification and examples of FCs [4] .....	31
Table 2 Calculation specifications of noise .....	82
Table 3 Optimization Results for the Multi-rotor Type.....	93
Table 4 Optimization Results for the Vectored-thrust Type.....	95
Table 5 Optimization Results for the Lift + Cruise Type .....	97
Table 6 Battery energy density comparison between the three aircraft types .....	100
Table 7 Parameter Study Results for the Multi-rotor.....	102
Table 8 Parameter Study Result for the Vectored-Thrust Type .....	103
Table 9 Parameter Study Results for the Lift + Cruise Type.....	104
Table 10 Constants in Equation (3) and (4).....	121
Table 11 Constants for the Spring Damper Model .....	124
Table 12 Mechanical Criteria by Injury [85] .....	135
Table 13 Vahana mission profile [94] .....	163
Table 14 Lilium-jet mission profile [94] .....	164
Table 15 Volocopter 2X mission profile [94].....	164

Table 16 List of criteria [94].....	171
Table 17 Aircraft Types and Average Attributes.....	178
Table 18 Coefficients Values Obtained by Multiple Regression Analysis.....	181
Table 19 Updated Share Distribution .....	182
Table 20 Share Distribution in Four Scenarios.....	183

## Nomenclature

$\vec{J}$	Vector of objective functions
$\vec{w}$	Vector of weights
$\vec{x}$	Vector of variables
$A$	Front projected area [m <sup>2</sup> ]
$A_{\text{Body}}$	Projected area of the airframe [m <sup>2</sup> ]
$A_{\text{Parachute}}$	Projected area of a parachute [m <sup>2</sup> ]
$AR$	Aspect ratio of a main wing
$B$	Amplitude of the spring-damper system [m]
$B_{\text{Rotor}}$	The number of a rotor blade
$BED$	Battery weight energy density [Wh/kg]
$C$	Damping Constant [N · s/ m]
$C_{D\_Body}$	Drag coefficient of an airframe body
$C_{D\_Body}$	Drag coefficient of a body

$C_{D\_Parachute}$	Drag coefficient of a parachute
$C_{D\_Wing}$	Drag coefficient of a main wing
$C_{L\_Body}$	Lift coefficient of a body
$C_{L\_Wing}$	Lift coefficient of a main wing
$C_P$	Power coefficient of a rotor
$C_{P_i}$	Induced power coefficient of a rotor
$C_{P_p}$	Parasite power coefficient of a rotor
$C_Q$	Torque coefficient of a rotor
$C_T$	Thrust coefficient of a rotor
$D$	Drag force [N]
$E$	Energy required for a mission [kWh]
$E_{Hover},$ $E_{Climb}, E_{Cruise}, E_{Descent}$	Energy required for each phase: hovering, climbing, cruising, or descending [kWh]
$F$	Destructive event of a TOLA
$F_{FC}$	Impulsive load on the airframe of a FC [kN]
$FM$	Rotor's figure of merit

$F_{\text{Vertiport}}$	Impulsive load on a TOLA [kN]
$H$	Area of a landing point [m <sup>2</sup> ]
$K$	Spring Costannt [kN · m]
$L$	Lift force [N]
$LF$	Load factor of a fuselage[m/s <sup>2</sup> ]
$MTOW$	Maximum takeoff weight [kg]
$N$	The number of a rotor
$Noise$	Noise value [dB]
$P_{\text{Hover}},$ $P_{\text{Climb}}, P_{\text{Cruise}}, P_{\text{Descent}}$	Rotor power for each phase: hovering, climbing, cruising, or descending [W]
$P_{\text{Japan}}$	Population of Japan
$P_{\text{Tokyo}}$	Population of Tokyo
$PW$	Sound power [Pa]
$P_f(T)$	Destruction probability of the TOLA in period T by crash
$P_{\text{impact}}(T)$	Crash probability of the aircraft in period T
$Q$	Rotor torque [N · m]

$R_e$	Effective radius of a rotor [m]
$T$	Covered Period
$T_{Hover},$ $T_{Climb}, T_{Cruise}, T_{Descent}$	Rotor thrust for each phase: hovering, climbing, cruising, or descending [N]
$U$	Downwash velocity at an observer [m/s]
$V_{Climb}, V_{Cruise}, V_{Descent}$	Horizontal velocity for each phase: climbing, cruising, descending [m/s]
$V_{Tip, Hover}$	Rotor's tip speed during hovering [m/s]
$W_{Battery}$	Battery weight [kg]
$W_{Empty}$	Empty weight [kg]
$W_{Fuselage}$	Fuselage weight [kg]
$W_{Landing\_Gear}$	Landing gear weight [kg]
$W_{Motor}$	Motor weight [kg]
$W_{Payload}$	Payload weight [kg]
$W_{Rotor}$	Rotor weight [kg]
$W_{Wing}$	Main wing weight [kg]
$C$	Rotor chord [m]

$D$	Diameter of a parachute [m]
$d$	Propeller diameter [m]
$d_{\text{Back}}$	Diameter of a propeller at the back of a fuselage [m]
$d_{\text{Observer}}$	Distance between a rotor and an observer [m]
$g$	Gravitational acceleration $\equiv 9.80665 \text{ m/s}^2$
$l$	Length of landing area
$m$	Mass of an airframe and a parachute [kg]
$m_{\text{Harmony}}$	Harmony number of rotational noise
$m_{\text{Fuselage}}$	Mass of a fuselage [kg]
$n_{\text{airtaxi\_day\_vertiport}}$	Average number of trips per day per a vertiport
$n_{\text{taxi\_year}}$	Average number of trips per year for taxis in Japan
$n_{\text{vertiport}}$	Number of Vertiports inn Tokyo
$p_{\text{airtaxi}}$	Probability of choosing air taxi among transportation modes
$p_{\text{ref}}$	Referential noise power [Pa]

$r$ [fare>5000]	Ratio of the taxi passengers who pay a fare of 5,000yen or more
$s$	Solidity of a rotor blade
$t$	Time [t]
$\Delta t$	Time variation [t]
$t_{\text{Rotor}}$	Thickness of a rotor blade [m]
$v$	Relational velocity of a fluid [m/s]
$v_h$	Induced velocity under a rotor [m/s]
$v_z$	Velocity in z direction of an airframe and a parachute
$\Delta v_z$	Variation of $v_z$
$w$	Width of a landing area
$w_{\text{span}}$	Wingspan [m]
$z$	Altitude of an airframe and a parachute [m]
$a$	Sound speed [m/s]
$\alpha$	Initial phase of the spring-damper system [rad]

$\alpha_{\text{Rotor}}$	Rotor degree against airspeed vector [rad]
$\delta$	Dimensionless initialization speed of spring-damper system
$\zeta$	Attenuation ratio
$\theta_{\text{Attack}}$	Angle of attack [rad]
$\theta_{\text{Body}}$	Advanced angle of a body [rad]
$\theta_{\text{Observer}}$	Azimuthal angle between a rotor and an observer [rad]
$\kappa$	Induced power ratio
$\kappa_{\text{Int}}$	Interference-induced power ratio
$\lambda$	Occurrence probability of an accident
$\lambda_{\text{Tapper}}$	Tapper ratio of a main wing
$\mu$	Advance ratio
$\rho$	Air density [kg/m <sup>3</sup> ]
$\rho_{\text{Air}}$	Air density $\equiv 1.225 \text{ kg/m}^3$
$\varphi$	Weighted objective function
$\omega_0$	Natural angular frequency of the spring- damper system [rad/s]



# **Chapter 1**

## **Introduction**

# **1.1 Background**

## **1.1.1 Why is a Flying Car (FC) Emerging?**

Currently, serious traffic jams, especially in urban areas, are being generated by population explosion and urbanization all around the world. These problems will become much worse toward 2050. In 2018, the world population is more than seven billion, and will increase to about 10 billion according to the report of United Nations [1]. India will have the highest population in the world. China will turn to have the second highest population then.

Moreover, urbanization becomes much worse as well as the increasing world population. Currently, that more than one half of the world population lives now in urban areas, and virtually all countries of the world are becoming increasingly urbanized [1]. As a fact, globally, more people live in urban areas than in rural areas, with 55 % of the world's population residing in urban areas in 2018. In 1950, 30 % of the world's population was urban, and by 2050, 68 % of the world's population is projected to be urban [1]. For example, Tokyo, which is a capital of Japan, is the world largest city with an agglomeration of 37 million inhabitants [2]. This number is much more than those of Shanghai, Mexico City and Sao Paulo. However, the urbanization is

shared by not only developed countries, but also developing countries [1]. Just three countries- India, China as mentioned before, and Nigeria together are expected to account for 35 % of the growth in the world's urban population between 2018 and 2050 [1].

In recent years, FCs have been expected to be the next generation of air mobility, sparked by a white paper published by Uber in 2016, and expected to be used as air taxis to alleviate urban congestion [3]. According to a survey by Electric VTOL News, more than 400 eVTOLs have been developed [4]. FCs are sometimes referred to as eVTOL, Urban Air Mobility (UAM), or Passenger Drone [22]. In this paper, we call this new type air mobility as a FC.

## 1.1.2 Applications

Uber's white paper describes the future of air taxis, where FCs will ease traffic congestion in cities [3]. Expected market for FCs is not limited to air taxis. This figure classifies use cases from social acceptance and profitability. There is a wide range of applications, including local transportation, disaster relief, remote island transportation, depopulated areas, emergency medical services, and leisure [22]. Some of the use cases will be introduced later. Some of the use cases will be presented in detail in the following subsections.

In many cases, air traffic in rural areas is operated from regional airports to Haneda Airport, the hub. Alternatively, there are many flights connecting government-designated cities to government-designated cities. Manufacturing plants are often located in regional areas, and managers in those areas have a need to travel from regional airports to regional airports. The availability of air traffic can also help attract companies to the region. These are not the mobility needs of ordinary consumers, but the needs of companies and corporations. If the author consider FCs as transportation between rural areas in Japan, a certain amount of market scale can be expected.

There are many local governments that are currently utilizing helicopters for disaster relief. Because of the urgency of this use case, it is expected to

have high social acceptance. However, since the number and frequency of operations are not expected to be large, the use of helicopters during normal times is an issue. In addition, since the TOLAs are not always at well-developed heliports, flexibility in landing functions is required.

There are about 254 remote islands in Japan which people live in [5]. Most of the traffic between the islands and the mainland or between the islands is unprofitable. Helicopters have been introduced to the islands of Tokyo for inter-island transportation, but they are operated on a subsidized basis. Since the helicopter flies over the sea, it is easy to gain a certain level of understanding for safety and environmental friendliness. On the other hand, if the aircraft lands in the water or crashes, the cost of salvaging it would be in the hundreds of millions, so the reliability of the aircraft is important.

Due to the declining birthrate and aging population in Japan, depopulation has been increasing in rural areas. There are 61,000 marginal villages in Japan [6]. The public transportation in these villages is mostly loss-making routes for both buses and trains. FCs have potential as a means of transportation in depopulated areas, as it is easy to secure land. However, in depopulated areas, traffic congestion is less frequent, and it is not always possible to travel faster than by car.

Medical Emergency applications are expected to have high social acceptability as well as disaster relief. The purpose of this application, called "doctor helicopter" in Japan, is not primarily emergency transport, but to

reach the sick or injured as quickly as possible. Therefore, there is a high demand for the use of FCs, even if they are small in size and have a short cruising range. However, FCs are still not as fast as helicopters. Since half of all injuries and illnesses occur at night, nighttime flight requires nighttime equipment. In addition, considering the decrease in the number of flight doctors and the fact that the fire department must arrive at the rendezvous point before the existing doctor helicopter can land, not only the operation system but also the landing process must be manpower-saving.

The use case of sightseeing and leisure, as the name suggests, corresponds to scenic flights in tourist areas. This is not a problem even if it is a single-seater, and it is possible to realize a FC within the current technological constraints. While attracting the attention of tourism businesses, there is a possibility that FCs can only play an active role during the specific season of a tourist destination.

### **1.1.3 Vehicle Types**

Nowadays, FCs are called Urban Air Mobility, Passenger Drone, or eVTOL, and 100 types of airframe have been announced to the world [4]. They can be classified according to the shape of the airframe and the thrust system. In terms of airframe shape, they can be divided into winged and wingless types [4]. The wingless type has many multicopters that are derived from the so-called drone form. The winged type can be divided into Vectored Thrust, which changes the direction of thrust, and Lift+Cruise, which does not change the direction of thrust. The thrust system can be divided into electric and hybrid. Examples of each are shown in Table 1 below. In this article, the author will keep to the three simple categories. FCs are not all classified in this way. For example, the Openner BlackFly is a winged model, but it cannot be classified as a pure multicopter because it flies using eight rotors without rotating rotors or wings.

Table 1 Classification and examples of FCs [4]

	Multicopter (Wingless)	Vectored Thrust	Lift+Cruise
Electric	SkyDrive, Volocopter, EHang, City Airbus	Airbus Vahana, Joby Aviation S4 , Lilium, Archer	Boeing Aurora Flight Science, Wisk Cora, Kitty Hawk Heavyside, teTra Aviation
Hybrid	-	Bell Nexus	Terrafugia TF- 2

## **1.1.4 Infrastructure**

FC systems require not only an airframe, but also TOLAs for maintenance and operation, charging facilities, air traffic control (flight management system), communication facilities, and service providers such as dispatchers in order to achieve safe and efficient operations [7].

TOLAs are also sometimes referred to as Vertiports [8]. It has the same function as an existing heliport. A TOLA is a place where FCs take off and land, and the selection of the site, the maximum number of parked aircraft, operating rules, and environmental standards must be considered. Charging facilities are facilities for charging the batteries of flying vehicles. There are two types of charging systems: one is to charge the FC via a charging station, and the other is to replace the battery each time the car is operated. Each type of charging system requires appropriate equipment and charging specifications. To achieve efficient and safe takeoffs and landings, communication facilities are needed to enable communication between people, between people and systems, and between systems. Based on the required communication speed and volume, an appropriate communication system must be defined.

The factors that affect the availability of a TOLA for flying vehicles [8]. All of these issues must be considered comprehensively, along with control and operation methods and communications. The factors can be divided into two categories: the ability to locate TOLAs in desirable locations and the operational capability of the sites. The former can be divided into constraints on the development of TOLAs and constraints due to legal policies. The latter includes not only constraints on the development of the TOLA (such as wind speed patterns, landing encroachment routes, price and availability of surrounding airspace and land, etc.) and legal policies, but also operational constraints, the terrain of the TOLA, takeoff and landing operations of flying vehicles, and passenger boarding and disembarkation processes.

# 1.2 Conventional Research

Flying Car Research Lab  
→Halistic system design

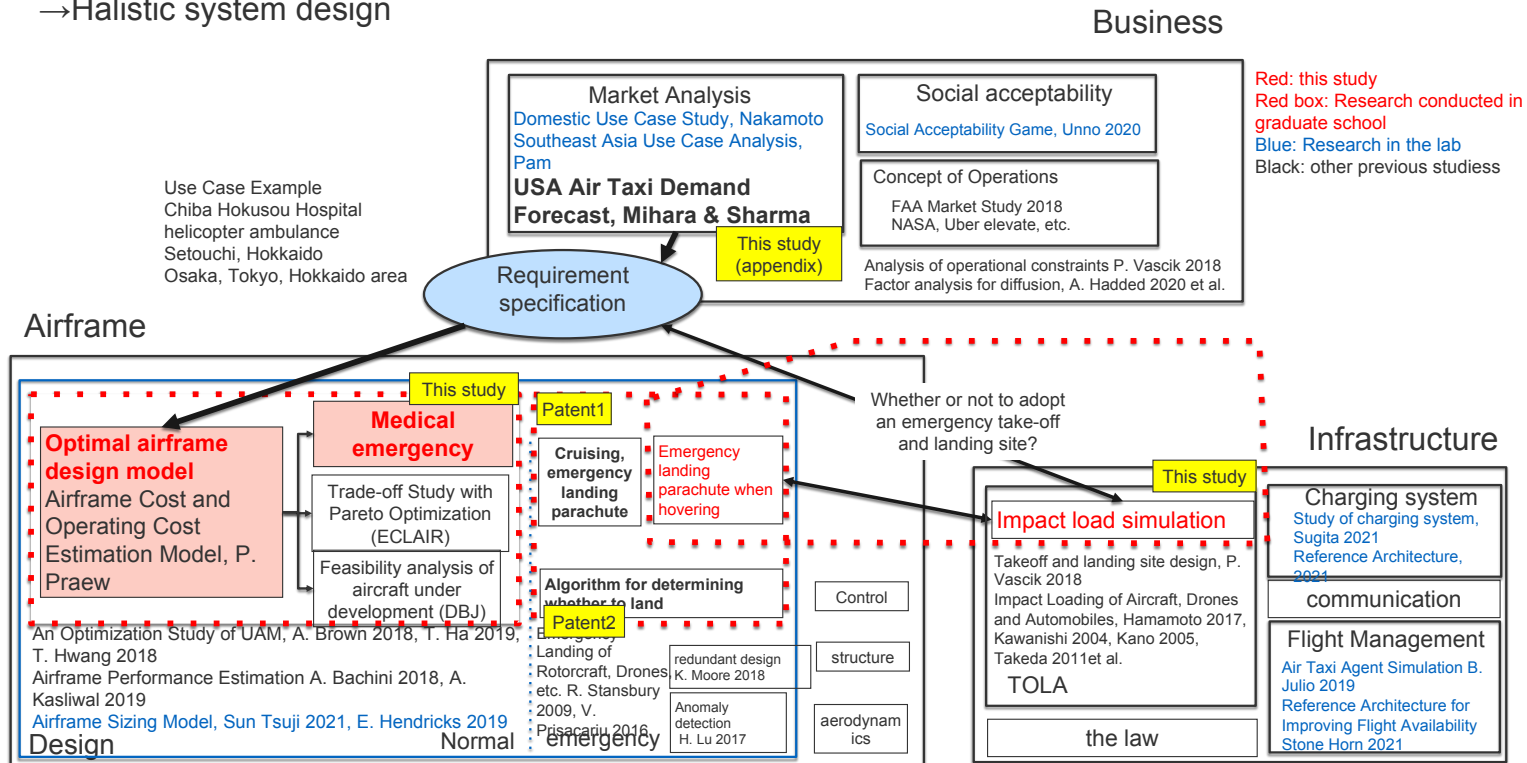


Figure 1 Map of Conventional Research and This research

Figure 1 shows a map which puts this research contents and conventional research inside and outside Flying Car Research Lab in Keio University. The lab focuses on not only an FC vehicle but also its infrastructure and business. This study focuses airframe optimization model and emergency landing inside red frames.

Figure 2 shows the overview of main FC system issues [8][9]. FC vehicles have short-range and passenger capacity due to limited battery capacity, especially lithium-ion batteries. These issues limit FC operation. Therefore, with the battery evolution, an FC market has high potential. Moreover, the noise from multiple rotors of an FC affects social acceptance. Although a FC is free from engine noise, an FC cannot avoid rotational noise because rotating rotors provide thrust power. Furthermore, to increase operational scalability, placement of tools and traffic management system design should be considered with vehicle designs also. In Tokyo, because there are few spaces for FC's TOLAs, with the increased number of TOLAs, FC's market size can be increased. Also, safety is one of the most important issues for FCs for obtaining aviation certifications. Due to choosing multiple rotors for an FC vehicle design, an FC is expected to have higher redundancy than other rotorcraft. However, to consider social acceptance and ensure its safety, an FC needs an emergency landing solution for crashing by any chance [10][11][12].

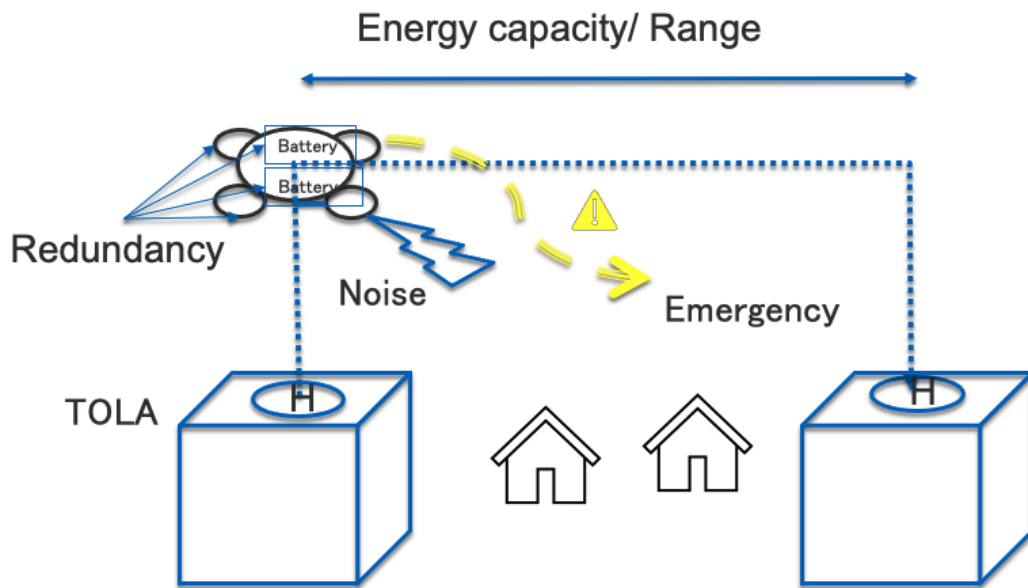


Figure 2 Overview of Main FC's Issues

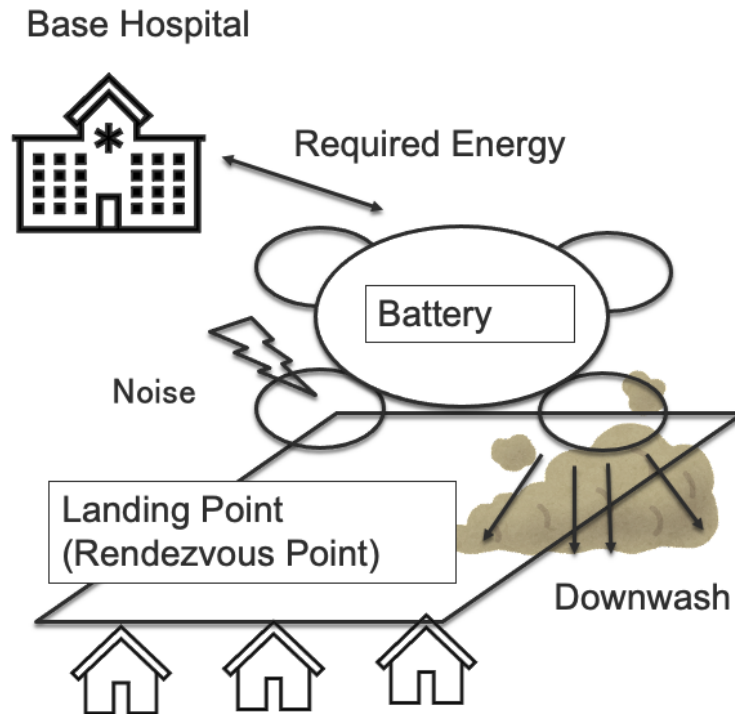
## **1.2.1 Airframe analysis for a medical emergency for a normal flight in the medical emergency use case**

FC airframe models of an FC are divided into three types, namely, multi-rotor, vectored thrust (tilt-rotor, tilt-wing), and lift + cruise [13]. From the perspective of airframe design, there is no dominant design in the FC sector [14]. Some studies have conducted research into airframe designs that have been identified as highly feasible. However, due to the anticipated size of the market, most of the FCs under development are destined for use as air taxis [15], [16], [17]. The research which has analyzed the requirements for using FCs in a medical emergency and discusses the airframe design in the mission profile based on the requirements of medical emergencies has not been found. Some previous studies have investigated the airframe models of the vectored-thrust and lift + cruise aircraft types [37], [38], [39]. However, based on an interview with a medical doctor with extensive experience working with the helicopter emergency medical service (HEMS), a short-range multi-rotor-type aircraft is sufficient for use by the Japanese HEMS. P.Praew (2019) estimates capital expense and direct operational cost of an FC HEMS with the DAPCA model [18]. Although the research shows these costs can decrease

with distributed electrification, its scope is limited to the economical issues of FCs.

Compared with existing aircraft, an FC has the potential to contribute more to the improvement of business sustainability because of the anticipated reduction in operating costs due to downsizing and electrification [39]. Previous studies [37], [38], [39] have used optimized aircraft and included performance parameters, such as the range and operating cost of FCs. However, to date, the optimal design of an FC from a social perspective, including airframe noise and downwash, has not been defined. Therefore, the current study analyzes the requirements of medical emergency applications and performs an optimum design simulation of an FC within the mission profile of a medical emergency from a system design perspective. Because a research method for FCs is yet to be established, the optimization is limited to a first-order analysis [19].

This study scope is limited to a medical emergency. However, the author researched other use cases. In the ÉCLAIR consortium, which discusses electrical aircraft among the industry, we have output the optimized vehicle model for other applications such as Tokyo, Hokkaido, and other rural areas [20]. Moreover, the author discusses the feasibility of the eVTOL aircraft which is under development with DBJ (Development Bank of Japan Inc) by estimating the cost, battery capacity, noise, downwash in this model [21].



The author summarizes the research questions below.

In a medical emergency, what is the performance of an FC in terms of weight, energy required for flight, noise level, etc.? This main research question is decomposed into two.

1, Which aircraft model (Multi-rotor, Vectored Thrust, Lift+Cruise) is appropriate for the mission profile of a medical emergency application?

2. With the requirements analysis results, to what extent can the values of the four objective functions of energy requirement, noise value, downwash, and landing site area be reduced?

## **1.2.2 Safety analysis by a impulsive load simulation for emergency landing**

In particular, for the safe operation of air taxis over cities, it is necessary to consider the impact on passengers, TOLAs, and aircraft due to emergency landings at TOLAs in case of aircraft trouble [22][23]. After taking off, a FC has emergency landing approach because it unstably flies in 30-50 m. However, multicopter type FCs do not have glide or auto-rotation functions. Therefore, the author propose that a parachutes are one solution to mitigate the impact of a collision. In Tokyo, when a FC flies, a TOLA candidate is an emergency heliport on a high building. However, the effects of emergency landing are not sure.

In the past, there have been studies on emergency landing methods for helicopters, airplanes, and drones using parachutes, but there is no similar research on FCs [24] [25] [26] [27]. In addition, although there are studies that have analyzed the impact load when an aircraft or helicopter crashes into a take-off or landing area while gliding or autorotating, there are no studies which have investigated the impact load when an FC makes an emergency landing on take-off or landing area [28] [29] [30] [31]. ICAO has published design criteria for heliport construction, but there is no study on the TOLAs for flying vehicles to calculate the design criteria [32]. The ICAO has

published the design criteria for heliport construction, but there is no study on the TOLA of flying vehicles to calculate the design criteria, and there is no study from the viewpoint of system design that considers the impact of landing on the TOLA, airframe system, and passengers.

This research is targeting the phase of taking off and landing. In the conventional research of the author, we discuss two stages parachute for an emergency in the phase of cruising. This parachute enables an FC to glide with a ram-air parachute. Reaching near a landing target, an FC can land on the ground with a mushroom parachute as shown in Figure 3. However, in the phase of hovering in taking off and landing, an FC needs to land on the near TOLA to avoid damaging other than that. Therefore, in this phase, we apply a mushroom parachute for an emergency landing to decrease damages.

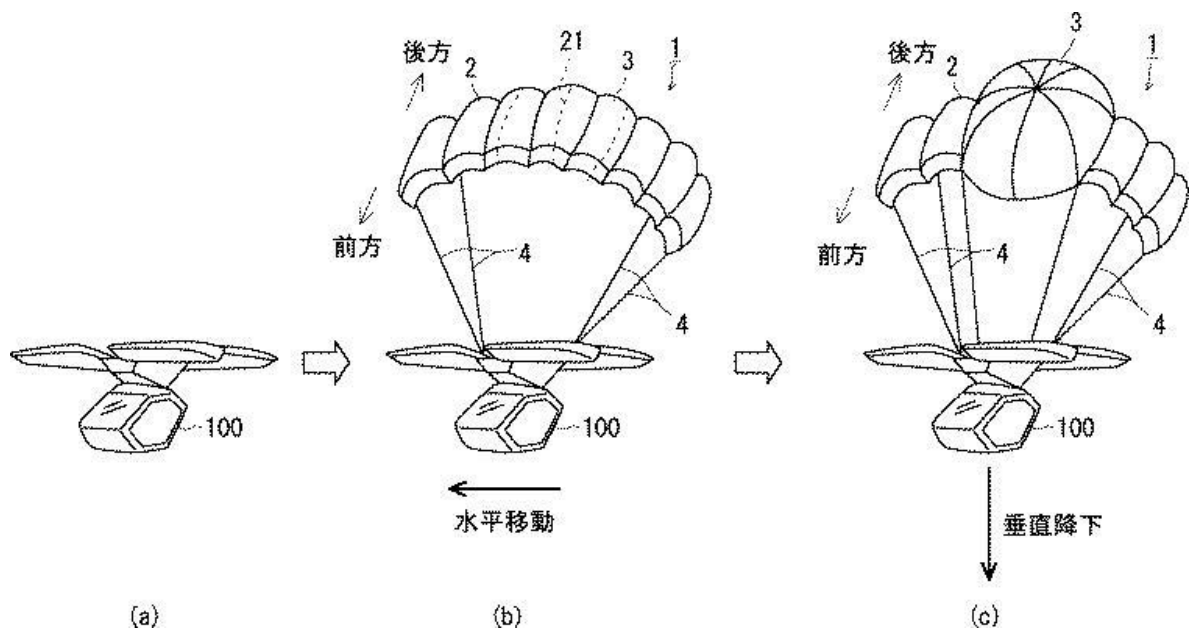


Figure 3 Two Stages Parachute for Emergency Landing [33]

There are two types of heliports: public heliports and emergency TOLAs. The first type of TOLA for air taxi operations in Tokyo is the existing heliport. In addition, there are about 80 emergency TOLAs in Tokyo for firefighting helicopters to take off and land in the event of a fire or other emergency. However, compared to heliports, it is unclear whether emergency TOLAs, which have less stringent installation standards set by each municipality, can withstand the take-off and landing of FCs [34]. In addition, when taking off and landing from the rooftop of a high-rise building, there is a possibility that the FC will be exposed to danger due to the building wind in the sky. Therefore, it is an issue to analyze the impact of a soft landing at an existing heliport when the FC loses control during the hovering phase of takeoff and landing.

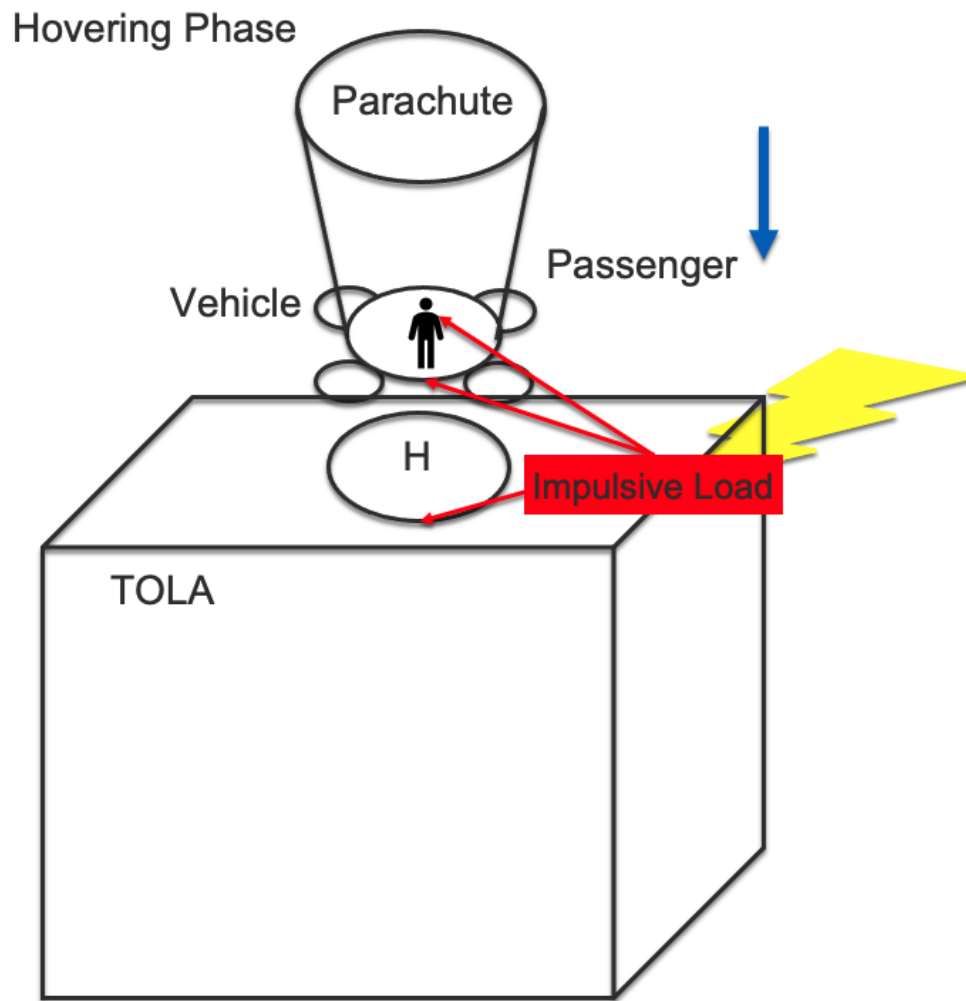


Figure 4 Emergency Landing with a Mushroom Type Parachute in the Phase of Hovering

The author summarizes the research questions bellow.

When an FC needs emergency landing as show in Figure 4, can the FC lands on the ground safely with a mushroom parachute? How much impact does the landing has?

1, When the FC lands and hovers on a TOLA, How much impact does the landing has on a TOLA, a vehicle, and a passenger?

2, When the FC lands with or without a parachute, how is his or her injury? How high should the FC use a parachute?

3, Is the impulsive load on a TOLA under the criteria of the coventional emergency heliports for a helicopter on over 100m buildings?

## 1.3 Purpose

The main purpose of this research is to clarify whether a FC is feasible for the use cases of medical emergency and an FC. These main purposes are divided into two.

The first sub-purpose of this study is to verify the applicability of the multi-rotor, vectored-thrust, and lift + cruise types of FC in a medical emergency.

The second sub-purpose of this study is to clarify whether emergency landing with a mushroom parachute is effective in terms of impulsive load in the case which the FC hovers on a TOLA in the take-off and landing phases. Moreover, this study aims to clarify whether conventional emergency heliports for helicopters is applicable for the FC use case.

## 1.4 Overview of This Paper

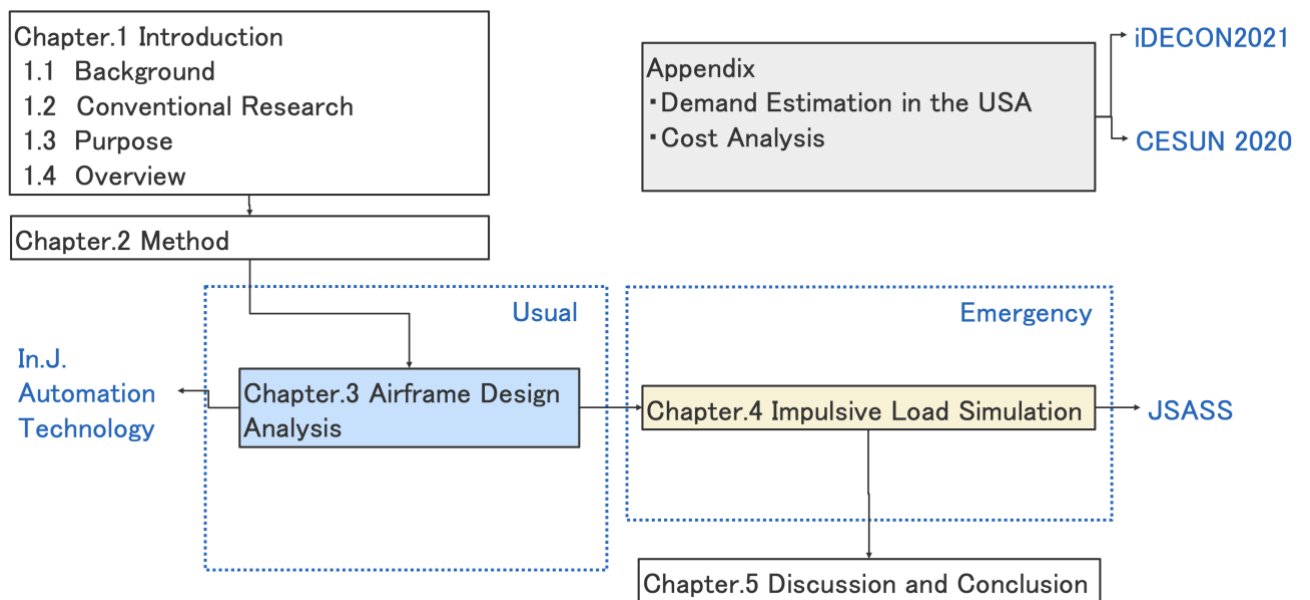


Figure 5 Overview of This Paper

Figure 5 shows the overview of this paper. First of all, the author introduces this paper. In the background section, an explanation about an FC is separated into three: vehicle, infrastructure, and applications. Chapter 2 summarizes and explains the method of this paper. After elucidating the overall method, the next subsection introduces the contents of a method, including parameters, input, output, and governing equations inside a model in each chapter. Next, in Chapter 3, the author discusses medical emergency in Japan based on actual operation data. After that, in Chapter 4, the author manipulates an air taxi service use case. Each chapter is composed of problem

definition, purpose, method, result, discussion, and conclusion as well as a usual research paper.

In Chapter 3, the author conducts modeling and simulation of an FC airframe design optimization for medical emergencies. A paper “Airframe Design Optimization and Simulation of FC for Medical Emergencies” is reviewed and published in International Journal of Automation Technology.

In Chapter 4, the author proposes the modeling and simulation of the FC impulsive load in emergency landings to design a safety TOLA. This chapter is published in the Japan Society of Aeronautical and Space Sciences in Japanese.

Finally, the author discusses and concludes this paper in Chapter 5.

## **1.5 Conclusion**

In this chapter, the introduction of this paper is explained. First, it describes the background FC aircraft, infrastructure (TOLAs), and applications. From the case of helicopter operation services, it enumerates the factors that hinder the spread of the technology and argues that it must be considered comprehensively from the perspective of system design. Next, from the survey of previous studies, the paper describes several issues that emerge from the existing studies. Next, from there, the overall originality of this research and the purpose for the multiple remaining issues mentioned earlier are mentioned. In the next section, a description of the methods used to study the system design of FCs is given.

# **Chapter 2**

## **Research Methods**

## 2.1 Method Overview

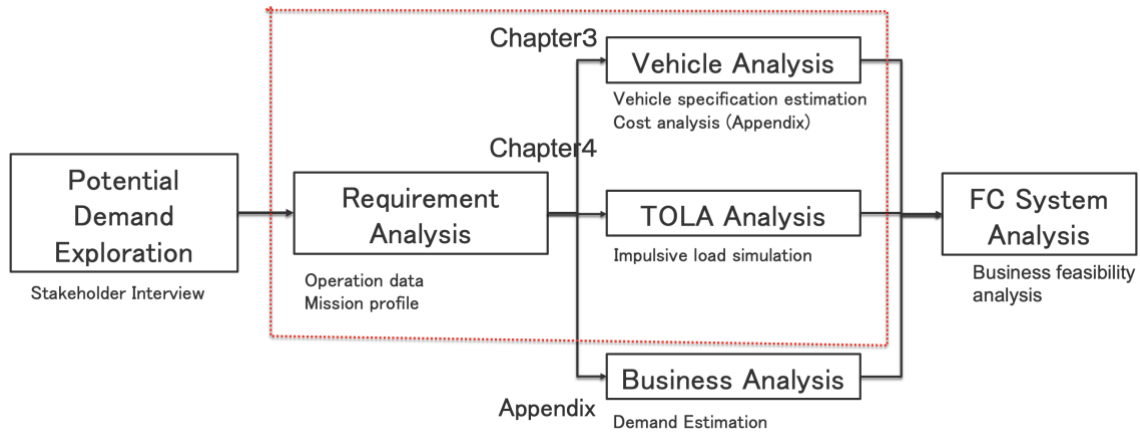


Figure 6 Method Overview

Figure 6 shows the overall picture of the method used in this paper. This model starts with a potential demand exploration. Based on the potential demand of a use case, the author defines requirements. As requirement analysis, the author analyzes real operation data to create a mission profile for flight and a concept of operation. Decomposing the requirements into subsystems of an FC system, the author can evaluate a vehicle and infrastructure, especially a TOLA in this study. In this study, the author estimates vehicle airframe specifications in a medical emergency application by airframe design optimization. Moreover, the author evaluates the

impulsive load effect on a TOLA, passengers, and a vehicle by impulsive load simulation. As a business analysis, the author executes multi logit model for estimating the demand for an air taxi service in the USA. However, the appendix section includes this study because it is out of the scope of this research.

Moreover, although the author also researches FC cost analysis including a purchase cost and direct operational cost, and demand estimation in the USA by multi logit model, the author inserts those research contents into the appendix section because these topics are out of scope in this research. Also, the details of each simulation method are explained in Chapters 3 and 4.

What makes this research unique? Although in general, a researcher focuses on a specific area in Figure 1, our target is a holistic system design of an FC. Our lab is connected to each stakeholder of a use case. Therefore, this enables us to find stakeholder needs, which can be the requirements of the use cases. Because the author belongs to the lab for a long time, he comes up with the ideas about multi-disciplinary system design optimization of an FC in the HEMS use case and whether an emergency heliport on a high-rise building can be a TOLA for an FC.

## 2.2 Airframe Design Optimization Model

This chapter targets mainly a vehicle design based on a use case of a medical emergency under technical and law constraints. The author develops a simulation model to optimize an airframe design of an FC in terms of society and economy. The purpose of the chapter is to verify the applicability of the multi-rotor, vectored-thrust, and lift + cruise types of an FC in a medical emergency in terms of society and economy. To date, conventional research, in which the airframe of an FC is optimized for use in medical emergencies, has not identified a sustainable solution. Therefore, the author executes modeling and simulation by system optimization for an FC airframe in a medical emergency use case.

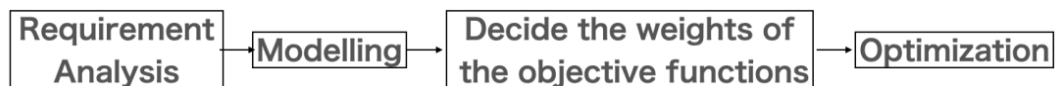


Figure 7 Research Flow in an Airframe Design Optimization Model

Figure 7 shows a research process of an airframe design optimization model. The author analyzes the requirements of a use case for a medical emergency using data from interviews with stakeholders from the HEMS system. Based on the interviews, a mission profile is created for the operation of FCs in a medical emergency. To optimize the system, the energy required for a round-trip flight and the noise, downwash wind speed, and landing point area are

selected as objective functions. Optimization is performed using weighted sum optimization, and the weighting coefficients are determined in terms of priority as identified in the above-mentioned stakeholder discussions. Since stakeholder consensus is required, weight optimization is used instead of Pareto's optimal solution.

Equation (1) shows the optimization problem.  $J(\vec{x})$  is the vector of the objective function, and  $\vec{w}$  is the weighting vector.  $\vec{x}$  indicates a variable vector. The aim is to minimize the weighted single-objective function. A solution by weighted optimization is limited to a weak Pareto solution although it can support decision-making for design [44]. As future research, the author needs to obtain a Pareto-line on a multi-objective optimization problem.

$$\min \Phi = \min[\vec{w} \cdot \vec{J}(\vec{x})] \quad (1)$$

The objective function vector comprises the amount of energy required for one flight ( $J_1 \equiv E$ ), the noise level ( $J_2 \equiv Noise$ ), the landing point area ( $J_3 \equiv H$ ), and the downwash wind speed ( $J_4 \equiv U$ ), as shown in Eq. (2):

$$J(\vec{x}) = \begin{bmatrix} E \\ Noise \\ H \\ U \end{bmatrix} \quad (2)$$

The design variables are the rotor diameter ( $d$ ) and the thrust coefficient ( $C_T$ ) (Eq. [3]). For the lift + cruise type of aircraft, the rear rotor diameter ( $d_{back}$ ) of the fuselage is included in the design variable.

$$\vec{x} = \begin{cases} \begin{bmatrix} d \\ C_T \end{bmatrix} & \text{for multi-rotor and vectored thrust} \\ \begin{bmatrix} d \\ C_T \\ d_{back} \end{bmatrix} & \text{for Lift + cruise} \end{cases} \quad (3)$$

## **2.3 Impulsive Load Model for Designing a Safety TOLA**

This subsection focuses on a TOLA in the infrastructure of an FC. The purpose of this subsection is to calculate the effects on the occupants and the aircraft and the required specifications of the TOLA field design strength for the safety design of both the TOLA and the aircraft by simulating the impact loads of an FC in the case of loss of control due to aircraft failure. Also, in this subsection, the author conducts a requirement analysis in a use case of an air taxi service in Tokyo with ground taxi data. The author finds that there are sixty to eighty trips per day in Tokyo in this use case. To operate with the trip number in Tokyo, the author finds that the number and locations of the TOLAs are an important issue to implement an ATS because the areas in Tokyo are quite limited. Therefore, the author proposes that current emergency heliports on high buildings in Tokyo are candidates for an FC TOLA because most of them are currently free assets. Thus, the author develops a physics model to simulate the impulsive load of an FC on a TOLA when a FC regularly lands on a TOLA, crush on a TOLA with or without a mushroom-type parachute. In, this model evaluates not only a single impact on a TOLA but also a failure possibility of a TOLA by repeated landings.

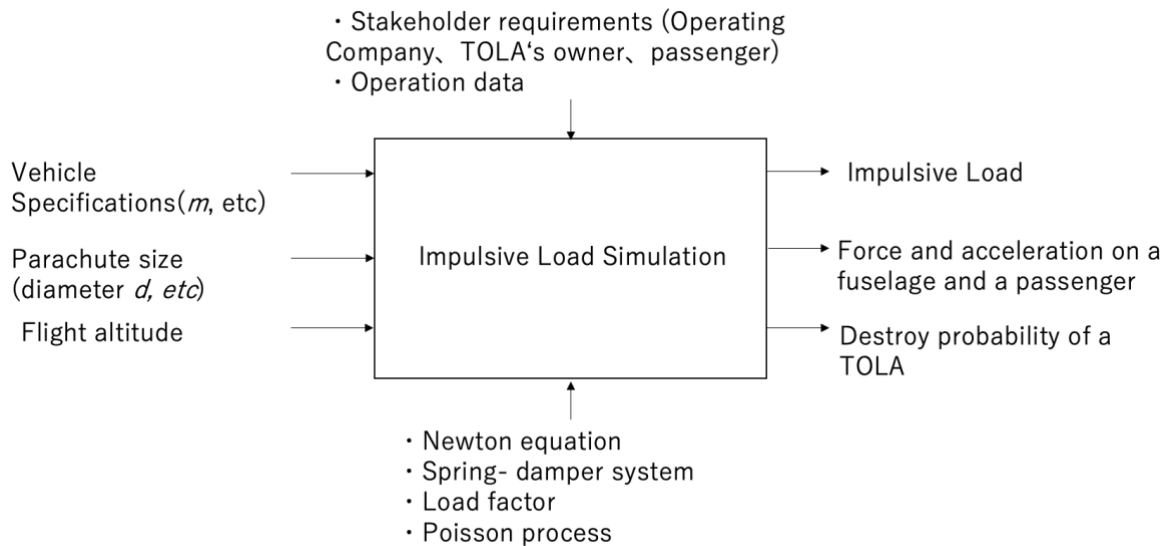


Figure 8 Conceptual Diagram of Impulsive Load Simulation

Figure 8 is a conceptual diagram of the simulation of impact loads due to the landing of a FC as an overview of the research method. On the left are inputs such as specifications of the aircraft and parachute, and flight altitude. The output is the impact load on the TOLA, the impact force and acceleration on the fuselage and passengers, and the destruction probability of the TOLA. The upper part is constraint conditions. The bottom is a means (enabler) to realize the model.

Stakeholders include operators, TOLA managers, and passengers. All of them want to reduce the damage to the aircraft, the TOLA, and the passengers by safe landing. Impact load simulation is performed under these constraints.

This study consists of four simulations. The details of the simulations are described in 5.2. It consists of the following four simulations.

1) Firstly, this study calculates the floor strength that a TOLA for an FC should have by calculating the impact load when the aircraft falls from the existing ICAO standard of 0.66 m (Subsection 4.2.2.1) [32].

2) Next, the results are compared with the design criteria of existing heliports and emergency TOLAs in the cases with and without mushroom-shaped parachutes. At the same time, a parameter study is performed by changing the diameter of the parachute, the altitude at which the parachute opens, and the maximum take-off weight of the FC (Subsection 4.2.2.2).

3) Next, the author considers the force applied to the fuselage and the landing gear of the aircraft immediately after landing, and calculate the impact force that should be absorbed by the crushable of the aircraft, the seat, and the airbag from the force to the fuselage. In addition, to consider the effect on the human body, the acceleration applied to that fuselage is calculated and the injury criteria of the acceleration on the human body are compared (Section 4.2.2.3).

4) Finally, the events that repeatedly land FCs and destroy the TOLAs when impact loads are generated are modeled as Poisson processes and their destruction probabilities are calculated (Section 4.2.3). Since there are no records of FC operations yet, the frequency of air taxi operations is estimated from taxi operation records.

## **2.4 Conclusion**

In this section, the author explains the method overview from a system design view and each method in the chapter. The details of each method in subsection 2.2-2.4 is provided in next chapters with results and discussion.

# **Chapter 3**

## **Vehicle Design Analysis**

## 3.1 Problem Definition

Airframe models of an FC are divided into three types, namely, multi-rotor, vectored thrust (tilt-rotor, tilt-wing), and lift + cruise [35]. From the perspective of airframe design, there is no dominant design in the FC sector [36]. Some studies have conducted research into airframe designs that have been identified as highly feasible. However, due to the anticipated size of the market, most of the FCs under development is destined for use as air taxis [37], [38], [39]. The research which has analyzed the requirements for using FCs in a medical emergency and discusses the airframe design in the mission profile based on the requirements of medical emergencies has not been found. Some previous studies have investigated the airframe models of the vectored-thrust and lift + cruise aircraft types [37], [38], [39]. However, based on an interview with a medical doctor with extensive experience working with the helicopter emergency medical service (HEMS), a short-range multi-rotor-type aircraft is sufficient for use by the Japanese HEMS.

Compared with existing aircraft, an FC has the potential to contribute more to the improvement of business sustainability because of the anticipated reduction in operating costs due to downsizing and electrification [39]. Previous studies [37], [38], [39] have used optimized aircraft and included performance parameters, such as the range and operating cost of FCs.

However, to date, the optimal design of an FC from a social perspective, including airframe noise and downwash, has not been defined. Therefore, the current study analyzes the requirements of medical emergency applications and performs an optimum design simulation of an FC within the mission profile of a medical emergency from a system design perspective. Because a research method for FCs is yet to be established, the optimization is limited to a first-order analysis [40].

The purpose of this study is to verify the applicability of the multi-rotor, vectored-thrust, and lift + cruise types of FC in a medical emergency in terms of sustainability. This paper analyzes the requirements of a use case for a medical emergency using data from interviews with stakeholders from the HEMS system. Based on the interviews, a mission profile is created for the operation of FCs in a medical emergency. To optimize the system, the energy required for a round-trip flight and the noise, downwash wind speed, and landing point area are selected as objective functions. Optimization is performed using weighted sum optimization, and the weighting coefficients are determined in terms of priority as identified in the abovementioned stakeholder discussions. Since stakeholder consensus is required, weight optimization is used instead of Pareto's optimal solution.

Section 3.2 analyzes the requirements of a medical emergency use case and describes its resulting mission profile. Additionally, the airframe optimization model is explained. Section 3.3 presents and explains the

results of the optimization and the parameter studies, and the required specifications for the aircraft are estimated based on these outcomes. Finally, Section 3.4 summarizes this study and provides some suggestions for future research.

## **3.2 Method**

### **3.2.1 Method Overview**

Fig. 1 outlines the methodology used in this study. First, a requirement analysis [41] involving stakeholder interviews is performed, and a mission profile for the use case of a medical emergency is created based on the interview results.

Next, a feasible proposal (multi-rotor, vectored thrust, or lift + cruise) for the design of an FC airframe is derived based on the mission profile created from the requirement analysis. The sustainability [42] issues of FCs are then extracted from the analysis. A sustainability analysis integrates environmental, economic, and social factors [43]. In a medical emergency, the energy required for the flight plus the noise, the landing point area, and the downwind are critical for FCs, so these parameters are selected as objective functions in the optimization problem. The weighting coefficient is determined by considering the priority identified during the stakeholder discussions mentioned above. A genetic algorithm implemented in Python is used to solve the weighted optimization problems [44], [45].

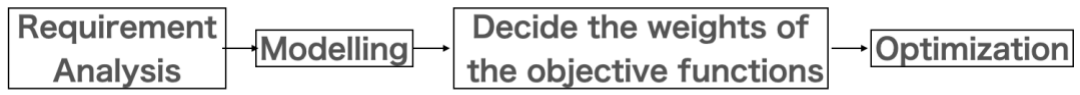


Figure 9 Research method process

## **3.2.2 Requirement Analysis for a Medical Emergency**

The medical helicopter system was introduced in Japan in 2001. In this scheme, a doctor is dispatched via helicopter to an emergency site where they provide “prehospital emergency medical treatment” [46]. The following stakeholders in the conventional HEMS system were interviewed to determine the requirements for medical emergencies:

### **(1) Flight doctor**

Interview with a flight doctor with a medical doctor’s license and experience of over 550 HEMS missions over 5 years.

### **(2) Helicopter pilot**

Interview with a HEMS pilot who flies a helicopter that belongs to the operating company.

### **(3) Operating company**

Interview with an operating company about the operational requirements of FCs. Note that the medical helicopter is operated by the operating company, not the base hospital of the HEMS system.

### 3.2.3 Vehicle Model

From the requirement analysis, three models of FCs (multi-rotor, vectored-thrust, and lift + cruise types) are selected (Fig. 2), which are expected to be capable of achieving the required cruising distance. Caused by choosing eVTOL in this paper, a propeller and a propeller is included in the mass load. As shown below in each model of the four objectives, the diameter of propeller is to affect not only a required energy for flight but also a noise value, a downwash speed, and vehicle miniaturization.

Like the Ehang 184 [47], the multi-rotor type has eight rotors (coaxial rotors with two upper and lower stages) with a diameter ( $d$  [m]) arranged at its four corners. It has a fuselage to accommodate the pilot and passengers.

The vectored-thrust type has four wings at the front, back, left, and right. During VTOL, the wings and rotor move vertically. When cruising, the wings and eight rotors produce lift and horizontal thrust, respectively, by rotating through  $90^\circ$ . When cruising, the wing area of the vectored-thrust aircraft supports the maximum takeoff weight (MTOW) with the lift force of four wingspans. In terms of general aviation parameters [16], the wing's aspect ratio ( $AR$ ) is 7, and the taper ratio ( $\lambda_{\text{Tapper}}$ ) is 1.0.

The lift + cruise type of aircraft achieves VTOL without rotating its main wing and rotor. When cruising, one rotor behind the fuselage is utilized for

advancing. For convenience, the diameters ( $d$ ) of the eight lift rotors are assumed to be identical. The wing area of the lift + cruise type supports the MTOW with the lift of two wings when cruising. The  $AR$  of the wing is 7, and the  $\lambda_{Tapp\text{er}}$  is 0.5, which is the same as the vectored thrust. When cruising, the lift + cruise aircraft uses the rotor (rotor diameter [ $d_{\text{back}}$ ]) at the rear of the fuselage to advance.

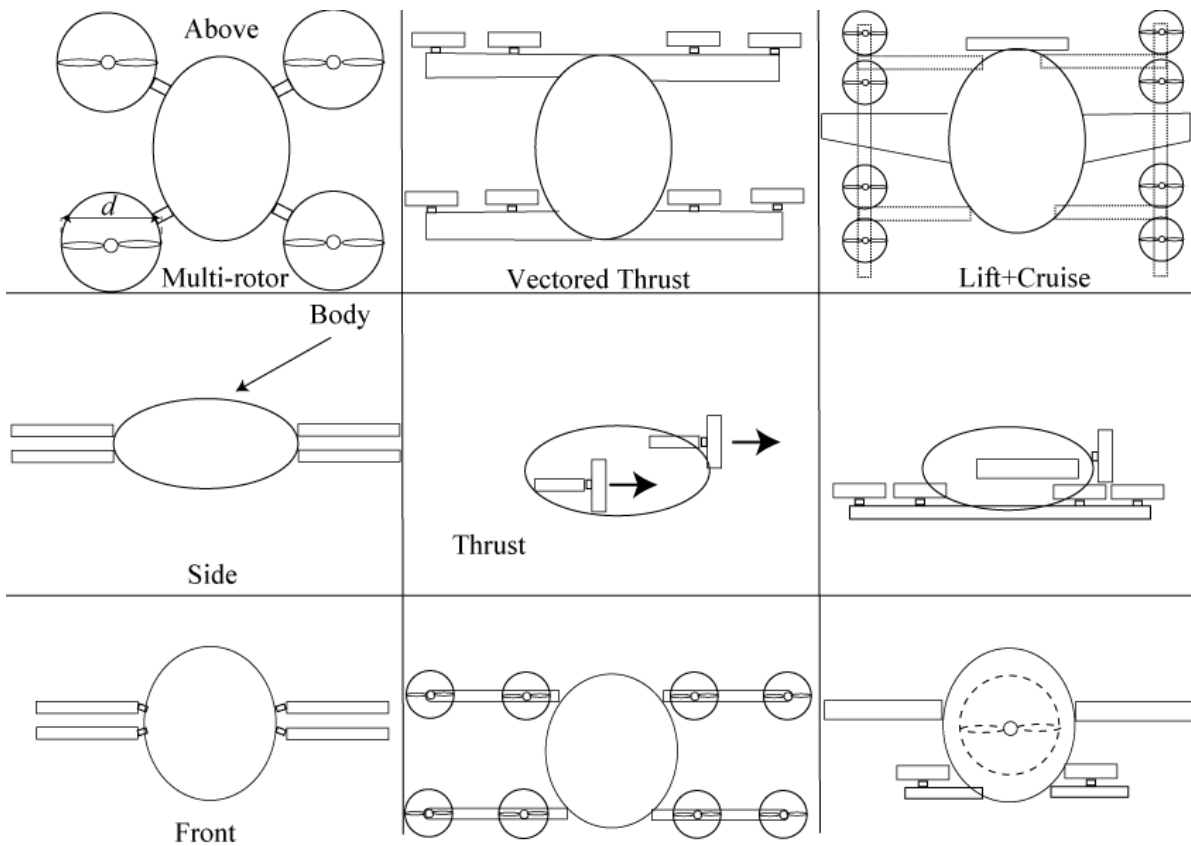


Figure 10 Three FC configurations

### 3.2.4 Optimization Model

Equation (1) shows the optimization problem.  $J(\vec{x})$  is the vector of the objective function, and  $\vec{w}$  is the weighting vector.  $\vec{x}$  indicates a variable vector. The aim is to minimize the weighted single-objective function. A solution by weighted optimization is limited to a weak Pareto solution although it can support decision-making for design [44]. As future research, the author needs to obtain a Pareto-line on a multi-objective optimization problem.

$$\min \Phi = \min[\vec{w} \cdot \vec{J}(\vec{x})] \quad (4)$$

The objective function vector comprises the amount of energy required for one flight ( $J_1 \equiv E$ ), the noise level ( $J_2 \equiv Noise$ ), the landing point area ( $J_3 \equiv H$ ), and the downwash wind speed ( $J_4 \equiv U$ ), as shown in Eq. (2):

$$J(\vec{x}) = \begin{bmatrix} E \\ Noise \\ H \\ U \end{bmatrix} \quad (5)$$

The design variables are the rotor diameter ( $d$ ) and the thrust coefficient ( $C_T$ ) (Eq. [3]). For the lift + cruise type of aircraft, the rear rotor diameter ( $d_{back}$ ) of the fuselage is included in the design variable.

$$\vec{x} = \begin{cases} \begin{bmatrix} d \\ C_T \end{bmatrix} & \text{for multi-rotor and vectored thrust} \\ \begin{bmatrix} d \\ C_T \\ d_{back} \end{bmatrix} & \text{for lift + cruise} \end{cases} \quad (6)$$

The constraint condition is that the speed of the propeller's blade tip [m/s] is subsonic or lower to prevent the generation of a shockwave resulting from the blade tip speed exceeding the speed of sound (Eq. [4]). In the multi-rotor aircraft, the cruising speed ( $V_{Cruise}$ ) + the tip speed of a propeller wing ( $V_{Tip}$ ) must be subsonic (270 m/s) or lower, because the directions of rotation and the rotating propeller correspond during cruising.

$$V_{Tip} \begin{cases} < 0.8a - V_{Cruise} & \text{for multi-rotor} \\ < 0.8a & \text{for others} \end{cases} \quad (7)$$

### (1) Energy

The amount of energy required from takeoff to landing is calculated. First, the weight model of the aircraft is determined. The amount of energy required for flight is calculated from the power required by the rotor during hovering, ascending/descending, and cruising for one flight (Eq. [5]).

The MTOW is the sum of the empty weight ( $W_{Empty}$ ), battery weight ( $W_{Battery}$ ), occupant weight ( $W_{Crew}$ ), and the payload weight ( $W_{Payload}$ ) [47].  $W_{Battery}$  is set at one-third of the MTOW because the optimal batteries available are estimated to increase the weight of a small aircraft by around

one-third [48]. The loading weight ( $W_{\text{Payload}}$ ) is 180 kg, which includes two 70-kg crew members and 40 kg of cargo.

$$MTOW = W_{\text{Empty}} + W_{\text{Battery}} + W_{\text{Crew}} + W_{\text{Payload}} \quad (8)$$

The empty weight is calculated by adding together the weights of the fuselage, rotor, landing gear, motor, and main wings, as shown in Eq. (6) [47]. Each weight above is calculated using Mohammad's weight estimation model [47]. The fuselage length is 6.0 m, the height and width are 2.0 m, and the material is aviation aluminum with a density of 2,711 kg/m<sup>3</sup>. The main wing is constructed from the same aeronautical aluminum: its thickness ratio is 0.2, the wing density coefficient is 0.0011, the load factor (including the safety factor) is 4.725, and the wing lift ratio is NACA0015, of which the Reynolds number is 100,000 and the air turbulence is Ncrit. From reference [40],  $C_{D\_Wing}$  and  $C_{L\_Wing}$  are 0.028 and 1.35, respectively [49]. When estimating the weight, the angle of attack ( $\theta_{\text{Attack}}$ ) of the main wing is considered to be 15°. From Table 10.5 of the Mohammad model, the landing gear's weight is 7.39% of the empty weight [47]. The rotor's weight uses the empirical formula of the weight and diameter of the Helix propeller used in UAV and Volocopter's e-volo aircraft [50]. The motor's weight is calculated empirically from the maximum torque required for turning the propeller, which is obtained from the Mohammad model [47].

$$W_{\text{Empty}} = W_{\text{Fuselage}} + W_{\text{Rotor}} + W_{\text{Landing Gear}} + W_{\text{Wing}} + W_{\text{Motor}} \quad (9)$$

Next, the power output of the rotor during one flight is considered (Eq. [7]). The amount of energy that the battery requires per single flight is calculated from the hovering, ascending/descending, and cruising times and the power outputs of the rotor at each stage. The duration of hovering, ascending/descending, and cruising is determined from the requirement analysis.

$$E = \begin{bmatrix} P_{Hover} \\ P_{Climb} \\ P_{Cruise} \\ P_{Descent} \end{bmatrix} \cdot [t_{Hover}, t_{Climb}, t_{Cruise}, t_{Descent}] \quad (10)$$

Equations (8)–(10) show the calculation formulas [3] [21] of Leishman's model. Typically, this is utilized to calculate the rotor's thrust during the hovering phase of a rotary wing aircraft and its power. Drag considers both induced and profile drag (Eq. [8]).

$$C_p = \kappa_i C_{pi} + C_{pp} \quad (11)$$

$$C_{pi} = \frac{1}{2} C_T^{1.5} \quad (12)$$

$$C_{pp} = \frac{1}{4} s C_{d0} \quad (13)$$

The power of induced drag is proportional to the thrust coefficient to the power of 1.5 [47]. The induced power factor ( $\kappa_i$ ) is 1.2[47]. The profile drag coefficient is proportional to the solidity ( $s = 0.1$ ) and rotor blade 2D zero-lift drag coefficient ( $C_{d0} = 0.01$ ) [51].

#### (A) Hovering

During hovering, the thrust of the rotors is considered to support the gravity of a FC with  $N$  rotors.  $v_h$  is the induced velocity of a rotating rotor while hovering. The wing tip velocity ( $V_{Tip, Hover}$ ) is calculated from the thrust ( $T$ ). Equations (11)–(13) are used to calculate the rotor power ( $P_{Hover}$ ). The power of the rotor during hovering ( $P_{Hover}$ ) is obtained using Leishman's rotor model [51]. The multi-rotor type is considered to consist of four co-axis rotors. The induced power coefficient is assumed to be  $\kappa$  ( $= 1.16$ ), and the interference-induced power coefficient is  $\kappa_{int}$  ( $= 1.15$ ) [51].  $\pi (d / 2)^2$  indicates the rotor area. The rotor's figure of merit ( $FM$ ) is set to 0.75.

$$v_h = \sqrt{\frac{MTOW \cdot g}{N \cdot \left(2 \cdot \rho \cdot \pi \cdot \left(\frac{d}{2}\right)^2\right)}} \quad (14)$$

$$V_{Tip,Hover} = \sqrt{\frac{T_{Hover}}{0.5 \cdot \rho \cdot C_T \cdot \pi \cdot \left(\frac{d}{2}\right)^2}} \quad (15)$$

$$P_{Hover} = \begin{cases} \frac{N}{2} \left( \frac{\kappa \kappa_{Int} (2T)^{1.5}}{\sqrt{4\rho A}} + \rho \pi \cdot \left(\frac{d}{2}\right)^2 V_{Tip,Hover}^3 \frac{2\rho C_{d0}}{8} \right) & \text{for multi-rotors} \\ N \cdot 0.5 \cdot C_p \cdot \rho \cdot (V_{Tip,Hover})^3 \cdot \pi \cdot \left(\frac{d}{2}\right)^2 & \text{for others} \end{cases} \quad (16)$$

### (B) Climbing and Descending

Next, the study considers the output power of one rotor when climbing and descending. It is calculated from the relationship between the climb and descent velocities ( $V_{Climb}$  or  $V_{Descent}$ , respectively), the induction velocity of the hovering rotor ( $v_h$ ), and the output power ( $P_{Hover}$ ) of one rotor during hovering [51].

$$\frac{P_{Climb}}{P_{Hover}} = \frac{V_{Climb}}{2v_h} + \sqrt{\left(\frac{V_{Climb}}{2v_h}\right)^2 + 1} \quad (17)$$

$$\frac{P_{Descent}}{P_{Hover}} = \frac{V_{Descent}}{2v_h} - \sqrt{\left(\frac{V_{Descent}}{2v_h}\right)^2 - 1} \quad (18)$$

### (C) Cruising

The energy required by one rotor during cruising is divided into the multi-rotor and the vectored thrust/lift + cruise, because the position of the FC is different from that during climbing and descending.

(i) Multi-rotor

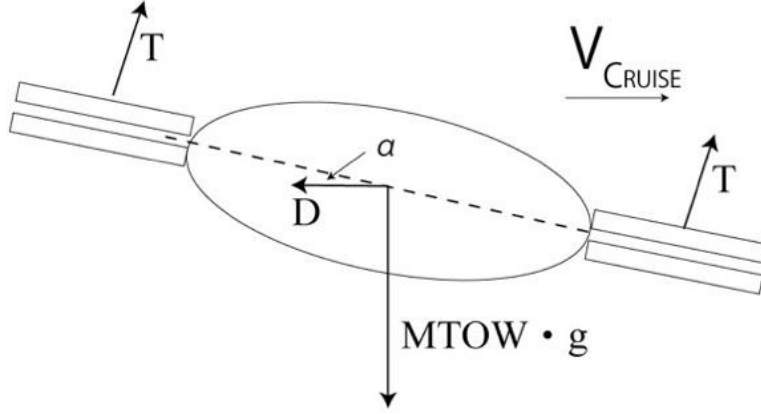


Figure 11 Equilibrium of the forces exerted on a multi-rotor aircraft during cruising

Figure 11 shows the equilibrium of the forces exerted on a multi-rotor aircraft during cruising. A forward rate ( $\mu$ ) is considered, which comprises a cruising speed ( $V_{Cruise}$ ), a rotor tip speed ( $V_{Tip, Cruise}$ ), and a turning radius ( $d/2$ ). From Eq. (17) using the forward rate ( $\mu$ ), the inflow rate ( $\lambda$ ) into the rotor is calculated from repeated calculations until the error ( $\varepsilon$ ) becomes 0.005 or less [51].

$$\mu = \frac{V_{Cruise} \cos(\alpha_{Rotor})}{V_{Tip, Cruise} \left(\frac{d}{2}\right)} \quad (19)$$

$$\lambda_{n+1} = \mu \tan(\alpha_{Rotor}) + \frac{C_T}{2\sqrt{\mu^2 + \lambda_n^2}} \quad (20)$$

$$\varepsilon = \frac{\lambda_{n+1} - \lambda_n}{\lambda_{n+1}} \quad (21)$$

Let  $\alpha_{Rotor}$  [rad] be the angle between the air velocity passing through the rotor surface of the multi-rotor and the rotor surface. The drag ( $D$ ) is proportional to the fluid density  $\rho_{Air}$  and the flow velocity ( $v$ ) and is expressed by the following general mathematical model using the projected area ( $A$ ) and the drag coefficient ( $C_D$ ). The drag coefficient ( $D_{Body}$ ) applied to the FC during cruising is assumed to be the air density ( $\rho_{Air} = 1.225 \text{ kg/m}^3$ ), the drag coefficient of the aircraft ( $C_{D\_Body} = 0.6$  [52]),  $A_{Body} = 4 \text{ m}^2$ , and the airflow velocity as a constant value of the cruising speed ( $V_{Cruise}$ ) obtained from Eq. (19). To consider the total thrust of the rotor so as to oppose the combined force of the drag force ( $D$ ) and the gravity of the airframe,  $\alpha$  is calculated using the following formulas:

$$D = 0.5 \cdot \rho \cdot C_D \cdot A \cdot v^2 \quad (22)$$

$$\alpha = \tan^{-1}\left(\frac{D}{MTOW \cdot g}\right) \quad (23)$$

From the converged inflow rate ( $\lambda$ ), the inflow rate ( $\lambda_h$ ) during hovering ( $\lambda_f = \sqrt{0.5C_T}$ ), the rotor angles ( $\alpha_{Rotor}$ ), and the forward rate ( $\mu$ ) with respect to the airspeed, the power of one rotor during cruising is calculated from Eq. (21) [51], as follows:

$$\frac{P_{Cruise}}{P_{Hover}} = \frac{\mu}{\lambda_h} \tan(\alpha_{Rotor}) + \frac{\lambda_h}{\sqrt{\mu^2 + \lambda^2}} \quad (24)$$

(ii) Vectored Thrust/Lift + Cruise

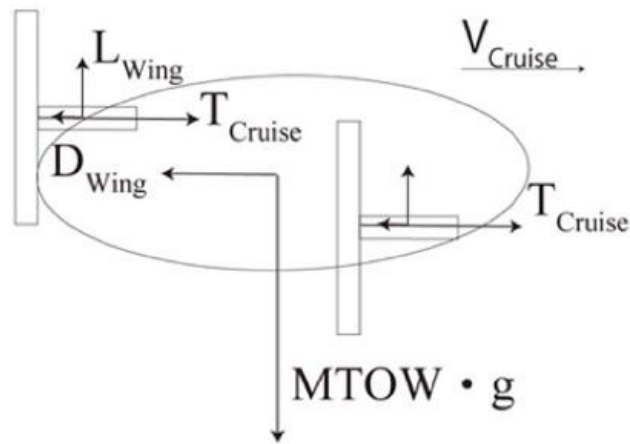


Figure 12 Equilibrium of the forces exerted on a vectored-thrust aircraft during cruising

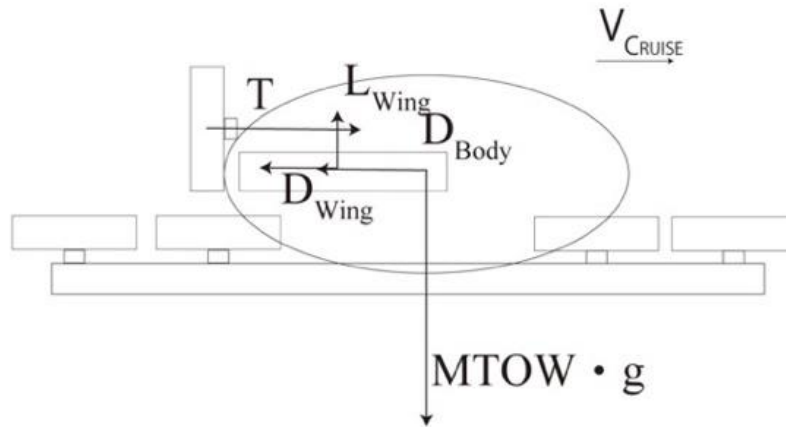


Figure 13 Equilibrium of the forces exerted on a lift + cruise aircraft during cruising

Figure 12 and Figure 13 illustrate the equilibrium of the forces exerted on a vectored-thrust and lift + cruise types during cruising. The gravity of the airframe is considered to be equal to the lift of the main wings, and the drag of the airframe is equal to the thrust of the rotors ( $T$ ). The thrust and power of the rotor are then calculated [53]. This study assumes that the center of gravity of the airframe and the aerodynamic center are equal, and the magnitude and direction of the thrust of each rotor are the same. The balance of the pitching moment, including the positioning of the fixed wing and the rotor, is not considered.

Eric. S (2019) and Christopher. C (2018) compare the performance of the conceptual design for urban air mobility (UAM). In the study, the thrust of the rotor is estimated from the equilibrium of the airframe gravity, thrust, drag, and lift forces. Meanwhile, the present study compares not only the amount of energy required during one flight but also the noise, downwash, and landing point area. However, in the winged types, it is assumed that the configuration of the rotors at the front of the main wing and the fuselage is such that the pitching moments of each axis are balanced. Based on these assumptions, the thrust of each phase is considered from the relationship between the gravity exerted on the FC and the lift and drag forces [54], [55].

The vectored-thrust type of aircraft cruises with eight rotors mounted on its main wings. Conversely, the lift + cruise type cruises with a single rotor at the rear of the fuselage. It is assumed that the gravity of the FC is supported by the lift force of the main wings. The drag coefficient ( $D_{\text{Body}}$ ) exerted on the FC during cruising is calculated using the values of air density ( $\rho_{\text{Air}} = 1.225 \text{ kg/m}^3$ ) and drag coefficient ( $C_{D\_Body} = 0.6$ ) [52] of the airframe under the assumption that the airspeed is a constant value at the cruising speed ( $V_{\text{Cruise}}$ ) (Eq. [22]). For the vectored-thrust type of aircraft,  $A_{\text{Body}} = 4 \text{ m}^2$ . In the case of the lift + cruise type, the author considers the drag force during cruise other than the fuselage and main wings, and  $A_{\text{Body}}$  is assumed to be 20% more than the vectored-thrust type after considering the project area of

the connectors between a fuselage and rotors. For the weight and wing area of the main wing, Mohammad's aircraft model is referenced [47].

$$\begin{cases} 8 \cdot T_{Cruise} = D_{Body} + D_{Wing} & \text{for vectored thrust} \\ 1 \cdot T_{Cruise} = D_{Body} + D_{Wing} & \text{for lift + cruise} \end{cases} \quad (25)$$

Thrust ( $T_{Cruise}$ ), cruise velocity ( $V_{Cruise}$ ), and induced velocity during cruise ( $v_{i\_Cruise}$ ) can be used to calculate the cruising output power of the two FC types. The induced velocity is expressed from Leishman's model due to the orthogonality of the velocity vectors of the air passing through the rotor surface and the rotor surface [51]:

$$P_{Cruise} = \begin{cases} 8 \cdot T_{Cruise} (v_{i_{Cruise}} + V_{Cruise}) & \text{for vectored thrust} \\ 1 \cdot T_{Cruise} (v_{i_{Cruise}} + V_{Cruise}) & \text{for lift + cruise} \end{cases} \quad (26)$$

$$v_{i_{Cruise}} = 0.5 \left( -V_{Cruise} + \sqrt{V_{Cruise}^2 + v_{Hover}^2} \right) \quad (27)$$

## (2) Noise

Here, noise comprises the rotational noise of  $N$  rotors (load noise and blade thickness noise), vortex noise, and blade-slap noise [38]. The engine sound is excluded from this research because the engine is excluded in an airframe mode. In this study, the blade tip speed does not include blade-slap noise because the constraint condition (Eq. [4]), in which the blade tip speed is

80% or lower of the speed of sound, is set considering the relative speed against the forward speed [52].  $p_{ref}$  is a reference sound pressure.

$$SPL = 10 \log \left[ N \left( \frac{p_{mL}^2 + p_{mT}^2}{p_{ref}^2} + p_{Vortex}^2 \right) \right] \quad (28)$$

Rotational noise is expressed by the sound pressure ( $p_{mL}$ ) of the load sound and the sound pressure ( $p_{mT}$ ) of the wing thickness.  $m_{Harmony}$  is the harmonic number, and  $B_{Rotor}$  is the number of rotor blades.  $\Omega$  is the rotor angular velocity,  $V_{Tip, Hover}$  is the blade tip velocity, and  $N (= 8)$  is the number of rotors.  $a$  is the speed of sound.  $\Delta S$  is the distance between the rotor and the observer (Figure 14), and  $Q$  is the rotor torque.  $R_e$  is the effective rotor radius ( $= 0.8 \cdot d/2$ ),  $J_{mB}()$  is a first-class Bessel function, and  $c$  is the length of the rotor blade chord.  $t$  is the thickness of the rotor blade.  $\theta_{Observer}$  is an angle determined by the positional relationship between the observer and the rotor, as shown in Figure 14.

$$p_{mL} = \frac{m_{Harmony} B_{Rotor} \Omega}{2\sqrt{2}\pi a (\Delta S)} \left[ T \cos(\theta_{Observer}) - Q \frac{a}{\Omega R_e^2} \right] J_{mB} \left( \frac{m_{Harmony} B_{Rotor} \Omega}{a} R_e \sin(\theta_{Observer}) \right) \quad (29)$$

$$p_{mT} = \frac{-\rho (m_{Harmony} B_{Rotor} \Omega)^2 B_{Rotor}}{3\sqrt{2}\pi (\Delta S)} c t_{Rotor} R_e J_{mB} \left( \frac{m_{Harmony} B_{Rotor} \Omega}{a} R_e \sin(\theta_{Observer}) \right) \quad (30)$$

Equation [28] is an expression of vortex noise.  $T/A$  is the disc loading on the rotating surface of the rotor,  $s$  is the rigidity of the rotor, and  $K_2$  is a

constant at  $0.4258 \text{ s}^3/\text{m}^3$  [47]. With reference to [47] and [51], the value of solidity ( $s$ ) is 0.1.  $A$  is the rotor area.

$$p_{vortex} = K_2 \frac{V_{Tip,Hover}}{\rho(d_{Observer})} \sqrt{\frac{NT}{s} \left(\frac{T}{A}\right)} \quad (31)$$

$d_{Observer}$  is the distance between the observer and the rotors. Equation (12) is used to calculate the blade tip speed of the rotor. The gravity of the FC is supported by the thrust of the rotors. Table 1 summarizes the calculation specifications. The torque coefficient ( $C_Q$ ) is identical to the power coefficient ( $C_P$ ) of the rotor. Equation (29) is used to calculate the torque of the rotor:

$$Q = \frac{1}{2} \rho (V_{Tip,Hover})^2 \left( \pi \left( \frac{d}{2} \right)^3 \right) C_Q \quad (32)$$

Figure 14 shows the positional relationship between the observer and the rotor. The interview with an in-flight doctor revealed that a convenience store's parking lot should be considered as a landing site since the location could serve as a rendezvous point. Considering the impact on both the airfield and the neighborhood,  $d_{Observer} = 14.141 \text{ m}$  is considered in this study ( $r = h = 10 \text{ m}$ ).

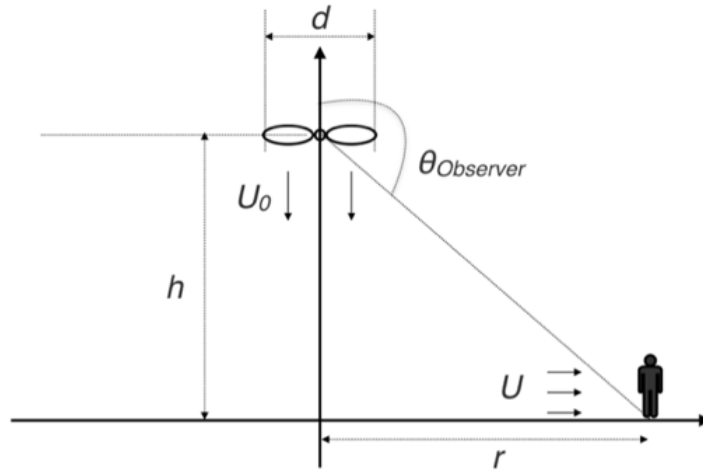


Figure 14 Positional relationship of the rotors and the observer during hovering

Table 2 Calculation specifications of noise

Variable/Constant	Value	Unit
$\rho_{Air}$	1.225	kg/m <sup>3</sup>
$d_{Observer}$	14.141	m
$N$	8	
$m$	3	
$B$	2	
$a$	1225	km/h
$\theta_{Observer}$	135	°

$R_e$	$0.8 \cdot d/2$	m
$p_{\text{ref}}$	$2.0 \times 10^{-5}$	Pa
$s$	0.1	
$c$	$\pi(d/2) s / B$	m
$t$	$0.12 \cdot c$	m

### (3) Downwash

Next, the study considers the wind speed of the downwash when hovering. The wind speed under the rotor is determined from the law of the conservation of momentum [56], [57], [58], as follows: It is assumed that the gravity of the airframe is supported by one virtual rotor with an area of  $N \cdot \pi (d / 2)^2$ . Downwash interactions from each rotor are not considered. However, as in the previous study [57], the error between the measured value of the blowdown wind of the drone and the predicted value by the CFD simulation is around 7–11%. Since this research focuses mainly on conceptual design, a detailed analysis for pursuing accuracy is not considered necessary [59].

The downwash speed received by the observer can be modeled empirically by the diameter ( $d$ ) of the rotor and the horizontal distance ( $r = 10$  m) from the center of the rotor to the observer (see Figure 14) [58].

$$U_0 = \sqrt{\frac{MTOW \cdot g}{2\rho N \left( \pi \left( \frac{d}{2} \right)^2 \right)}} \quad (33)$$

$$U = \frac{1.03}{\frac{r}{d}} U_0 \quad (34)$$

#### (4) Landing Area

The landing point area is estimated to be the value of the multiplication of the maximum horizontal length and width of the FC as viewed from above. It is difficult to obtain an accurate estimation of how aircraft configurations on takeoff and landing are affected by pilot control (based on flying abilities) and the weather conditions at the landing point. The area margin is set to 20% irrespective of the configuration [60].

$$H = \begin{cases} 1.44 \cdot (2d + 2) \left( \frac{8}{\pi} + 2d \right) & \text{for multi - rotor} \\ 1.44 \cdot (2w_{span} + d + 2) \left( \frac{8}{\pi} + d \right) & \text{for vectored thrust} \\ 1.44 \cdot (2w_{span} + 2) \left( \frac{2w_{span}}{7} + 4d \right) & \text{for lift + cruise} \end{cases} \quad (35)$$

Figures. 15–17 show the established models to obtain the area of the landing site. The configuration of the fuselage is an ellipse with a major axis of  $4/\pi$  m and a minor axis of 1 m.

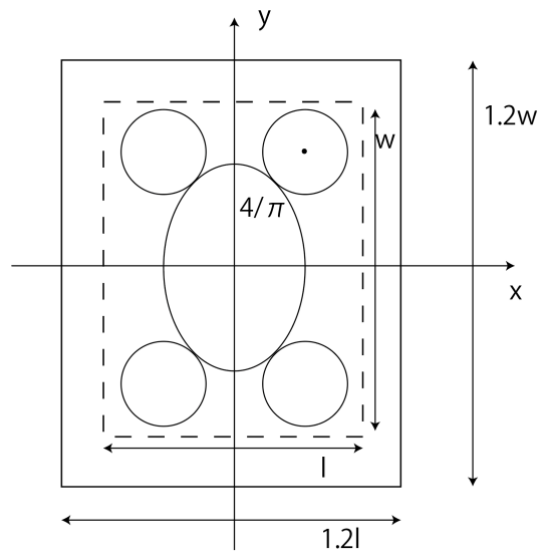


Figure 15 Landing area model of the multi-rotor type

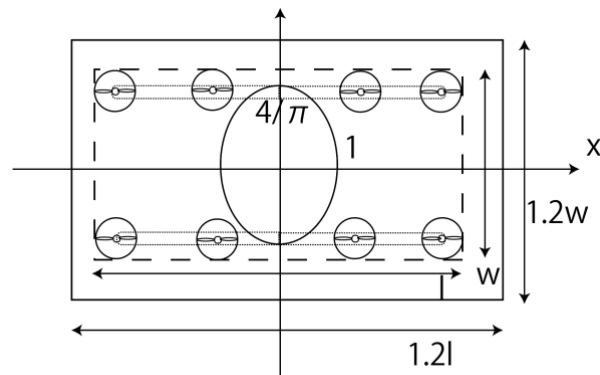


Figure 16 Landing area model of the vectored-thrust type

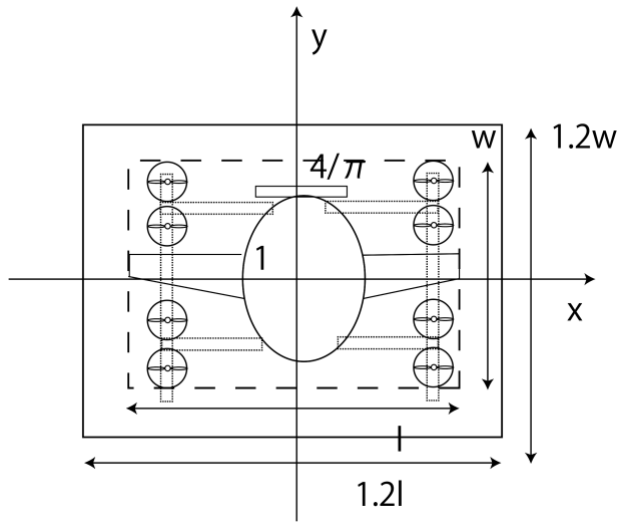


Figure 17 Landing area model of the lift + cruise type

### **3.2.5 Determining the Weighting**

The weighting vector ( $\vec{w}$ ) is critical for solving the optimization problem. In this study, these values were determined using stakeholder interviews with flight doctors, operators, pilots, and authors.

## **3.3 Result and Discussion**

### **3.3.1 Requirement Analysis Result and Mission**

#### **Profile**

From the interviews with the HEMS stakeholders, the key requirements for medical emergencies are listed by the interviewee, as follows:

(1) Flight Doctor

- In the initial stage, it is sufficient to dispatch pilots and doctors in FCs, since the main purpose of introducing an FC is to reduce the travel time between the doctor and the patient.

- The patient should be reached within 15 min. Considering the golden hour curve, it is desirable to reduce the time between request and patient contact by as much as possible [61].

- Noise from an FC for medical emergencies should be reduced to improve social acceptance.

(2) Helicopter Pilot

- The FC lands after the fire department confirm the safety of the landing point. It is desirable to reduce the downwash that causes brownout, which is an in-flight visibility restriction due to airborne dust or sand [62].

### (3) Operating Company

- The duration of one flight is about 30–60 min across one or two missions, i.e., one mission takes at least 30 min. Since continuous dispatch is possible, it is essential that batteries can be either charged in flight or replaced quickly.

- Currently, there is no time to warm up a helicopter engine before takeoff. Eliminating this could reduce takeoff time.

- It takes 15 min for a one-way flight.

- In the round trip between the base hospital and the rendezvous point, historical operational data reveal the round-trip distance to be  $49.18 \pm 79.72$  km. This is the average round-trip distance plus the standard deviation multiplied 3 times for 438 flights per year.

- A FC operates at an altitude of 150–1,000 m with a cruising height of 300 m.

According to German Parliament [42], “*Sustainability is the concept of robust future development in the ecological, economic and social dimension of human existence.*” Based on the stakeholder interviews of the HEMS, the author considers that noise, a downwash, and a landing area size should be

included in the objective functions because a sustainable system design of a FC should not only the economical but also social and environmental parameters.

Moreover, from these interviews, a mission profile for FCs for deployment in medical emergencies can be created. The arrival time to the patient is 1 min for hovering time ( $t_{\text{hover}}$ ), 2 min for VTOL ( $t_{\text{climb}}$ ,  $t_{\text{down}}$ ), plus 12 min for cruising time ( $t_{\text{cruise}}$ ), making a total of 15 min (30 min for the round trip). The distance of a round trip is 50 km at a cruising speed of 150 km/h and a cruising altitude of 300 m. There are two passengers (a medical doctor and a pilot).

### 3.3.2 Weighting for Optimization

Based on the results of the interviews to determine the weighting (priority) of the four objective functions, the resulting weights ( $\vec{w}$ ) are provided in Eq. (32) under the condition which the weight sum is to be 1.0 for normalization. Assigning different numerical values to the weighting vector with a margin should be also discussed in future research.

The author sets  $w_1$  to be 0.4. It is essential for each flight to have sufficient energy for the entire round trip. Without the enough energy for flight, social and environmental parameters such as noise are not worth discussing. Therefore the amount of energy is given top priority in the four objective functions.

The author sets  $w_2$  to be 0.1. In terms of noise, HEMS aircraft rarely land at the same landing point repeatedly. Noise can be tolerated due to the emergency's potential life-threatening consequences. Therefore, noise is the lowest priority in the four objective functions.

The author set  $w_3$  to be 0.2. In terms of landing area size, vehicle miniaturization increases the probability to land on a landing point. When smaller landing points can be selected in operation, the number of landing points can increase, which means faster response times. Although a downwash effects landing stability of a FC, a pilot cannot decide to land on

the ground when the size of a landing point is too small to land. Therefore, the second priority is a landing area size in the four objective functions.

The author set  $w_4$  to be 0.3. In cases of a strong downwash, according to a helicopter pilot, dust (brownout) is generated at the landing point, creating difficult landing conditions. Including the ground effect, a strong downwash makes landing unstable. As mentioned above, because ensuring the landing size before landing inside a generated downwash is more significant than the downwash. Therefore, the third priority is a downwash speed in the four objective functions.

$$\vec{w} = \begin{bmatrix} w_1 \\ w_2 \\ w_3 \\ w_4 \end{bmatrix} = \begin{bmatrix} 0.4 \\ 0.1 \\ 0.2 \\ 0.3 \end{bmatrix} \quad (36)$$

### 3.3.3 Optimization Result

Tables 2–4 summarize the results of the design variables, objective functions, and constraints obtained by optimizing the multi-rotor, vectored-thrust, and lift + cruise types. For the blade tip speed, which is a constraint condition, the maximum value during operation is selected. In each case, the optimum solution is found within the constraints.

#### (1) Result for Each Aircraft Type

Table 3 Optimization Results for the Multi-rotor Type

<b>Design Variable</b>	<b>Value</b>	<b>Unit</b>
$d$	1.104	m
$C_{Thrust}$	0.0250	
Weight	Value	Unit
$MTOW$	803.386	kg
(Breakdown)		
$W_{Empty\_weight}$	377.290	kg
$W_{Battery}$	301.238	kg

$W_{\text{Payload}}$	180	kg
$W_{\text{Rotor\_weight}}$	11.647	kg
$W_{\text{Fuselage}}$	189.528	kg
$W_{\text{Motor}}$	148.203	kg
$W_{\text{Landing Gear}}$	27.912	kg
$W_{\text{Avionics}}$	45.186	kg
<b>Objective Functions</b>	<b>Value</b>	<b>Unit</b>
$\varphi$	70.800	
$E$	121.786	kWh
$Noise$	91.413	dB
$U$	9.885	m/s
$H$	39.853	m <sup>2</sup>
<b>Constraint</b>	<b>Value</b>	<b>Unit</b>
$V_{\text{Tip}}$	202.695	m/s

Table 4 Optimization Results for the Vectored-thrust Type

<b>Design Variable</b>	<b>Value</b>	<b>Unit</b>
$d$	0.931	m
$C_{Thrust}$	0.0250	
<b>Weight</b>	<b>Value</b>	<b>Unit</b>
$MTOW$	803.429	kg
<b>(Breakdown)</b>		
$W_{Empty\_weight}$	355.619	kg
$W_{Battery}$	267.810	kg
$W_{Payload}$	180	kg
$W_{Rotor\_weight}$	8.586	kg
$W_{Wing}$	26.423	kg
$W_{Fuselage}$	189.528	kg
$W_{Motor}$	67.573	kg
$W_{Landing\ Gear}$	23.337	kg
$W_{Avionics}$	40.171	kg
<b>Objective Functions</b>	<b>Value</b>	<b>Unit</b>
$\varphi$	57.389	
$E$	78.302	kWh

<i>Noise</i>	95.176	dB
<i>U</i>	4.660	m/s
<i>H</i>	52.059	m <sup>2</sup>
<b>Constraint</b>	<b>Value</b>	<b>Unit</b>
<i>V</i> <sub>Tip</sub>	269.707	m/s

Table 5 Optimization Results for the Lift + Cruise Type

<b>Design Variable</b>	<b>Value</b>	<b>Unit</b>
$d$	0.745	m
$d_{back}$	3.551	m
$C_{Thrust}$	0.0250	
<b>Weight</b>	<b>Value</b>	<b>Unit</b>
$MTOW$	774.795	kg
<b>(Breakdown)</b>		
$W_{Empty\_weight}$	297.791	kg
$W_{Battery}$	258.266	kg
$W_{Payload}$	180	kg
$W_{Rotor\_weight}$	5.797	kg
$W_{Wing}$	21.429	kg
$W_{Fuselage}$	189.528	kg
$W_{Motor}$	59.006	kg
$W_{Landing\ Gear}$	22.031	kg
$W_{Avionics}$	38.739	kg
<b>Objective Functions</b>	<b>Value</b>	<b>Unit</b>
$\varphi$	73.188	

$E$	98.935	kWh
$Noise$	98.383	dB
$U$	4.577	m/s
$H$	76.201	m <sup>2</sup>
Constraint	Value	Unit
$V_{Tip}$	262.563	m/s

## (2) Accuracy in Comparing Each Vehicle Configuration

The calculated amount of energy is compared with previous studies for validation, and the accuracy of the data is compared with the energy of the multi-rotor type. Priyank (2019) simulated the same multi-rotor model with eight rotors, which cruises with a rotor diameter of 1.6 m and a weight of 240 kg for 1 min at a constant cruise speed. The energy consumption per minute is 0.756 kWh [63]. Conversely, when this study's model is used under the same conditions, the energy consumption per minute during cruising is 0.742 kWh with an error of 1.82%. Therefore, it is considered that the model in this study has comparable validity. Although this study has compared the amount of energy of other aircraft types in terms of noise, downwind, and landing point area, no comparable data have yet been found.

### (3) Battery Weight Energy Density

Table 5 compares the weight energy density of the battery system ( $BED$  [Wh/kg]), which is obtained from the required energy amount ( $E$ ), as follows:

$$BED = \frac{E}{W_{Battery}} \quad (37)$$

In existing electric vehicles, the energy weight density of installed batteries is between 150 and 200 Wh/kg [64], which is unfeasible from an energy perspective for any type of FC. From the perspective of the battery, with a fixed-wing aircraft, it is considered that the vectored-thrust type of aircraft is more feasible than the other two types. However, considering the hovering standby time before landing, the reserve energy to be loaded for a safe and affordable flight, and the battery's deterioration, it is suggested that a battery with a high energy density of 300 Wh/kg or more is required. Based on the assumption of an advancement in battery technology for electric vehicles as predicted by Japan's New Energy and Industrial Technology Development Organization, the operation of electric multi-rotor aircraft will be realized after the latter half of the 2020s [65].

Table 6 Battery energy density comparison between the three aircraft types

Multi-rotor	404.287 Wh/kg
Vectored Thrust	292.403 Wh/kg
Lift + cruise	383.074 Wh/kg

Regarding noise at a flight test level [66], the distance to the observer is set to 150 m, considering distance attenuation. The noise levels of the multi-rotor, vectored-thrust, and lift + cruise types are 70.901, 74.664, and 77.851 dB, respectively, which are lower than the standard for helicopter noise [67]. However, for an observer closer than 50 m, the noise will sound as loud as a train [67]. A comparison between the rotational noise and the vortex noise produces  $(p_{mL}^2 + p_{mT}^2)/(p_{ref}^2) \gg p_{vortex}^2$ , which represents a difference of four digits. Therefore, it is confirmed that the rotational noise due to the noises of the load and the blade pressure will be dominant.

The downwash is observed on the ground at a maximum of about 5 m/s. The landing area is up to 127 m<sup>2</sup>, although it is distributed by the rotors and the rotor area. In MD 902 [68], which is also used for the HEMS, the total length and width are 12.37 and 10.3 m, respectively, and the landing zone area must be at least 183.47 m<sup>2</sup>. This is expected to be about 25% smaller than for a conventional helicopter, which will allow FCs to land in tighter spaces.

### 3.3.4 Parameter Study

Next, the flight distance of the mission profile is changed to the average value + standard deviation of the round-trip distance, the average value + 2 × standard deviation, and the average value + 3 × standard deviation to perform the optimization for the parameter study. When considering the distribution of the round-trip operational distance of the HEMS in 1 year as a normal distribution, 50% of the flights (mean round-trip distance), 84% (mean round-trip distance + 1 × standard deviation), 97.5% (round-trip distance + 2 × standard deviation), and 99.85% (mean round trip + 3 × standard deviation) are compared for discussing the feasibility of a FC. This subsection discusses only the energy required for one flight and the battery's weight energy density due to the prioritization of these parameters.

Tables 6–8 present the results of the parameter study with modifications of the round-trip distance and cruising speed. The cruising speed is set to enable the round-trip distance to be covered in 24 min. The blank part (-) indicates no optimum solution result due to the blade tip velocity exceeding the constraint condition. As the cruising speed of the FC increases, the thrust against the drag force also increases. Therefore, the blade tip speed of the rotor increases the constraint condition in proportion to the thrust, and the optimum value cannot be obtained.

Even if the distance of the round trip is extended, the cruising speed must be increased because of the requirement to reach the target point within 15 min. Therefore, the amount of energy in the battery mounted onto the airframe and its weight density both increase. Existing batteries cannot attain the energy density values required, and the development of batteries with high weight energy densities is critical to the development of FCs. Additionally, an increase in cruising speed causes the lift of the main wing to increase, resulting in a decrease in the required main wing. Consequently, the airframe becomes slightly lighter. As a result, it is possible to fly a round trip, although it requires the amount of energy for a long-distance flight, resulting in a large amount of energy per kilogram of battery.

Table 7 Parameter Study Results for the Multi-rotor

Round-Trip Distance[km]	Cruise Velocity [km/h]	$d$ [m]	$MTOW$ [kg]	$E$ [kWh]	$BED$ [Wh/kg]
50	150	1.460	903.713	121.786	404.287
75	200	-	-	-	-
101.52	260	-	-	-	-
128.89	320	-	-	-	-

Table 8 Parameter Study Result for the Vectored-Thrust Type

Round-Trip Distance[km]	Cruise Velocity [km/h]	$d$ [m]	$MTOW$ [kg]	$E$ [kWh]	$BED$ [Wh/kg]
50	150	1.104	803.386	78.304	292.403
75	200	1.111	774.190	150.372	582.694
101.52	260	-	-	-	-
128.89	320	-	-	-	-

Table 9 Parameter Study Results for the Lift + Cruise Type

Round-Trip Distance[k m]	Cruise Velocity [km/h]	$d$ [m]	$MTOW$ [kg]	$E$ [kWh]	$BED$ [Wh/kg]
50	150	0.731	774.194	99.641	386.107
75	200	0.855	759.427	180.249	712.047
101.52	260	-	-	-	-
128.89	320	-	-	-	-

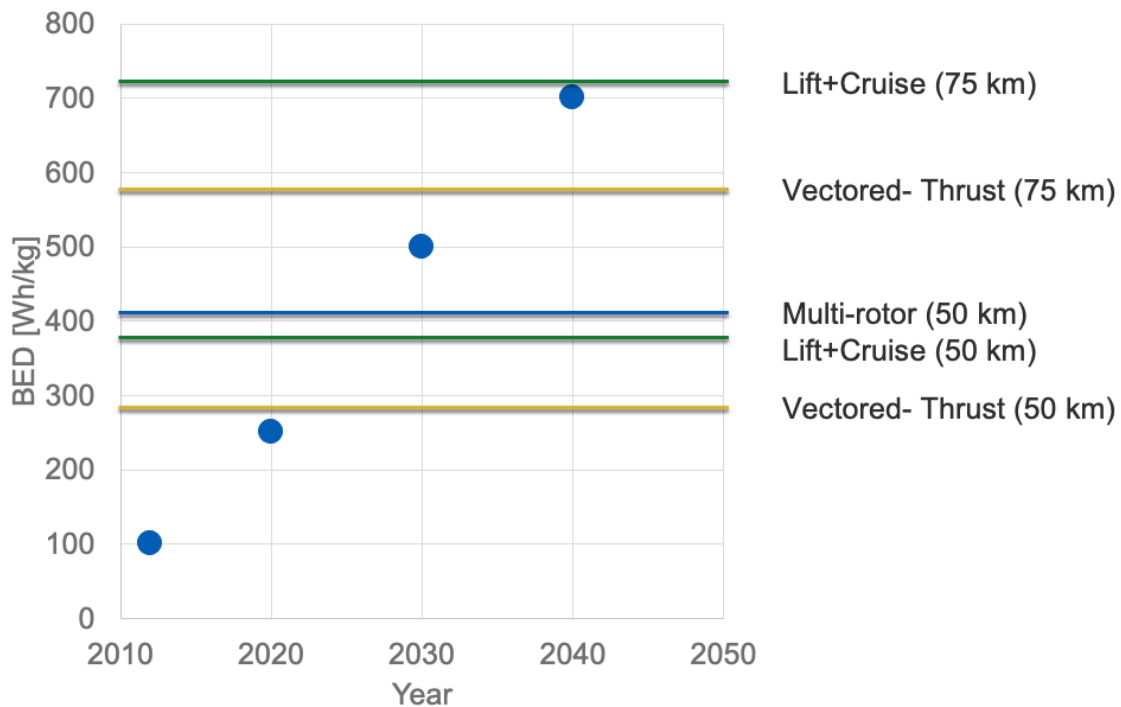


Figure 18 Comparison between the NEDO Battery Roadmap and the Results [65]

Figure 18 shows the comparison between the results and the NEDO rechargeable battery roadmap. The circle plots in the figure are expected battery specifications in Wh/kg in each year. The line plots in the figure are the results of this parameter study. The vehicle type which is implemented earlier is estimated to be a vectored-thrust. In this study, when a vehicle ascends and descends, it moves vertically. Ascending and descending obliquely, a Vectored-Thrust and a Lift+Cruise can fly more efficiently in terms of energy although this decreases a merit of a VTOL function.

### 3.4 Conclusion

This study verified the applicability of multi-rotor, vectored-thrust, and lift + cruise types of FCs (UAM) for use in medical emergencies. From the system design perspective, a requirement analysis for application in medical emergencies was conducted to define a mission profile. A system optimization was conducted based on a simulation of a FC airframe in the mission profile with the following conditions: arrival time to the patient is 1 min for hovering + 2 min for VTOL + 15 min for cruising time. Thus, a round trip takes 30 min. The round trip is 50 km with a cruising speed of 150 km/h. The cruising altitude is 300 m, and there are two passengers (a medical doctor and a pilot).

Tables 2–4 and Tables 6–8 present the results of the design variables, objective functions, and constraints. Based on the above mission profile, the vectored-thrust type produced highly feasible results. From the perspective of the battery weight energy density, a value of at least 293 Wh/kg is required, which is considered to be difficult to achieve with existing battery technology.

In future research, it will be necessary to evaluate CO<sub>2</sub> in terms of life cycle analyses [43]. Additionally, the cost of each type of FC and its

operating expenses should be assessed with higher accuracy to determine the feasibility of FCs from the viewpoint of sustainability.



# **Chapter 4**

## **TOLA Design Analysis**

## 4.1 Problem Definition

In particular, for the safe operation of air taxis over cities, it is necessary to consider the impact on passengers, TOLAs, and aircraft due to emergency landings at TOLAs in case of aircraft trouble [69][70]. In particular, multicopter type FCs do not have glide or auto-rotation functions, and only parachutes are currently available to mitigate the impact of a collision. In the past, there have been studies on emergency landing methods for helicopters, airplanes, and drones using parachutes, but there is no similar research on FCs [71] [72] [73] [74]. In addition, although there are studies that have analyzed the impact load when an aircraft or helicopter crashes into a take-off or landing area while gliding or autorotating, there are no studies that have investigated the impact load when a FC makes an emergency landing on a take-off or landing area [75] [76] [77] [78]. ICAO has published design criteria for heliport construction, but there is no study on the TOLAs for flying vehicles to calculate the design criteria [79]. The ICAO has published the design criteria for heliport construction, but there is no study on the TOLA of flying vehicles to calculate the design criteria, and there is no study from the viewpoint of system design that considers the impact of landing on the TOLA, airframe system, and passengers.

There are two types of heliports: public heliports and emergency TOLAs. The first type of TOLA for air taxi operations in Tokyo is the existing heliport. In addition, there are about 80 emergency TOLAs in Tokyo for firefighting helicopters to take off and land in the event of a fire or other emergency. However, compared to heliports, it is unclear whether emergency TOLAs, which have less stringent installation standards set by each municipality, have the capacity to withstand the take-off and landing of FCs [80]. In addition, when taking off and landing from the rooftop of a high-rise building, there is a possibility that the FC will be exposed to danger due to the building wind in the sky. Therefore, it is an issue to analyze the impact of a soft landing at an existing heliport when the FC loses control during the hovering phase of takeoff and landing.

The purpose of this study is to calculate the effects on the occupants and the aircraft and the required specifications of the TOLA design strength for the safety design of both the TOLA and the aircraft by simulating the impact loads of a FC in the case of loss of control due to aircraft failure. When considering the design load of the TOLA, it is necessary to consider not only the instantaneous impact load in a crash, but also the probability of failure due to repeated landings in daily use.

Parachutes are mainly considered as a shock mitigation method. In addition, one application of the FC that has not been implemented in the society is defined, and the mechanical study at the conceptual level that

simplifies the airframe model first is kept while many airframes are under development. After identifying the airframe model of the FC, it is one of the future researches to improve the accuracy of the detailed analysis of the impact load from the detailed model of the airframe, mechanical properties and boundary conditions.

Section 1 gives an overall overview of this study; Section 3.2 describes the research methodology; Section 3.3 presents the results and discussion of the above four computational simulations; Section 3.4 concludes with a conclusion. Finally, in section 4, the conclusion of this study is attached as a conclusion.

## 4.2 Method

### 4.2.1 Method Overview

The first figure is a conceptual diagram of the simulation of impact loads due to the landing of a FC as an overview of the research method. On the left are inputs such as specifications of the aircraft and parachute, and flight altitude. The output is the impact load on the TOLA, the impact force and acceleration on the fuselage and passengers, and the destruction probability of the TOLA. The upper part is constraint conditions. The bottom is a means (enabler) to realize the model.

Stakeholders include operators, TOLA managers, and passengers. All of them want to reduce the damage to the aircraft, the TOLA, and the passengers by safe landing. Impact load simulation is performed under these constraints.

This study consists of four simulations. The details of the simulations are described in 3.2.1-3.2.4. It consists of the following four simulations.

- 1) Firstly, this study calculates the floor strength that a TOLA for a FC should have by calculating the impact load when the aircraft falls from the existing ICAO standard of 0.66 m (Section 2.1) [79].

- 2) Next, the results are compared with the design criteria of existing heliports and emergency TOLAs in the cases with and without mushroom-shaped parachutes. At the same time, a parameter study is performed by

changing the diameter of the parachute, the altitude at which the parachute opens and the maximum take-off weight of the FC (Section 3.2.2).

3) Next, the author considers the force applied to the fuselage and the landing gear of the aircraft immediately after landing, and calculate the impact force that should be absorbed by the crushable of the aircraft, the seat and the airbag from the force to the fuselage. In addition, in order to consider the effect on the human body, the acceleration applied to that fuselage is calculated and the injury criteria of the acceleration on the human body is compared (Section 3.2.3).

4) Finally, the events that repeatedly land FCs and destroy the TOLAs when impact loads are generated are modeled as Poisson processes and their destruction probabilities are calculated (Section 3.2.4). Since there are no records of FC operations yet, the frequency of air taxi operations is estimated from taxi operation records.

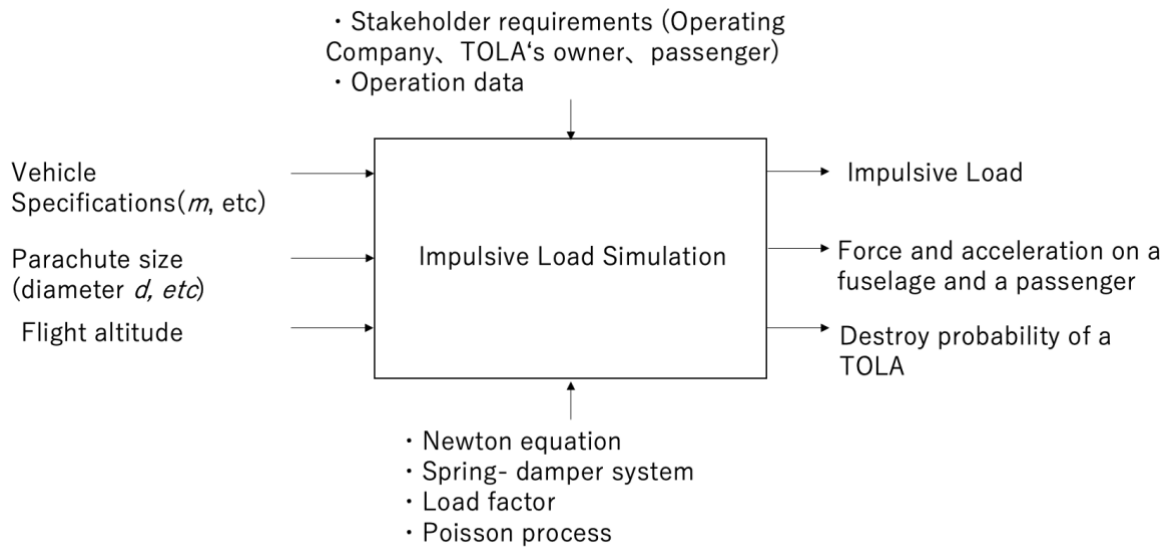


Figure 19 Conceptual Diagram of Impulsive Load Simulation

## 4.2.2 Impulsive Load Model

### 4.2.2.1 TOLA Floor Strength

Use  $z = 0.66$  m because the ICAO Heliport Manual includes a criterion that the TOLA for rotary wing aircraft must be able to withstand a drop impact from a height of 0.66 m [47]. The aerodynamic drag force is neglected for the low altitude drop. From the law of conservation of mechanical energy, the author considers the velocity just before the crash.

$$mgz = 0.5 \cdot mv_z^2 \quad (38)$$

Based on the criteria of the design load of the Architectural Institute of Japan (AIJ), the impact load is larger than the case of plastic deformation of the landing site and the aircraft, and a hard impact is assumed in this study which gives a result on the safe side compared with the actual impact load [81]. The author assumes that the time  $\Delta t$  from the landing site to the velocity of 0 m is 0.1 - 0.2 s. In reference [76], which deals with the impact load of a car traveling at 20 km/h,  $\Delta t$  is given as 0.1. Given that the speed of the aircraft at the time of impact is 10-20 km/h, the upper limit of 0.2, the lower limit of 0.1 and the intermediate value of 0.15 are given as  $\Delta t$ . In addition, the impact load waveform is assumed to be triangularly distributed [82]. From

the force product and the momentum conservation law, the force  $F_{\text{Vertiport}}$  ( $=F_{\text{FC}}$ ) is added to the ground point of landing as shown in equation (2).

$$F_{\text{FC}}\Delta t = \Delta m v_z \quad (39)$$

#### 4.2.2.2 Impulsive Load on a TOLA of a FC

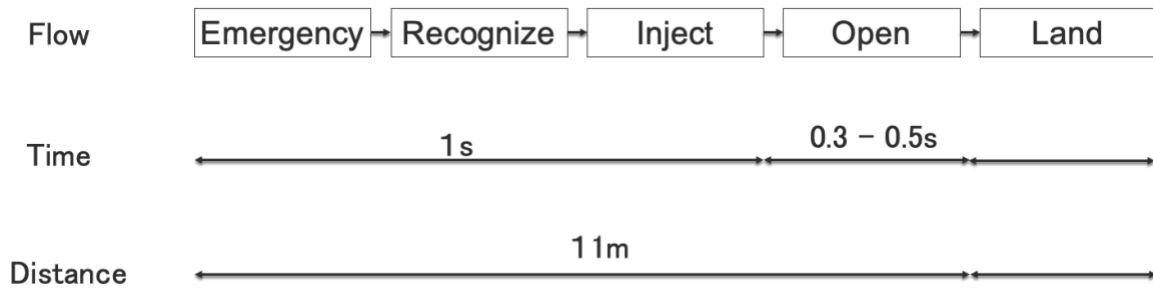


Figure 20 Functional Flow of a Ballistic Parachute System

Figure 20 shows the flow of a parachute system after an emergency event happens. After an emergency event happens, a parachute function to decrease the vehicle velocity starts in 1.5 seconds. This data come from the interview which the author asked a parachute manufacturer a parachute functional process. In the 1.5 seconds, the altitude of a vehicle decreases by eleven meters including vehicle drags. Also this testimony is verified by the video which a eVTOL manufacturer “opener” experiments a parachute test in about 300 meters altitude [83]. In the video, a FC vehicle whose empty weight is 155.582 kg falls with 20 seconds from 120 m to the ground. The open time of a parachute is estimated to be 2 seconds in the video. When a heavier vehicle has 1000kg MTOW, a parachute will open earlier because the initial falling

time can be decided by the MTOW and an umbrella of a parachute is filled with the air earlier.

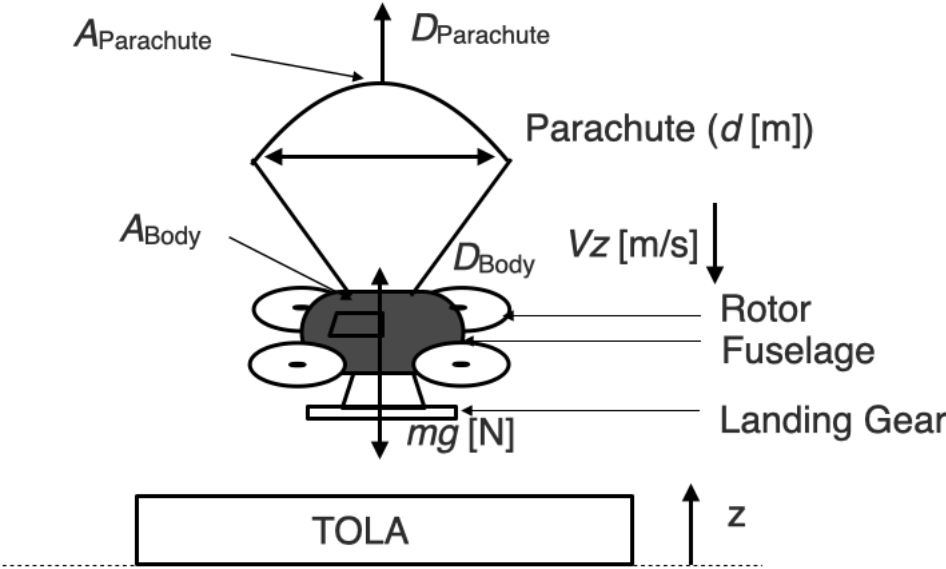


Figure 21 Mechanical Model of an Airframe and a Parachute

The second figure is a model of the system of a falling mushroom-shaped parachute and an FC. Let  $\underline{m}$  be the total weight of the FC. Let  $z$  be the distance from the landing site to the aircraft.

The aircraft and the parachute are subjected to drag force  $D_{Body}$  and  $D_{Parachute}$  force respectively. To assume an emergency landing, the author assumes that the rotor is not functioning and  $D_{Body}$  includes the drag force of

the rotor. The equation of motion of the aircraft and parachute in the  $z$ -direction is equation (3). Assuming an FC with two to four passengers, the mass  $m$  is 1000 kg. The drag force  $D$  is proportional to the square of the airspeed, where  $\rho$  is the air density,  $A$  is the projected area, and  $C_D$  is the drag coefficient. The calculation parameters are summarized in Table 10. The parachute is considered as a mushroom shape with a length of diameter  $d$ . The projected area  $A_{\text{Parachute}}$  is  $\pi (d/2)^2$ . The magnitude of the impact load is given by equation (2).

$$m\ddot{z} = -mg + D_{\text{Body}} + D_{\text{Parachute}} \quad (40)$$

$$D = 0.5 \cdot \rho \cdot C_D \cdot A \cdot v_z^2 \quad (41)$$

Table 10 Constants in Equation (3) and (4)

Constant	Value	Unit	Reference
$m$	1000	kg	
$C_{D\_Body}$	1.2		[4]
$C_{D\_Parachute}$	0.83		[74]
$A_{Body}$	6.4	m <sup>2</sup>	[4]
$A_{Parachute}$	$\pi(d/2)^2$	m <sup>2</sup>	[74]
$d$	10	m	[74]
$g$	9.80655	m/s <sup>2</sup>	SI
$\rho$	1.225	kg/m <sup>3</sup>	ISO

### 4.2.2.3 Mechanical Model of a FC's Body

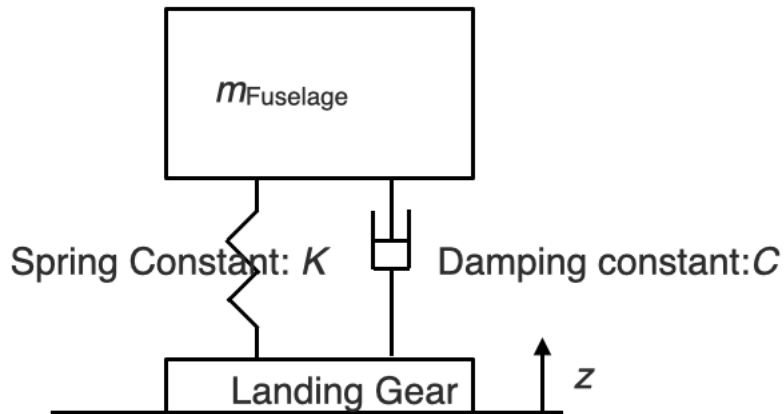


Figure 22 Springer Damper Model of One-Mass System

For the safety design of a FC, in order to consider how much impact a passenger may be subjected to introduce the damping vibration model of the one mass system of the airframe + landing gear at the moment of landing (Fig.3). Immediately after the crash, the landing gear is glued to the ground, and the deceleration by the parachute is considered to be invalid. Consider a spring constant  $K$  ( $=100 \text{ kN} \cdot \text{m}$ ) and a damping coefficient  $C$  ( $=284.60 \text{ N} \cdot \text{s/m}$ ) [76]. Since the dominant design of the FC is not clear and the composite material cannot be identified at present, the author consider a simplified model in which  $K$  and  $C$  are constant values.

According to the criteria of design loads of the Architectural Institute of Japan in reference [77], when considering the collision between a rotorcraft

such as a FC or a helicopter and a building, the aircraft has a crushable zone and the building is assumed to be rigid enough. Since the structure including the crushable zone and the collision load data of the FC are not found yet, the general equivalent 1-DOF model is used for the evaluation of the collision load. In addition, the elastic deformation in the spring-damper system has larger values of impact loads to both the passenger and the landing site, and the physical effects on the passenger and the landing site are larger. In order to focus on the results of impact loads on the safer side, this study focuses only on the elastic deformation [77][78]. The equation of motion of this one-mass system is expressed by equations (5) and (6).

$$m_{fuselage}\ddot{z} = -m_{fuselage}g + K \cdot z + C \cdot \dot{z} \quad (42)$$

$$z = B \exp(-\zeta \omega_0 t) \cos(\omega_0 \sqrt{1 - \zeta^2} t - \alpha) \quad (43)$$

By solving the equation of motion, the author can obtain a damped vibration solution with amplitude  $B$  (Eq. 7), initial phase  $\alpha$  at  $t=0$  (Eq. 8), damping ratio  $\zeta$  (Eq. 10), and dimensionless initial velocity  $\delta$  ( $=v_{z0} / z_0 \omega_0$ ).  $\omega_0$  is the natural angular frequency, which can be calculated from Equation 9. The values of each constant are summarized in Table 11 [81]. Since the first half cycle of the damped vibration has the highest force, the author considers the force and acceleration only in the first half cycle.

$$B = z_0 \sqrt{1 + \left( \frac{\delta + \zeta}{\sqrt{1 - \zeta^2}} \right)^2} \quad (44)$$

$$\alpha = -\tan^{-1}\left(-\frac{\delta + \zeta}{\sqrt{1 - \zeta^2}}\right) \quad (45)$$

$$\omega_0 = \sqrt{\frac{K}{m_{fuselage}}} \quad (46)$$

$$\zeta = \frac{C}{2\sqrt{m_{fuselage}K}} \quad (47)$$

Table 11 Constants for the Spring Damper Model

Value	Value	Unit
$m_{Fuselage}$	900	kg
$K$	100	kN · m
$C$	284.60	N · s/m
$\zeta$	0.03	
$\omega$	10.541	rad/s
$\alpha$	-0.532	rad
$B$	1.161	m

### 4.2.3 Fracture Probability Model

Next, the author considers the probability  $P_f(T)$  of the destruction of the landing site due to the repetition of the FC landing in a certain period  $T$  [75]. The probability that the impact load is generated by the landing of the aircraft and destroys the building can be considered as the following equation (11).

$$P_f(T) = P_{impact}(T) \int_0^{\infty} P(F|L=l) f_l(l) dl \quad (48)$$

The probability of destruction of a landing site by an aircraft landing in period  $T$  can be modeled as a Poisson process with probability  $\lambda$  [75].  $n$  is the number of takeoffs and landings of a FC per short period,  $T$  is the period of interest, and  $\lambda$  is the probability of an accident during takeoff and landing. To consider the use case of air taxis, the  $n_{airtaxi\_day\_vertiport}$  is estimated from taxi operation data.

$$P_{impact}(T) = n_{airtaxi\_day\_vertiport} T \lambda \quad (49)$$

$F$  is the destruction event. The probability of destroying the landing site when the impact load  $l$  is equal to the impact load criterion  $L$  is  $P(F|L=l)$ . Assuming that the impact load occurs only once, the probability

density function  $f_l(l)$  for the magnitude of the impact load  $l$  can be calculated as in equation (13).

$$f_l(l) = \lambda \exp(-\lambda l) \quad (50)$$

# 4.3 Numerical Results and Discussion

## 4.3.1 Weight and Impulsive Load

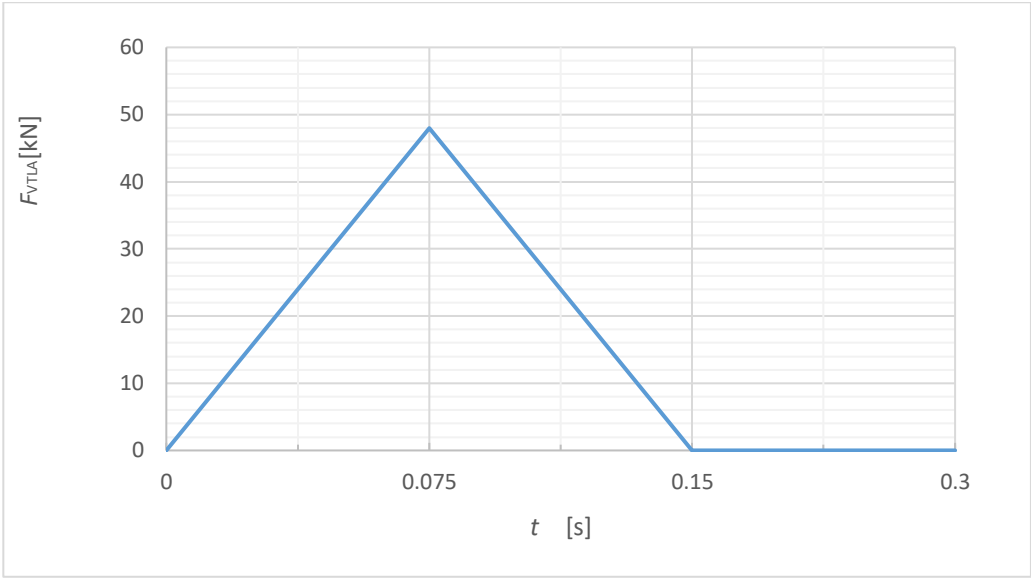


Figure 23 Time Series Variation of Impulsive Load at  $\Delta t=0.15$ ,  $m=1000$

Figure 23 shows the time series profile of the impact load when the total weight  $m$  is 1000kg and  $\Delta t$  is 0.15s. Since the shock waveform is assumed to be a triangular wave, it shows that the maximum value of 47.970 k N force is applied at the midpoint  $t=0.075$  s.

Figure 24 shows the relationship between the total weight  $m$  of the FC and the impact load  $F_{VTLA}$ . If the total weight of the FC is 700 kg to 2 t, the impact load will be the value of 27-144 kN. When designing a new TOLA for

FCs, the floor strength must be strong enough to withstand the force value of 27-144 kN.

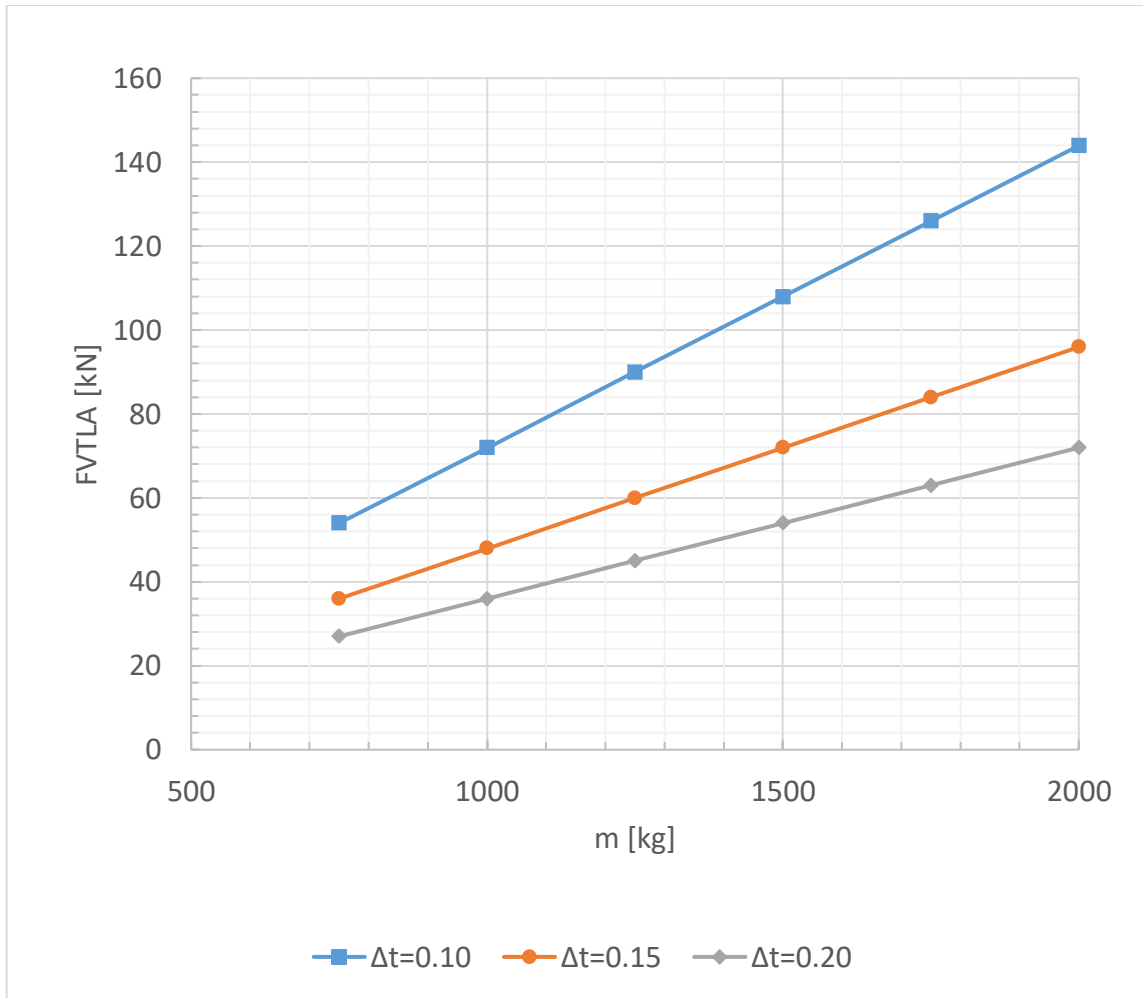


Figure 24 Total Weight and Impulsive Load by  $\Delta t$

### 4.3.2 Comparison with exist TOLA Design Criteria

Next, the author considers a case where a FC makes an uncontrolled emergency landing at an existing heliport. A FC with a total weight of 1000 kg and a parachute of 10 m in diameter falls from an altitude of 5-300 m. The author consider the impact load on the TOLAs for the cases with and without the parachute.

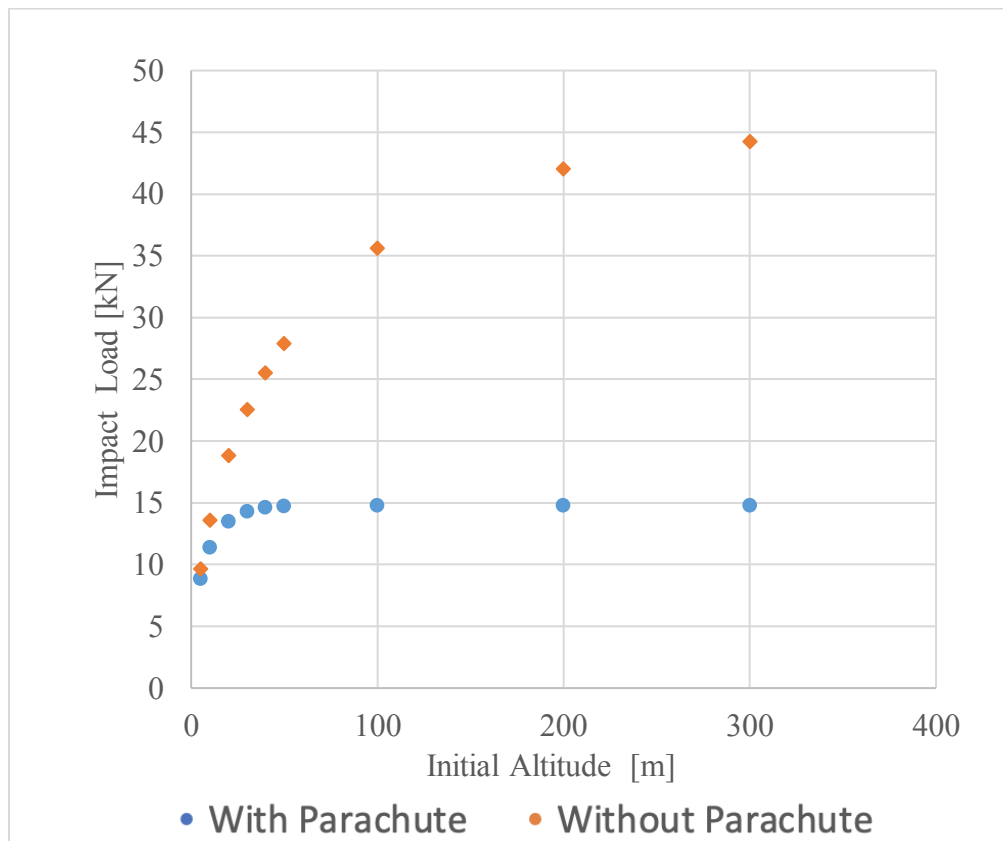


Figure 25 Impulsive Load by Altitude with and Without a Parachute

Figure 25 is the graph of impact load by initial altitude. The blue curve is the result of impact load by initial altitude in the case with parachute. Because there is a parachute, it reaches the terminal velocity at the point of 10m fall and the shock load becomes constant. On the other hand, the orange curve is the result of impact load by initial altitude in the case without parachute. Because there is no parachute, it does not reach the terminal velocity, and the impact load becomes larger at higher altitude. Next, the author considers whether the existing heliport can withstand these shock loads.

The ICAO design standard for existing heliports is 2.5 times the impact load of the helicopter's own weight multiplied by a safety factor of 1.31 [79]. The heliport at Tokyo Heliport Airport in Tokyo can land an aircraft up to 8.5 tons [84]. In other words, it is designed to withstand an impact load of up to 262 kN. On the other hand, the Tokyo Metropolitan Government's design standard for the floor strength of emergency TOLAs, which are grounded on the rooftops of high-rise buildings, is 10.625 tons [80]. This means that emergency TOLAs in Tokyo can withstand an impact load of up to 104 kN. In the case of a high-speed collision, the time  $\Delta t$  for the impact load to be applied is around 0.1s, and a FC with a total weight of 1.4t or more will be subjected to an impact load of 104kN or more [81].

Then, in order to analyze the influence of the parameters, a sensitivity analysis is performed to see how much the impact load is reduced by

increasing the weight  $m$  or the deceleration by the parachute. In general, rotorcraft, like most cars, have crushable structures that absorb shock. In addition, many TOLAs of buildings are made of aluminum, which is capable of absorbing impacts. In other words, this study assumes that the collision between the aircraft and the takeoff/landing area is a hard impact, but in order to calculate the impact load with more accuracy, it is necessary to simulate the structure of the aircraft and the takeoff/landing area or to verify the actual aircraft, which is a part of the next research subjects.

Figure 26 shows the impact load for each  $m$  of total weight with parachute. The design criterion of 110 kN (= 10.625t) for the emergency take

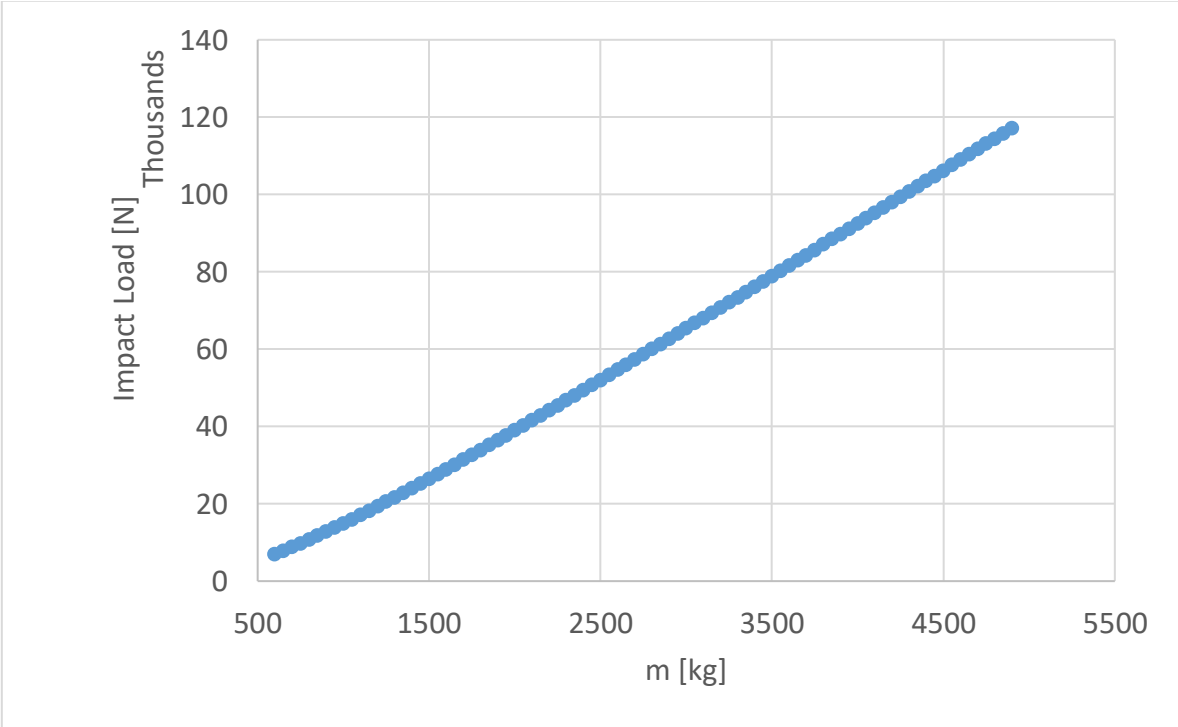


Figure 26 Impulsive Load by Total Weight

Figure 27 shows the relation between the size of the parachute and the impact load. As the diameter of the parachute increases, the drag force increases due to the larger projected area, and the impact load decreases. When the diameter is increased to 20 m, the impact load is reduced to about 7.5 kN, which is half of that of the existing ballistic parachute for aircraft (10 m). However, in actual operation, it is necessary to consider the combination of the size of the parachute and the size of the TOLA.

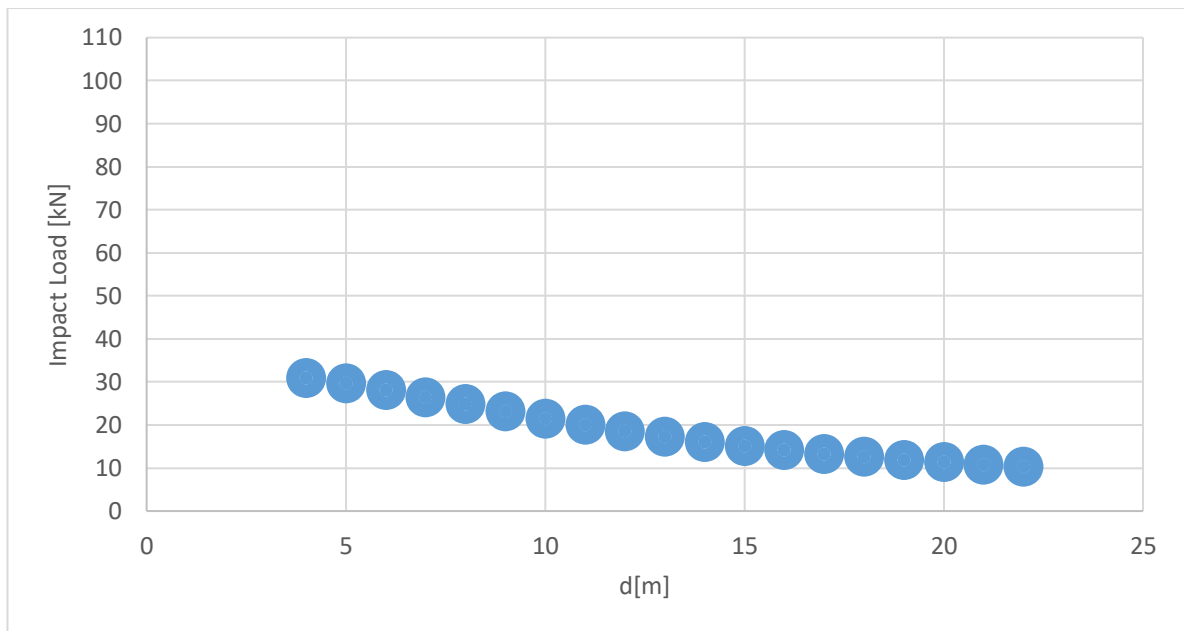


Figure 27 Impulsive Load by the Size of a Parachute

### 4.3.3 Effect of Impulsive Load on Passengers

From equation (5), the acceleration applied to the body can be calculated. From this, the force  $F_{\text{Body}}$  applied to the whole body can be calculated. Figure 28 shows the transition of acceleration in  $z$  direction in time series when the aircraft fell from the altitude of 100 m with the total weight of 1000 kg and the parachute diameter of 10 m. The author considered the weight of the fuselage of the aircraft to be 750 kg, the landing gear to be 100 kg, and the total weight of the two crew members to be 150 kg. As a result, an acceleration of up to 110-120  $\text{m/s}^2$  occurs in the fuselage of the aircraft. A maximum force of 110-120 kN is applied to the fuselage.

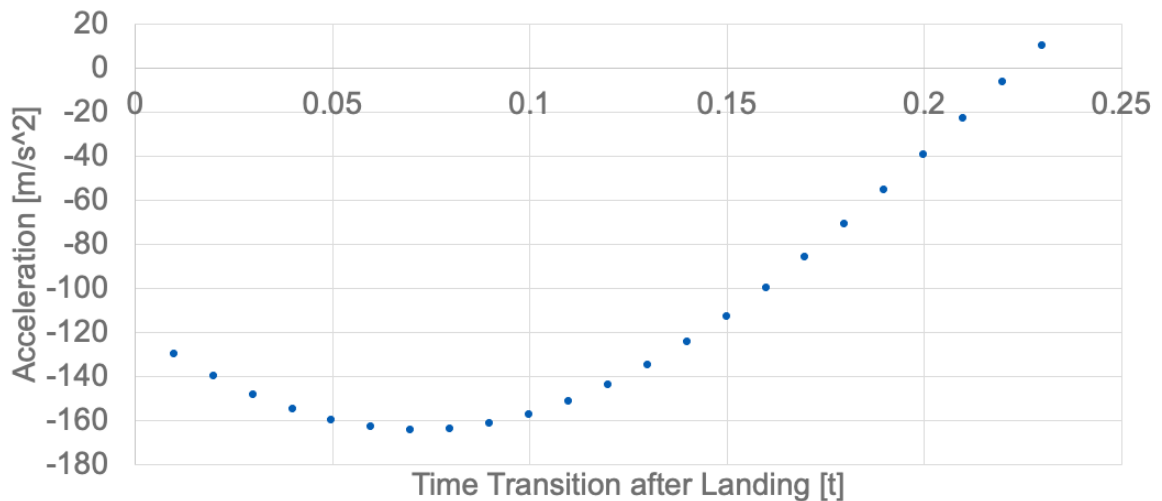


Figure 28 Acceleration of a Fuselage in Spring Damper System by time

In order to consider the criterion of the force applied to the fuselage, the author considers the Load Factor [ $\text{m/s}^2$ ](=LF), which is a measure of the

stress on the structure of an aircraft [85]. The value of  $LF$  of the existing helicopter fuselage is  $20 \text{ m/s}^2$  [47]. If the weight of the fuselage alone is 750 kg, the impact criterion is 15 kN. Therefore, the crashworthiness of the fuselage must be reduced to less than 1/8 by the crushable fuselage, seat and airbags.

Table 12 Mechanical Criteria by Injury [85]

Injury	Criteria	Remarks
Skull fracture	110 G	Dependent on cranial location and extent of impact
Brain injury	90 G	Depends on translational acceleration and rotational acceleration. Rotational acceleration is unknown.
Neck injury	190 N · m (Front), 55N · m (Back)	The value is the limit of tolerance that does not result in ligament damage
Chest injury	60G or deflection rate is less than 76 mm	Acceleration, force, and deflection should be considered
Abdominal injury	-	Shock tolerance has not been fully elucidated due to the multi-organ nature of the disease.

Leg injury	4-17 kN	Loading criteria for fractures of the femur, patella, pelvis, etc.
------------	---------	--

What is the effect on the human body when the maximum acceleration of 110-120 m/s<sup>2</sup> is applied? Table 12 shows [86] the injuries to the human body and their injury criteria. Except for the lower limb injury, the other injuries are fatal enough. From Table 12, the author can see that the impact on the human body should be kept below 60 G. Figure 28 shows that the maximum acceleration due to impact is about 12G (=110 [m/s<sup>2</sup>] /1g), which is not enough to meet the criteria for any fatal injury. However, since the acceleration applied to the human body is determined by the interaction of the seat, seat belt, airbag, and human body, detailed analysis will be left to future research.

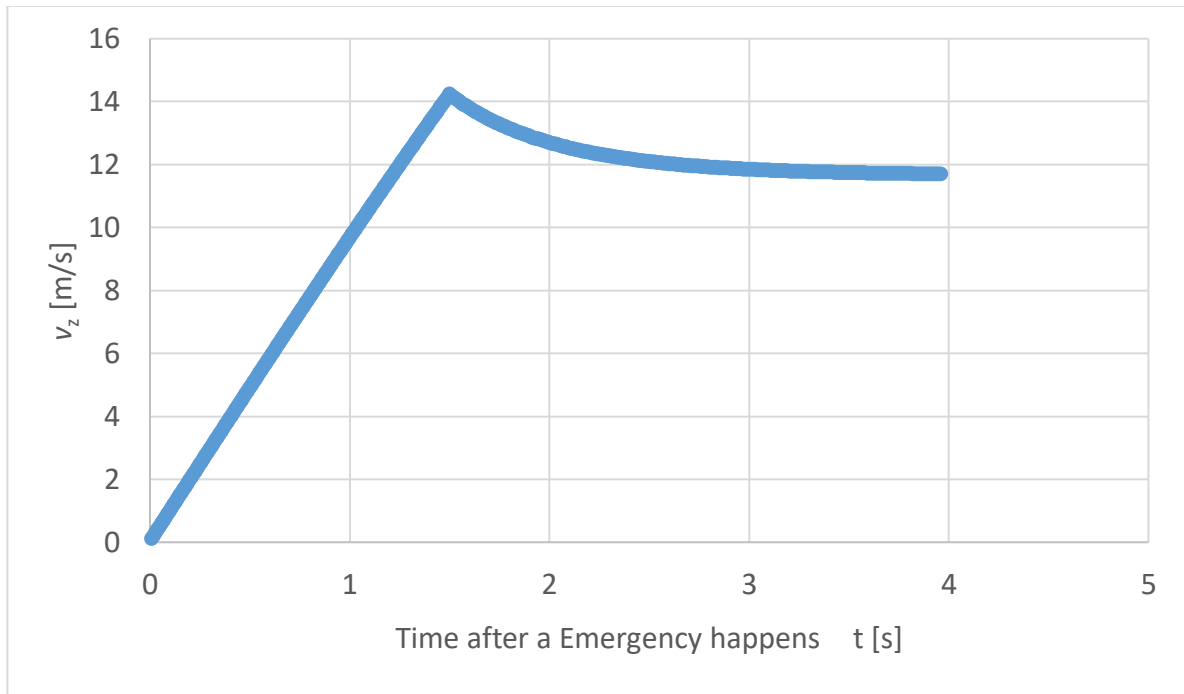


Figure 29 Vertical Velocity Transition

Figure 29 shows the vertical velocity transition. After a parachute opens in 1.5 seconds, the velocity decreases gradually to around 12 m/s. However, when a parachute is opening, the projected area increases. Considering the drag change by increased projected area is also future research.

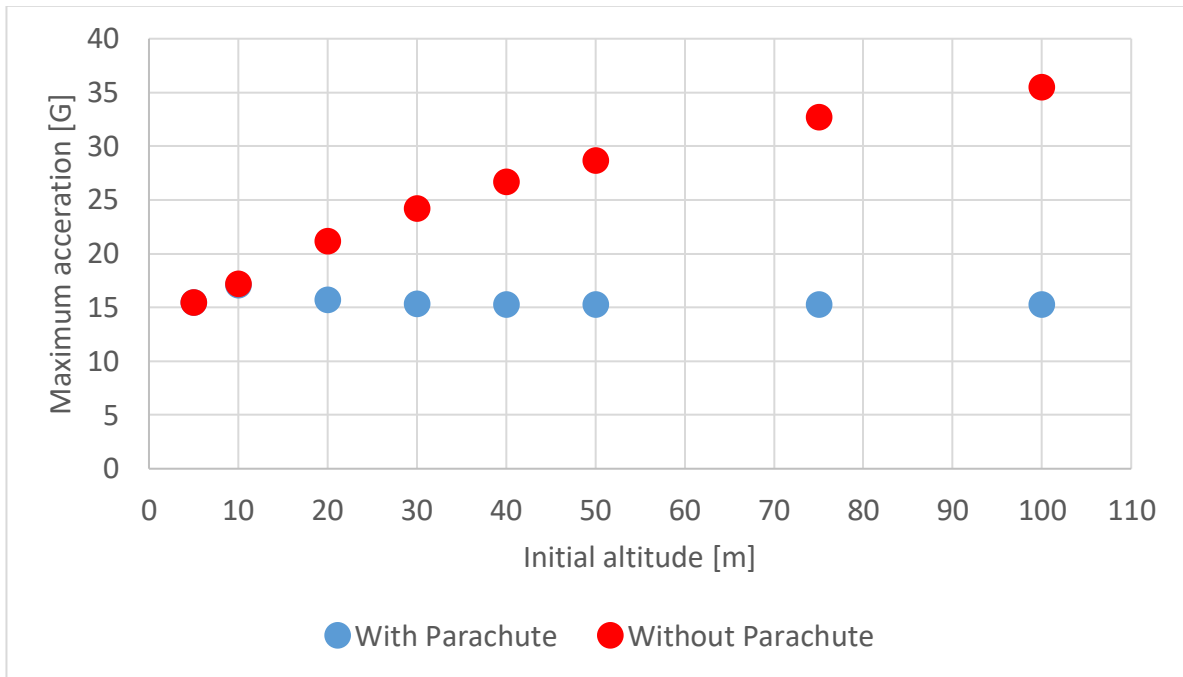


Figure 30 Maximum Acceleration by Initial Altitude

Figure 30 shows maximum acceleration by initial altitude. When the altitude is higher, the parachute effect is stronger. When the altitude is 30 meters and above, the acceleration is under the criteria of legs injury. However, when the altitude is lower than 11 meters, the parachute effect is limited therefore a vehicle needs crushable and air bags to absorb crush force. Also, when the altitude is higher than 50 meters, a vehicle can be whipped by high winds.

### 4.3.4 Probability of the TOLA Destruction by a FC

Consider the probability of destroying a TOLA in a period  $T$  if the FC is operated as an air taxi.

The author considers the frequency of FC operations in Tokyo. Since it is a use case of air taxi, the author estimates the frequency from the data of taxi operation. The number of taxi trips per day in Japan,  $n_{\text{taxi\_year}}$ , is 6 million trips [87]. From the data of Japan's population  $P_{\text{Japan}}$  124.3 million and Tokyo's population  $P_{\text{Tokyo}}$  13.99 million, the author linearly distributes the number of daily trips in Tokyo [88] [89]. The proportion of people who pay more than 5000 yen per trip,  $r$  [ $\text{fare} > 5000$ ], is 12.3% [90]. Of this estimated demand, the proportion of people who use a FC,  $p_{\text{airtaxi}}$ , is assumed to be 1%. The number of trips per day in Tokyo is estimated to be 8301. Here the author assumes that 80 emergency TOLAs in Tokyo will be  $n_{\text{vertiport}}$  of air taxi TOLAs.  $n_{\text{airtaxi\_day\_vertiport}}$  can be calculated as follows.

$$n_{\text{airtaxi\_day\_vertiport}} = n_{\text{taxi\_year}} \frac{P_{\text{Tokyo}}}{P_{\text{Japan}}} r[\text{fare} > 5000] p_{\text{airtaxi}} \frac{1}{n_{\text{vertiport}}} \quad (51)$$

Next, the target period  $T$  is assumed to be 365 days. The accident occurrence probability  $\lambda$  is given by Japan

Let  $\lambda$  for helicopters in the United States be equal to  $3.90 \times 10^{-5}$  (the average number of fatal accidents per 100,000 hours from 2001 to 2005) [91]. The impact load criterion  $L$  is assumed to be 10796 kg. From equation (11), it follows that  $P_f(T) = 4.909 \times 10^{-7}$ . The probability of destroying one TOLA during one year of air taxi operation is  $4.909 \times 10^{-7}$ . The legal service life of a steel reinforced concrete building is 47 years, and the probability of destruction of a TOLA during that period is less than  $10^{-5}$  [92].

### **4.3.5 Model Verification**

Finally, to verify the parachute+FC model, the author compares the video with this model. In the video of “Opener”, a vehicle lands on the ground in 20 seconds after a parachute opens [83]. In the video, the initial opening time is 2.5 seconds. Therefore, the effect of a parachute continues in 17.5 seconds. The average velocity is 5.71 m/s without the initial falling time. In the model including the same specifications of the “opener” vehicle, the average velocity is 8.07 m/s. The error value is 29.2 percentages. Although a parachute size is estimated to be 7.0 m, the drag coefficient is to be higher than the author’s setting.

## 4.4 Conclusion

This study analyzes the effects of impact loads on both the TOLAs and the aircraft by simulating the landing of a FC equipped with a parachute. The purpose of this study is to calculate the impact on the TOLAs and the occupants and the design strength requirements for the safety design of the total system of the FC. By the results of the landing simulation, the following are shown.

First of all, to design a new TOLA for FCs, the floor strength required for the TOLA was determined from the existing grounding standards of ICAO. As a result, considering that an FC of 1 to 2t class will land, the floor strength of 27kN is required at least.

Next, considering the utilization of existing heliports and emergency TOLAs, the author calculated the impact load of an FC on a TOLA by altitude, total weight, and parachute size. The calculation was done by using the fall model of the system of FC and parachute with air resistance. As a result, taking Tokyo as an example, if a parachute is used, it is possible to land at a heliport including an emergency TOLA from the viewpoint of floor strength. Therefore, when an FC is used as an air taxi and an emergency TOLA, which remains as an idle asset in Tokyo, is used as an arrival and departure site, the impact load of an emergency landing can be kept within the standard

regardless of whether a parachute is used or not. However, if the gross weight of the aircraft exceeds 3,900kg, it will exceed the standard.

Next, the author considered the force applied to the fuselage of the FC by considering the fuselage and the landing gear as a spring-damper system with one mass system. As a result, it was found that a force of 110-120 kN is applied to the fuselage. Considering the impact criterion based on the load factor of the fuselage of the aircraft, it is necessary to reduce the impact to 1/8 by using airbags, seats and ,a Crushable of the aircraft. The maximum acceleration of the fuselage is 110-120 m/s<sup>2</sup>, which is within the injury criteria for the human body.

Finally, if the probability that the impact load on the TOLA calculated above destroys the TOLA is regarded as a Poisson process, the probability of its destruction is  $4.909 \times 10^{-7}$  when operating in Tokyo as an air taxi. If the safety of FCs is expected to be improved over existing rotary-wing aircraft by distributed electric power, the probability will result in a drop of one order of magnitude compared to what it is.

In this study, the impact load was simulated by a simple model of a parachute and the airframe of an FC. As a prospect, the analysis for the design below the subsystem of the FC by the simulation of the structure interaction is expected to improve the accuracy of the impact load by making the model of the airframe and the TOLA of the FC detailed. In addition, although the floor strength was considered as a parameter of the design of the TOLA, it is

necessary to investigate whether aluminum, which is expected to be used as a flooring material, can withstand repeated impact loads calculated by simulation as a safety design.

# **Chapter 5**

## **Discussion and Conclusion**

The purpose of this research is to evaluate an FC system design including a vehicle airframe and a TOLA for the HEMS and an air taxi service in Tokyo. In the study, the author evaluates not only a vehicle design for sustainability and a TOLA design for safety but also air taxi operation with agent-based simulation in a viewpoint of system design. Based on conventional research papers, the author decomposes the purpose into three below.

The first purpose of this study is to verify the feasibility of the multi-rotor, vectored-thrust, and lift + cruise types of FC in a medical emergency in terms of economics and society. Conventional research, in which the airframe of an FC is optimized for use in medical emergencies, has not identified a sustainable solution. Therefore, the author develops a simulation model to optimize an airframe design of three FC types in terms of society and economics in a medical emergency use case. Tables 2–4 and Tables 6–8 present the results of the design variables, objective functions, and constraints. In the obtained mission profile, the vectored-thrust type produced highly feasible results. From the perspective of the battery weight energy density, a value of 293 Wh/kg is required at least, which is considered to be difficult to achieve with existing battery technology. This research is limited to first-order analysis because the author does not know the details of an FC airframe design. Therefore, future research should execute multi-disciplinary optimization on an FC detailed airframe from the viewpoints of sustainability: economics, society, and environment.

The second purpose of this study is to evaluate the effects on the occupants and the aircraft and the required specifications of the TOLA design strength for the safety design of both the TOLA and the aircraft by simulating the impulsive loads of an FC in the case of loss of control due to aircraft failure. This study analyzes the effects of impulsive loads on a TOLA, an aircraft, and a passenger inside a fuselage by simulating the landing of an FC equipped with a parachute. The author finds that an emergency landing with a parachute decreases the effect on a passenger although he or she may have a legs injury. This research is limited to first-order analysis because the author does not know the details of an FC airframe design. Therefore, the effect of emergency landing with detailed design is also future research.

## **Acknowledgments**

The author has to appreciate every people who support my study and research in Graduate School of System Design and Management. Each person written below is indispensable for this paper. For five years, all of his enthusiasm is instilled into the system desing of an FC.

Especially, Prof. Dr. Nakano always supervised all of the author's graduate research in the five years without changing his attitude toward the author. After his retirement, he keeps being a substantial supervisor. If the author has not chosen his laboratory five years before, the author would never have decied to study and research in the PhD program. The author needs to give him the most special thanks.

Prof. Dr. Yamagata was the major supervisor of the author for his final year. Although his profissional is not an FC, he always gave the author lots of precise advice. In the finaly year, the author was a teaching assistant for his three courses. However, the author learned urban city design and sustainability from him luckily. After the author's graduation, as a researcher, the author needs to support him and repay for his kindness which he accepted the author as a phd student after the retirement of Dr. Nakano.

- Graduate School of System Design and Management, Keio University

Not only Dr. Nakano, but also Prof. Dr. Yamagata, Prof. Dr. Haruyama supervised the author's doctorate thesis for the final three months with their enthusiasm as second supervisors. When the author was defending to their questions and advice, the author did not perceive that they were growing his up as one of the research doctors. Including Prof. Dr. Matsuo, they taught that writing this PhD thesis is a beginning of one researcher. The author appreciates this valuable time to discuss with them.

Also other professors inside Graduate School of System Design and Management provide me lots of research methods and contents. In this five years, the author learned not only physics, mathematics, and engineering but also politics, psychology, business, and philosophy. All of them is indispensable for thinking the SYSTEM DESIGN of an FC.

SDM officers helped the author's research and study in these five years. When the author went abroad twice, they supported me with their warmful messages. Their office work is absolutely professional. If there were not them in this graduate school, the author could not have concentrated on his research and study. As one of the graduate school students, the author appreciate very much that they provide him amazing research environment.

- Faculty of Science and Technology, Keio University

As mentioned above, Prof. Dr. Matsuo was the second supervisor of the author's PhD thesis. As one expert of aerospace engineering, she taught him

how to research and summarize his final paper. Also Prof. Dr. Matsumoto was a supervisor when the author was an undergraduate student in 2016. The experience to research the development of a PM2.5 measurement device is tightly connected with his decision to start studying systems engineering and system design. His bachelor research is still his fundamental to research. Finally, when he was in the faculty of science and technology, he appreciates that he learned lots of subjects in the STEM area for four years. He is proud that he learned for nine years totally in the perspective of engineering.

- Flying Car Research Lab

The author researched for these five years with Aki Nakamoto, Tsubasa Nakamura, Hajime Sagane, Kouichi Hommura, Keisuke Ishizumi, Yumi Tanaka, Hironomi Tagawa, Takashi Sugita, Daiki Hitsuji, Ryutaro Mori, Julio Budiman, Pawnlada Payuhavorakulchai, Patrisha Armi, Sharma Bhavya, Vincent Heurteur, and Geyue Shi. Each of them has an important part of the FC system design research. Their existence made the research area of the author prominent. Especially, her research area of Aki Nakamoto is requirement analysis by stakeholder interviews. Therefore, the author's research cannot exist without her effort, and vice versa. The author hope that this research helps her PhD thesis in the future. Also, Tsubasa Nakamura has been a project research assistant professor for a long time. He is the best boss, friend, and project manager for the author. When he leaded

collaboration research projects, the author learned not only how to research but also his project management. Finally, the author is sure that the best point to enroll in a graduate school is that a student can choose his or her boss. Choosing It is most lucky that the author could choose the three bosses Dr. Nakano, Aki Nakamoto, Tsubasa Nakamura as a first boss in the author's life.

Also the author greatly appreciates Business Engineering Lab members, Yamagata Lab member, other students who the author studied and researched with.

Moreover, the author needs to thank all industry collaborators: Toyota, Chodai, DBJ, JAXA, ECAIR, METI, Delloite, Aero Asahi, Hokusoh Hospital, Daiwa Taxi. Because the author was unskilled as one member of society, it was often trouble for them. However, his experience to research with them was one of the most valuable gift because the author learned lots of things from an industry viewpoint.

And the author went abroad twice to study. First, In ETH Zurich, Prof. Dr. Hacklin supported the author's master research and study in the D-MTEC. Secondly, in Purdue University, Prof.Dr. Crossley provided lots of insight for the author's phd research. There, his friends Naotaka, Takashi, Tshun, and Apoorv were essential fro the authors' studying abroad.

And this research is supported by research encouragement assosiate program in Keio University for three years, Keio Research Encouragement Scholarship three times, JST Support for Pioneering Research Initiated by

the Next Generation, JASSO Scholarship Programs for Studying Abroad twice, and the hire as a project assistant professor in SDM. Thankfully with amazing financial support for one graduate school student, the author never gave up his PhD research. The author has to repay for this investment in the industry and academia in the near future.

Finally, the author appreciates most his family support. Especially, his father financially supported him until the end of the PhD research. Without his father's financial assistance, he cannot keep my research and study. In five years, not only his best friends but also his family have never changed their attitude toward the author. The author appreciates their kindness. He also needs to repay for their kindness in all of his life. Moreover, Nana and Elizabeth, which are the lovely dogs of the author, always gave him nirvana. The author willingly devotes all of this PhD thesis to them.

# **Appendix A Cost Analysis of a FC Configuration Design for Medical Emergencies [76][77]**

## **A.1 Problem Definition**

In Japan, emergency medical helicopters are known as “doctor helicopters,” since doctors are onboard and are transported with the medical team to the site of the emergency. These systems ensure early treatment and result in high patient-survival rates according to HEM-net’s research. Due to the high running cost of approximately 250-million yen annually, doctor helicopters have not yet been fully deployed throughout Japan . Operators in the field also face problems of low ride quality due to noise and vibration, which complicate in-flight operation [93].

To find the best solution to the helicopter’s problems with cost, noise, and performance, short/vertical-takeoff-and-landing (S/VTOL) aircraft, have long been developed, but only some designs are safely operable. An eVTOL, which has promising small-size, low-cost, and low-noise characteristics, is anticipated to relieve problems and enhance existing helicopters for use in

urban areas. eVTOL is expected to reduce the total operating cost per seat mile by 26% compared to helicopters. The safety of air EMS will also be further increased by the development of flight controls, sense-and-avoid technologies, and fully autonomous aircraft, consequently reducing the current problem of a high crash rate .

In the usual case, four passengers, including a pilot, doctor, nurse, and passenger, are onboard for medical services. Due to battery-technology limitations, a 4-passenger vehicle will be available in the year 2025 only if hybrid systems are introduced. Hence, to cover needs in the year 2025, eVTOL capable of carrying 2 passengers (a doctor and a pilot) to the site of an emergency is proposed. Accordingly, the cost model for verifying the viability of 2-passenger eVTOL is studied in this research.

Conventional aircraft-cost estimation is performed using the cost-estimating relationship (CER) or a statistical equation such as the Eastlake cost model to predict an aircraft's acquisition cost using only typical input variables such as empty weight, maximum velocity, and production volume. The CER method breaks down costs into subcomponents such as material and engine-production costs. Hence, eVTOL's electric-systems components, including batteries, motors, and propellers, and additional costs, including ballistic parachute systems and sense-and-avoid systems, can be integrated into conventional cost estimation for cost analysis of the eVTOL configuration design. For components regarded as automotive parts, cost

estimation is related to automotive-manufacturing cost. Current eVTOL cost studies conduct estimates based on the vehicle cost per unit weight, especially for fixed-wing aircraft, and profitability analysis is necessary for air-taxi utility. This research focuses upon collecting actual data in Japan related to an air ambulance's requirements, and discusses the components affecting cost, such as battery utilization and deterioration. With this objective and the available data, the selected methodologies are a combination of top-down, bottom-up, and parametric-cost equation.

The purpose of this research is to estimate the cost of eVTOL by developing a mathematical-cost model and inputting different commercial-configuration designs for analysis. We aim to verify that the eVTOL's cost will be lower than the current expected cost; hence, the total cost of an air ambulance will need to be lower than the Japanese government's budget. Guidelines on the expected amount of eVTOL production for the needs of air-ambulance service, and realistic cost estimation for each configuration for aircraft for operators interested in expanding eVTOLs to air-ambulance usage are proposed in this study. Commercial configurations, including fixed-wing vectored thrust with 2 different propulsors for each configuration and multi-rotors, were collected from various companies; these include A3 Vahana's tilt-wing, Lilium jet's fixed-wing, and Volocopter 2X's wingless multirotor aircraft. We expect that this study will increase access to air-ambulance service in Japan.



## A.2 Method [94]

The cost model for an eVTOL is consisted of capital expense and direct operation cost (DOC). Capital expense of the configuration will be distinguished for different types of propulsor, where CapEx<sup>P</sup> (Capital expense for the configuration with a propeller) is used for analysis of Vahana and Volocopter 2X. Both configurations share variable-pitch propellers, but differ in size and number of propellers as a reference to the commercial model. CapEx<sup>D</sup> (Capital expense for the configuration with a ducted fan) shows a ducted-fan-type configuration, which is a Lilium jet. The fixed cost, which will not change depending on a vehicle's weight, velocity, propulsion systems etc., including SAACost, is given by:

$$CapEx^P = VPCost + (ManCost + SAACost + BatCost + PCCost + PropCost)zQDF^{AC} \quad (52)$$

$$CapEx^D = VPCost + (DucCost + SAACost + PCCost + PropCost)zQDF^{AC} \quad (53)$$

DOC is calculated per vehicle unit each year. DOC calculation depends upon capital expenditure, hours of flight, and total energy required. However, the capital expense cost from (3) will cover 5 years' production; thus, the parameter should be calculated by a following equation.  $CapEx^A$  (Capital expense per one unit) is one parameter for calculating DPCost (Depreciation

cost),  $ITCost$  (Interest Cost), and  $MMTCost$  (Maintenance-material cost in dollars per year).

$$CapEx^A = \begin{cases} \frac{CapEx^p}{z} & \text{if propeller} \\ \frac{CapEx^D}{z} & \text{or ducted fan} \end{cases} \quad (54)$$

$$DOC = DPCost + ITCost + FCCost + MTCost + MMTCost + ENCost \quad (55)$$

### **Direct-operational Cost**

In aircraft design, estimation of the direct operating cost (DOC), seat-mile cost, and price of the aircraft is a crucial aspect for certifying the aircraft's viability. The operating costs are categorized into the DOC and the indirect-operating cost (IOC) [95] [96]. However, IOC depends upon the services that the airline offers. Therefore, DOC is a parameter for comparative analysis in this research. Many methodologies have been developed to estimate DOC, by organizations such as the Air Transportation Association of America, the National Aeronautics and Space Administration. The DOC commonly breaks down into depreciation cost, interest cost, maintenance cost, maintenance-material cost, insurance cost, energy cost, and flight-crew cost. Regarding the detailed differences between conventional aircraft and eVTOL,

modification to the DOC is presented in [97] [98]. The estimation of the above cost follows [97].

The battery-replacement cost must be considered in the eVTOL's cost model because that battery will undergo loss in discharge capacity over time. Capacity loss has irreversible and reversible components. Reversible capacity loss can be recovered by charging the battery, while irreversible loss is related to degradation and cannot be recovered. Electric vehicles are typically designed so that the battery will never become wholly charged or discharged. However, to implement this practice in an eVTOL, the weight of the battery must be increased.

### **Capital Expense**

Capital expense consists of the airframe, motor, battery, propeller, sense-and-avoid system, and parachute costs. Airframe cost is modeled as the CER, which the model itself already provided reduction in cost with respect to production number. Component costs will be calculated using either cost estimation from the equation or the initial cost survey from the market. The quantity-discount factor (learning curve) [**Error! Bookmark not defined.**] is applied to other components, including motor cost, battery cost, propeller cost, sense-and-avoid-system cost, and parachute cost:

$$QDF^{AC} = F_{EXP}^{1.4427 \cdot \ln(z)} \quad (56)$$

Here,

$$z = \begin{cases} x^p z & \text{if apply to propeller — motor part} \\ z & \text{if others} \end{cases} \quad (57)$$

The vehicle-purchase price of fixed-wing and multi-rotor aircraft will be calculated using DAPCA IV's cost model [97], which is expected to be applicable for both UAVs and light-weight aircraft. The cost equation depends mainly upon statistical data from past models and provides maximum speed, number of productions, and empty weight as input parameters for analysis. Cost components include the total costs of engineering, development support, flight testing, tooling, manufacturing, materials, and quality control. Note that the costs of avionic and autonomous systems are not included. Research, development, testing, and evaluation (RDT&E) costs are divided into development support, quality-control, and flight-test costs from DAPCA IV. RDT&E and production cost are usually combined in CER because they are difficult to separate, since engineers spent hours in the RDT&E phase as well as supporting the production of the aircraft.

$$VPCost = DevCost + QCCost + FTCost + EngCost + TCost + ManCos + MatCost(58)$$

The propulsion systems of the eVTOL configuration include the motor, propeller-type (fixed pitch or variable pitch) or ducted fan-type propulsor,

and battery. Motor cost and Propeller cost (ManCost/ DucCost) are estimated by referring [99] [100].

Referring to [101], the costs of Li-ion-battery packs continue to decline and those among market leaders are much lower than previously reported. From the graph trend, battery cost reduction can be estimated as an exponential-decay function. Tesla model 3 SR's Li-ion battery has a pack cost of \$176/kWh (assuming from Fig. 16 which use Tesla's cost as one of the prices feed into an average) as of 2018 with 250 Wh/kg has been found promising for aircraft applications, providing very safe and high-energy battery packs. However, there is an alternative battery cost provided by NEDO of \$200/kWh and \$100/kWh in the years 2020 and 2030, respectively. Hence, for direct-operating-cost estimation, scenarios will be provided for both cases.

Battery cost will be calculated by accumulating the battery capacity of each configuration and cost in \$/kWh [102]. First, the battery mass is calculated by assuming one-third of the maximum takeoff weight to balance the weights of the vehicles [103] and to account for the fact that most transport aircraft have a maximum fuel weight of 1/3 of the maximum takeoff weight. Battery mass ( $xM$ ) is multiplied by the battery-energy density ( $BattD$ ) to learn the battery capacity of each configuration. With the available battery capacity (kWh) of each configuration and cost in \$/kWh ( $CellCost$ ), the battery cost can be predicted, as shown in equation (25). This can be recalled as the

bottom-up approach, since it breaks down parts into features and composes them to form the total battery cost.

$$BatCost = BatCap(CellCost) \quad (59)$$

Where

$$BatCap = x^M BatD \quad (60)$$

SAACost (Sense-and-avoidance systems cost) is calculated by referring [97] [104]. Also PCCost (Parachute cost) is calculated by referring [**Error! Bookmark not defined.**].

### A.3 Result

#### Mission Profile

From our interview data, the mission profile of each configuration will depend on the configuration's rate of climb/descent and cruising speed. With the required maximum operating distance of 31 km and a 15-minute constraint from calling, the following results can be concluded.

Table 13 Vahana mission profile [102]

Vahana		
Rate of climb/descent	5.6 m/s	Ref: [8]
Takeoff and landing time	1.8 min	Computed
Cruising time	10.2 min	Computed
Cruising speed	230 km/h	Ref: [8]
Cruising distance	39.1 km	Computed

Table 14 Lilium-jet mission profile [102]

Lilium jet		
Rate of climb/descent	5.6 m/s	Assumed
Takeoff and landing time	1.8 min	Computed
Cruising time	10.2 min	Computed
Cruising speed	280 km/h	Ref: [9]
Cruising distance	47.6 km	Computed

Table 15 Volocopter 2X mission profile [102]

Volocopter 2X		
Rate of climb	3.6 m/s	Ref:[10]
Rate of descent	2.5 m/s	Ref:[10]
Takeoff and landing time	3.7 min	Computed
Cruising time	8.3 min	Ref:[10]
Cruising speed	100 km/h	Computed
Cruising distance	13.8 km	Computed

Table 15-17 shows the mission profile of the Vahana where the rates of climb and decent are computed based on data given from Vahana’s official website, accumulated from the capable flight time to the ceiling height of the

air-taxi service. As it will reach within 90 sec given a rate of climb/decent of 5.6 m/s. Hence, for an air ambulance, assuming a service attitude of 300 m, it is possible to assume for takeoff and landing times of 1.8 minutes. As 15 minutes are required to increase the survival rates of patient (including 3 minutes for calling and 12 minutes for transportation), 10.2 minutes will be used for cruising; hence, with a cruising speed of 230 km/h, a distance of 39.1 km can be achieved.

### **Cost-analysis result**

Cost per unit in 2030 will be based on Tesla's battery roadmap, because slight differences in cost per unit do not show significant changes in cost. Calculation for each year's production cost, however, will still be necessary as the cost or capital expense per unit will be an input parameter for the DOC. The production profile of the 5-year results for the three commercial models is shown in Figure 31. The cost is expected to be lower than that of 16 R22 helicopters (31 million yen).

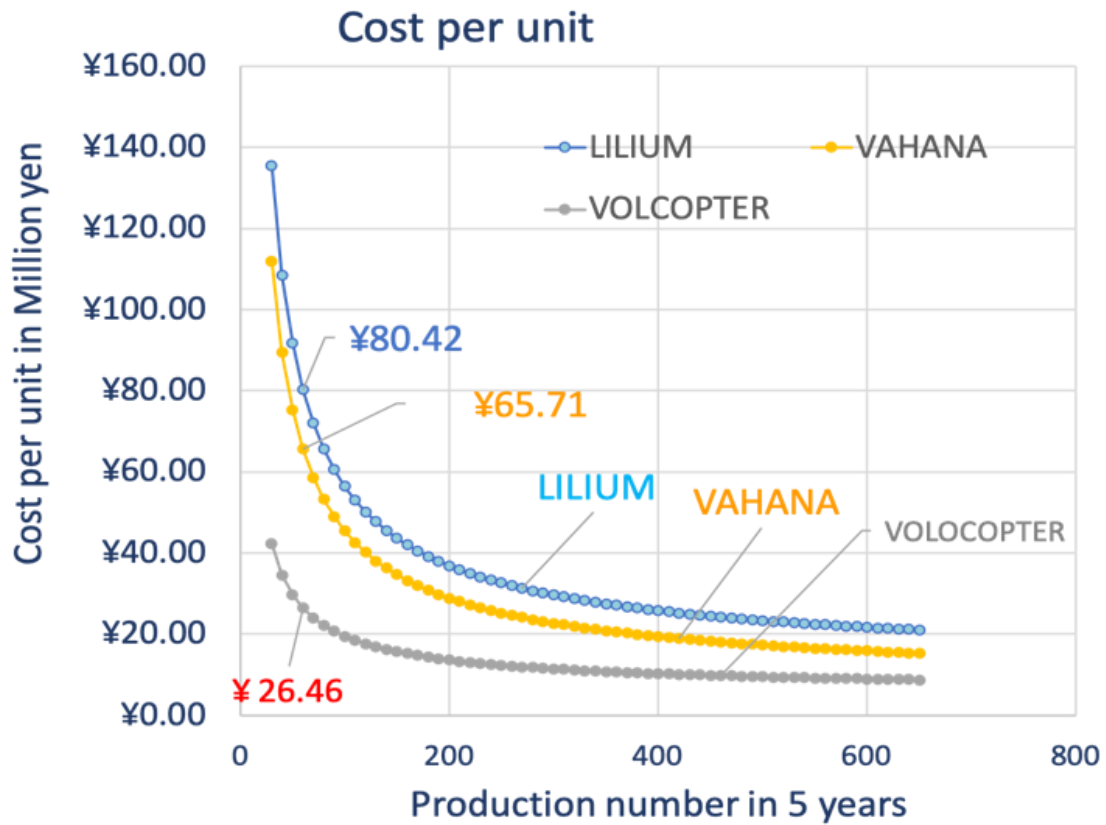


Figure 31 Cost per Unit [102]

The graph shows a rapid decrease in cost in the first region and then the curve becomes horizontal, indicating no significant change in price even when raising the production volume. Volocopter’s cost per unit approaches 11.47 million yen at 300 units and continues to reduce slowly. Vahana’s cost per unit approaches 17.3 million yen at 500 units and also declines slowly. Lilium jet’s trend line as well becomes almost horizontal at 500 units where it approaches the value of 23.3 million yen and continues to slowly decline.

Although 30 doctor-helicopter units are required, since they are 2-capacity vehicles, around 60 units or more are proposed to mitigate the problem of dual requests. For 60 vehicles the costs are 80.4, 65.7, and 26.5-million yen. respectively for Lilium jet, Vahana, and Volocopter.

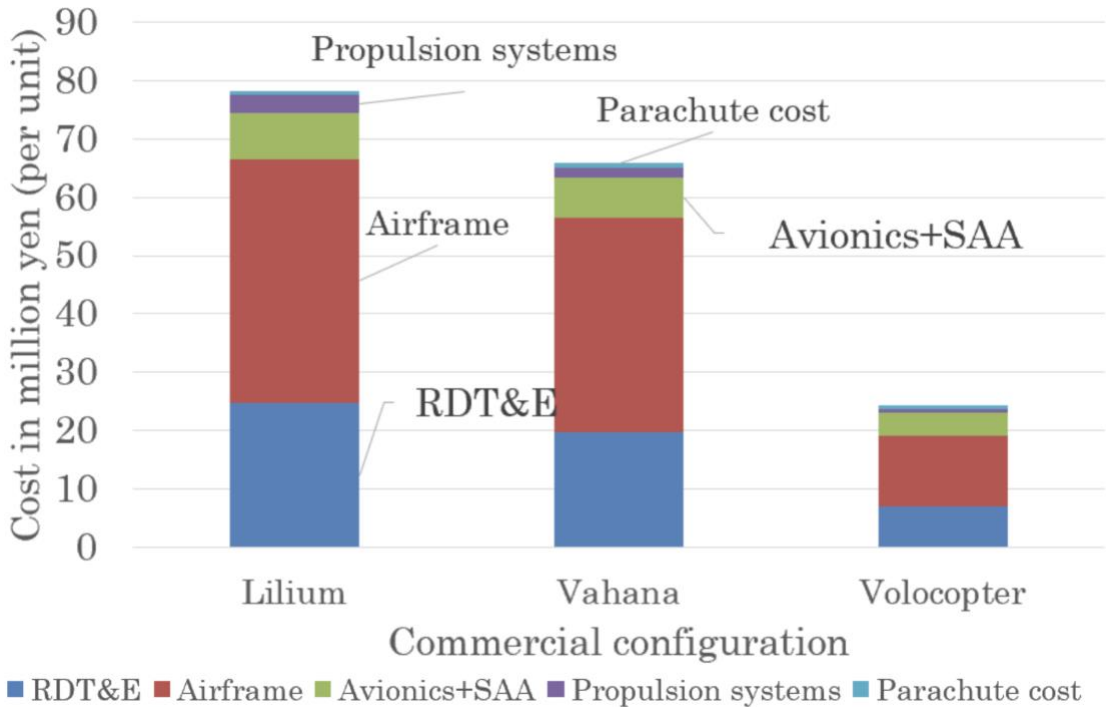


Figure 32 Component-cost breakdown [102]

The eVTOL purchase cost will breakdown into costs for RDT&E and production (airframe, SAA, Propulsion systems), and additional costs (Parachute cost). RDT&E costs include research-and-development, quality-control, and flight-test costs. Propulsion systems consist of batteries, propulsors (either ducted fan or propellers) and motors. At 60 units, eVTOL’s

highest cost is for airframe fabrication. Lilium jet's RDT&E cost is highest among the configurations at 25 million yen, while Volocopter is the lowest at 7 million yen. The chart implies that electric systems (which comprise only a small part of the overall cost) can lower the cost per unit compared with traditional helicopters.

DOC is broken down in Figure 33 into crew, maintenance, maintenance-material, battery replacement, interest, energy, and insurance costs. The result is separated into the cases of 200 flight hours with 60 vehicles (a case of a hospital in Chiba prefecture) and 500 flight hours with 100 vehicles (a case of a hospital in Hyogo prefecture) for years 2020 and 2030 by extrapolating the battery cost from the Tesla model (\$176/kWh in 2020 and \$62/kWh in 2030). The only fixed cost for the 2 scenarios is the crew cost of 80 thousand yen. Obviously, cost contributes to the battery-replacement cost in the year 2020, which for all configurations and both cases, accounts for approximately 50% of the DOC. Interest cost is primarily based upon vehicle cost; hence, it makes a higher cost at 60 units and becomes lower at 100 units. The energy cost becomes higher as the number of flight hours increases in Hyogo. The insurance cost is 6% of the operating cost and therefore changes with DOC.

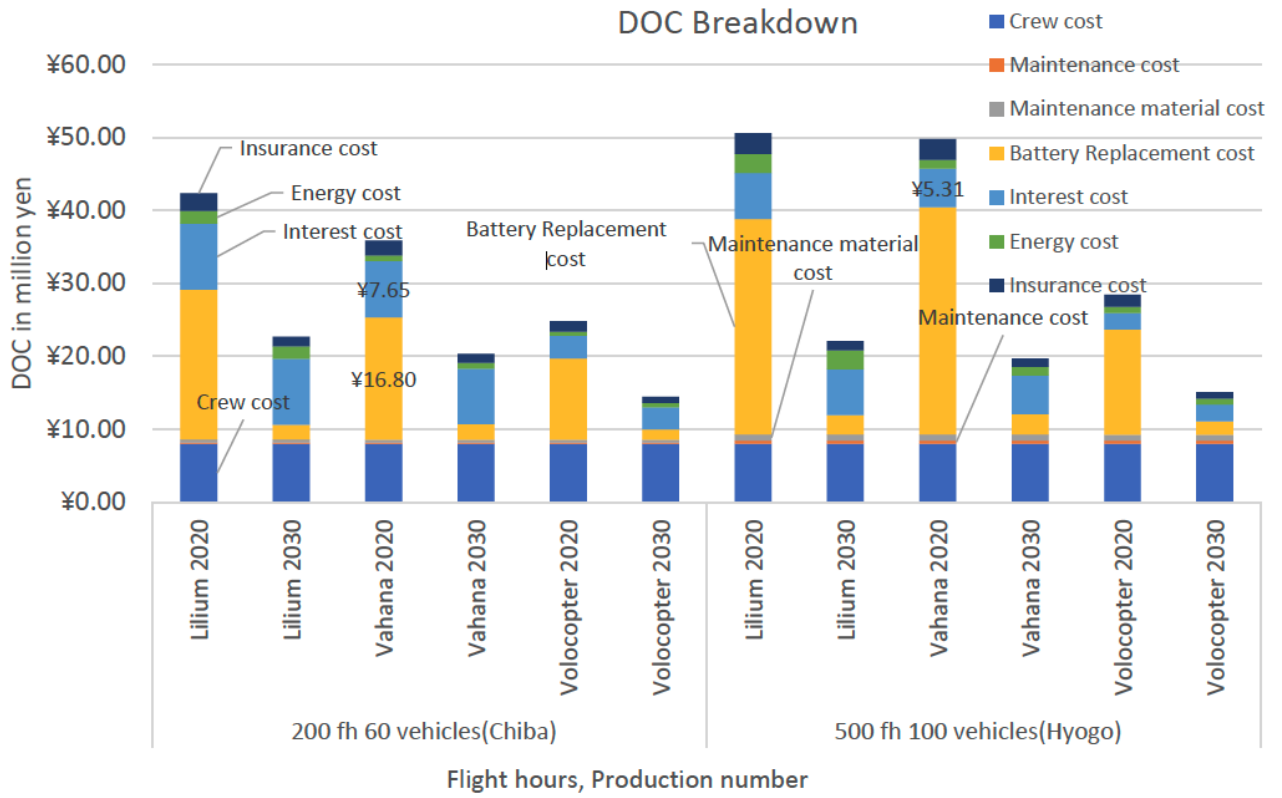


Figure 33 Cost breakdown of direct operating cost [102]

## **A.4 Discussion**

Volocopter, a multi-rotor configuration, is the only configuration that cannot meet operational requirements. Costs per unit at 60 units are 80.4, 65.7, and 26.7 million yen for Lilium jet, Vahana, and Volocopter, respectively. Hence, only Volocopter can achieve a lower cost than the R22 Robinson helicopter's cost of 31 million yen. Vahana and Lilium jet will need to raise production volume to 230 and 380 units to attain the same cost as Volocopter. The baseline for verifying the reduction and viability of the cost here is 25 million yen, which is 10 times lower than the current operating cost of 250 million yen. Volocopter is the only configuration that is applicable to achieve a DOC below 25 million yen with 90 production units, but only with the integration of a Tesla battery (\$176/kWh) and 200 flight hours per year (Chiba). The other configurations will only reach 25 million yen in the year 2030. At 60 units of production, all configurations can achieve a cost below 25 million for the best-case situation in 2030, when the Tesla battery has a cost of \$62/kWh and the advancement of the battery is increased to 500 kWh/kg, a doubling from 2020.

Table 16 List of criteria [102]

Criteria	Lilium jet	Vahana	Volocopter 2X
Meet requirements of operating distance ( $\geq 31.28$ km)	Yes (47 km)	Yes (39 km)	No (13 km)
Cost per unit (60 vehicles)	80.4 million yen	65.7 million yen	26.7 million yen
DOC worst case in Hyogo (60 vehicles)	58.8 million yen	57.2 million yen	32.3 million yen
DOC best case in Chiba (60 vehicles)	23.6 million yen	21.2 million yen	15.3 million yen

Reduce to $\leq$ 25-million-	At 100 units (NEDO,	At 60 units (NEDO,	
yen budget (DOC)	Hyogo) Or 70 units	Hyogo) Or 50 units	At 90 units (Tesla,
	(Tesla, Hyogo) Only	(Tesla, Hyogo) only	Chiba) 2020
	year 2030	year 2030	

---

## **A.5 Conclusion**

Cost-estimation results show a tradeoff between the performance and life-cycle cost of fixed-wing and wingless aircraft. The Lilium jet has the highest DOC but will be comparable to Vahana when both configurations need more batteries in the year 2020. Volocopter achieves the lowest cost, but suffers for not achieving the air ambulance's operating-distance requirement of 31 km. In conclusion, there is no configuration that meets the requirements in 2020. In the year 2030, all configurations meet the cost requirement.

This study shows the results for DOC and Japan's circumstances for only 3 commercial models: Lilium, Vahana, and Volocopter. In future studies, we suggest comparing the results of other eVTOL applications, which may give hints to eVTOL operators for markets in which they could implement their systems. With cost study, an optimized configuration design can be determined based on which configuration is more promising for integration with more precise cost estimation.

## **Appendix B Demand Estimation in the USA**

### **B.1 Problem Definition**

Christelle [105] uses a survey to identify the factors affecting the use of urban air mobility, such as eVTOLs. However, his study does not estimate the market share of FCs with identified factors. Also his studies consider only the case of Munich, Germany. Garrow [106] [107] presents two surveys representing the future market conditions among eVTOLs called FCs or urban air mobility, as compared with autonomous and traditional ground vehicles via a questionnaire targeting full-time workers with salaries of at least \$75k in five particular areas of the USA. Neither study considers other conventional on-demand services utilizing a rotorcraft, single/twin-engine piston aircrafts, or the like. Catalano [108] estimates the demand for carsharing services in Palermo, Italy via a multinomial logit model. In [108], Catalano considers competition between different transportation modes to calculate the shares of cars, carpooling, carsharing, and public transportation with the attributes of one-way travel time, one-way travel cost, and parking time. However, this study is limited to ground transportation and does not include aircraft as an on-demand service. Therefore, the present study focuses

on estimating FC demand in the USA by comparison with other fixed-wing aircraft and rotorcraft classified in FAA FAR Part 135 [109].

The purpose of this study is to explore the applicability of FCs to the air-taxi business in the USA. To estimate demand for this, we assume that FCs compete with current aircraft classified under Federal Aviation Administration (FAA) Federal Aviation Regulations (FAR) Part 135 [113]. Demand estimation helps to understand the degree by which modal characteristics affect how effectively FCs extract share from the current American air-taxi market. To calculate demand, a multinomial logit model is used. The model incorporates the current market share and characteristics of pre-existing air-taxi modes to generate an utility equation, and estimates the characteristics of FCs to calculate their share of the market. What-if analysis explores how demand for FCs is affected by changing the values of their characteristics.

This paper is composed of five sections. In Section 6.2, the research method is presented. Other aircrafts are specified as on-demand services. A multinomial logit model is introduced to estimate the share of each type of aircraft in the USA. After showing the result of the multinomial logit model solved by multi regression analysis in Section 6.3, what-if analysis is conducted to check the sensitivity of the model in Section 6.4.

## **B.2 Method**

### **B.2.1 Aircrafts Defined Under FAA FAR PART 135**

The FAA's Federal Aviation Regulation, Part 135, includes a fleet of aircraft categorized as 'Scheduled' or 'On-demand'. The On-demand category is further broken down into 'Passenger' and 'Cargo'. The 'Passenger' category has three main sub-divisions: 'Air Taxi,' 'Air Medical', and 'Air Tour' [110]. The aircraft/modes available in Part 135 have two types: 'Fixed-wing' and 'Rotorcraft'. The fixed-wing category is in turn composed of 'Single-engine Piston', 'Twin-engine Piston', 'Single-engine Turboprop', 'Twin-engine Turboprop', and 'Turbojet'. Rotorcraft breaks down into 'Piston Rotorcraft' and 'Turbine Rotorcraft'.

### **B.2.2 Model Characteristics**

To estimate demand, we identify a set of characteristics that significantly impact customer choice of aircraft. As shown Table 17, These factors are speed, cost per fare, capacity, noise, and accident rate, and are based on the Uber Elevate report [3] and a survey conducted by the University of Michigan, Ann Arbor [111]. The factor data are collected for each mode

defined by FAA FAR Part 135 for the aircraft models most commonly used in the United States. Information concerning aircraft models is extracted from Aircharterguide [112] and relevant articles online [113], [114] and [115].

Table 17 Aircraft Types and Average Attributes

Aircraft	Speed [knots] [114]	Cost/hour [\$] [112]	Noise [dBA] [110] [115]	Passenger Capacity [110]	Accident Rate [10 <sup>-5</sup> ] [113]	Average Share (2006-2017) [113]
Single- Engine Piston	170	493	66	5	3.30	0.513
Twin- Engine Piston	178	712	77	6	2.37	0.082
Single- Engine Turboprop	226	1357	81	9	1.12	0.051
Twin- Engine Turboprop	302	1641	79	9	2.17	0.056
Turbojet	302	1641	79	9	0.52	0.158
Piston Rotorcraft	109	577	81	3	3.81	0.033
Turbine Rotorcraft	141	1805	86	6	1.36	0.106
FC [13]	59.395	190	76	2	1.61	-

Aircraft safety is one of the most important factors affecting customer utility. The survey conducted by the University of Michigan, Ann Arbor [111Error! Bookmark not defined.] reveals that about 63% of the US citizens are ‘very concerned’ about the safety of FCs, while 20% are ‘moderately concerned.’ Data related to the safety of pre-existing modes of transport has been collected in the form of number of accidents per 100,000 hours of flight between the years 2004 and 2010.

To estimate FC market share, we need to decide the characteristics of a typical FC. In this study, the Volocity (Multicopter) is chosen as the FC model [116]. The total accident rate from FAA FAR Part 135, as describe is 1.61. Therefore, it can be assumed that a FC will have an average accident rate of 1.61.

### **B.2.3 Multinomial Logit Model**

The dependence of customer choice upon variables can be defined mathematically using the utility function [117]. In the study, alternatives for customers are the air-taxi modes defined by the FAA. The variables are speed, cost, noise, capacity, and accident rate. Hence, the utility function for a transportation MODE  $k$  ( $1 \leq k \leq 8, k \in \mathbf{N}$ ) is shown in Equation (1). The MODE  $k$  represents a transportation of Single-Engine Piston, Twin-Engine Piston,

Single-Engine Turboprop, Twin-Engine Turboprop, Turbojet, Piston Rotorcraft, Turbine Rotorcraft, or FC, in order.

$$\begin{aligned}
 U_{MODE\ k} &= \sum_{i=1}^5 \beta_i \cdot X_{i,k} + \varepsilon \\
 &= \beta_{Speed}X_{1,k} + \beta_{Cost}X_{2,k} + \beta_{Noise}X_{3,k} + \beta_{Capacity}X_{4,k} + \beta_{Accident\ Rate}X_{5,k} + \varepsilon \quad (61)
 \end{aligned}$$

Where  $U_{MODE\ k} = \beta_{SPEED}X_1 + \beta_{COST}X_2 + \beta_{NOISE}X_3 + \beta_{CAPACITY}X_4 + \beta_{ACCIDENT\_RATE}X_5 + \varepsilon$  here  $\beta_i (1 \leq i \leq 5, i \in \mathbb{N})$  is the coefficient of each variable defining the degree by which each factor affects the market share and  $k$  determines the number of modes shown in Table 17. The  $\beta_i$  represents coefficients of speed, cost, noise, capacity, or accident rate, in order. Seven of these alternatives are pre-existing modes define

$$S_{Mode\ k} = \frac{\exp(U_{Mode\ k})}{\sum_{k=1}^8 \exp(U_{Mode\ k})} \quad (62)$$

## B.3 Result and Discussion

### B.3.1 Numerical Result

Using multiple regression analysis on Equation (1-2) and Table 17, we can derive the value for each  $\beta_i$  in the utility Equation (1). On performing multiple regression analysis with SPSS Statistics 25, we obtain the following re

sult (Table 18). From the result, a multiple correlation coefficient is 0.9987, and a coefficient of determination is 0.9974.

Table 18 Coefficients Values Obtained by Multiple Regression Analysis

	$\varepsilon$	$\beta_{\text{Speed}}$	$\beta_{\text{Cost}}$	$\beta_{\text{Noise}}$	$\beta_{\text{Capacity}}$	$\beta_{\text{Accident Rate}}$
$\beta$ (Coefficient)	17.848	-0.00204	0.00147	-0.225	-0.372	-0.655
Standard Deviation	1.057	0.00177	0.000197	0.0126	0.0726	0.0915
t- Value	16.894	-1.154	7.472	-17.925	-5.121	-7.151
P-Value	0.0376	0.455	0.0847	0.0355	0.123	0.0885
Lower Bound 95%	4.424	-0.0245	-0.00103	-0.385	-1.295	-1.818
Upper Bound 95%	31.272	0.0204	0.00398	-0.0655	0.551	0.508
Lower Bound 90.0%	11.178	-0.0132	0.000229	-0.304	-0.830	-1.232
Upper Bound 90.0%	24.519	0.00913	0.00272	-0.146	0.0866	-0.0767

Note that since the coefficient values of noise and accident rate are high in the utility function, we obtain a very promising value for flying-car market share, as it is four times safer than pre-existing modes and less noisy.

Hence, upon substitution of the average values of all factors for competing modes, flying cars extract 29% of the market share in the FAA FAR Part 135 Flying Taxi market as shown Table 19.

Table 19 Updated Share Distribution

Single-Engine Piston	Twin-Engine Piston	Single-Engine Turboprop	Twin-Engine Turboprop	Turbojet	Piston Rotocraft	Turbine Rotocraft	Flying Car
0.370	0.0535	0.0379	0.0389	0.114	0.0244	0.0737	0.288

### B.3.2 What-if Analysis

In this subsection, four scenarios are analyzed to explore the dependence of flying-car market share upon three parameters: noise, capacity, and accident rate. The result of this ‘what-if’ analysis is shown in Table 20.

Scenario 1: what if the noise rate of a flying car decreases by 9 dB to 67 dB? According to the Uber report [3], the noise level must be less than 67 dB. The market share of a flying car becomes 75.4%.

Scenario 2: what if the capacity of a flying car increases by 2 to 4 people? Currently, the capacity is limited to 2 because of limitations on the battery. This scenario means that, as the battery’s energy density increases, the capacity to deliver passengers by flying car increases. The flying-car market share becomes 32.1%.

Scenario 3: what if the flying-car accident rate decreases by 75% to 0.41? The unit is not changed. According to the Uber report [3], flying cars have a high potential to be much safer than conventional aircraft due to their electrification and autonomy. The flying-car market share becomes 68.6%.

Scenario 4: what if the above three parameters simultaneously change? Flying cars would be much more widely accepted by citizens if this happened, owing to higher safety, lower environmental impact, and higher economical values. The result is shown as Table 20. The flying-car market share becomes 76.3%.

However, each variable value for flying car is somehow optimistic because a flying car is completely a brand new mobility on the earth. Thus, there is a possibility that these values cannot reach an ideal value such as Table 20.

Table 20 Share Distribution in Four Scenarios

Aircraft	Baseline	Scenario 1	Scenario 2	Scenario 3	Scenario4
Flying Car	0.288	<b>0.754</b>	<b>0.321</b>	<b>0.686</b>	<b>0.763</b>
Single-Engine Piston	0.370	0.128	0.352	0.163	0.123
Single-Engine Turboprop	0.0535	0.0185	0.0510	0.0236	0.0178
Single-Engine Turboprop	0.0379	0.0131	0.0361	0.0167	0.0126
Twin-Engine Turboprop	0.0389	0.0134	0.0371	0.0172	0.0129
Turbojet	0.114	0.0395	0.109	0.0505	0.0381
Piston Rotorcraft	0.0244	0.00842	0.0232	0.0108	0.00812

Turbine Rotor craft	0.0737	0.0255	0.0703	0.0326	0.0246
------------------------	--------	--------	--------	--------	--------

## B.4 Conclusion

This study analyzed the market share of flying cars compared to other conventional aircraft classified in FAA FAR, Part 135, with an eye to studying their applicability as air taxis. A multinomial logit model was utilized to estimate the market share of each aircraft. The five characteristics considered were speed, cost per hour, noise, capacity, and accident rate. The main results are presented Table 19 and Table 20. Flying-car market share is estimated to be 28.8%. When improving noise, capacity, and accident rate, the market share increases to three times the baseline (Table 20). This means that the social and environmental impacts on citizen and the economic value should be improved to increase the social acceptance of flying cars.

This study concludes that flying cars have sound potential to compete in the American air-taxi market as technology improves. The need to develop modern and more sophisticated modes of transport has arisen due to population increase and congestion problems in cities around the world.

The current study is limited in its scope, since it focuses specifically on one domain of Part 135 of FAA FAR. Flying cars will have applications in several domains including air ambulances, air tourism, logistics, and so forth, and the current model can be expanded to include these. Flying Cars are als

o expected to be purchased by individuals and companies around the world. The current model does not consider their use as private transport.

The introduction of new technologies will extract customers from the existing market as well as create new customers. The multinomial logit model estimates only the former. We cannot estimate the number of new customers that flying cars will potentially generate.

The current model uses historical data for current modes of transportation to generate the utility equation. With advances in technology, the characteristics of these modes will change and so too will the demand estimated for flying cars. Additionally, the flying-car characteristics used in this model are hypothetical. The actual values will have a different effect upon demand estimation.

The demand estimation introduced in this study can be taken as a base-model that can be expanded in the future to include more variables and more modes of transport and changed model-characteristic values. Especially, not only cruise range from the performance perspective but also CO<sub>2</sub> emission amount from the sustainability perspective should be considered for a future study. When UAM is operated in an urban area as a mode choice to deliver passengers, inserting other mobilities such as a ground taxi and public transportation into multi logit model is necessary for assuming share distribution among urban transportations.

## References

- [1] United Nations, “World Population Prospects”, <<https://population.un.org/wpp/>> (Accessed 2022-02-15).
- [2] Tokyo Metropolitan Government, “Population in Tokyo”, 2021, <<https://www.metro.tokyo.lg.jp/tosei/hodohappyo/press/2021/11/30/03.html>> (Accessed 2022-02-15).
- [3] J. Holden. and N. Goel, “Fast-Forwarding to a Future of On-Demand Urban Air Transportation”, Uber Elevate, Oct 27, 2017, <<https://www.uber.com/elevate.pdf>> (Accessed 2022-02-15).
- [4] Vertical Flight Society, “Electric VTOL News”, <<https://evtol.news/>> (Accessed 2022-02-15).
- [5] M-LIT, “Islands in Japan”, <<https://www.mlit.go.jp/common/001290710.pdf>> (Accessed 2022-02-15).
- [6] Ministry of Internal Affairs and Communications, “Survey of Depopulated Areas”, 2019 Dec 20th, <[https://www.soumu.go.jp/main\\_content/000660843.pdf](https://www.soumu.go.jp/main_content/000660843.pdf)> (Accessed 2022-02-15).

- 
- [7] Shahab.H, “Urban air mobility (UAM) market study”, NASA, 2019.
- [8] Parker. V, “Systems-level analysis of On Demand Mobility for aviation”, Massachusetts Institute of Technology, PhD Dissertation, 2017.
- [9] L. Garrow, B. German, etc, “Urban air mobility: A comprehensive review and comparative analysis with autonomous and electric ground transportation for informing future research”, Transportation Research Part C: Emerging Technologies, 2021, Vo. 132, 103377, DOI: 10.1016/j.trc.2021.103377.
- [10] A. Mathur, L. Panesar, etc, “Paths to autonomous vehicle operations for urban air mobility”, AIAA Aviation 2019 Forum, pp.1–17, DOI:10.2514/6.2019-3255.
- [11] O. COKORILO, “Urban air mobility: safety challenges”, Transportation research procedia, 2020, Vol.45, pp.21-29, DOI: 10.1016/j.trpro.2020.02.058.
- [12] EASA, “Proposed Special Condition for Small-category VTOL Aircraft”, Issue 1, 15th October 2018, <<https://www.easa.europa.eu/sites/default/files/dfu/SC-VTOL-01%20proposed.pdf>> (Accessed 2022-02-15).

- 
- [13] A. Bacchini, and E. Cestino, "Electric VTOL Configurations Comparison," *Aerospace*, Vol. 6, No.26, pp. 1–19, DOI: 10.3390 / aerospace 6030026, Feb 28, 2019.
- [14] J. M. Utterback, and W. J. Abernathy, "A dynamic model of process and product innovation," *Omega*, Vol.3, No.6, pp. 639–656, DOI: 10.1016 / 0305-0483(75)90068-7, 1975.
- [15] T. Ha and J. T. Hwang, "Large-scale Design-economics Optimization of eVTOL Concepts for Urban Air Mobility," *AIAA Scitech 2019 Forum*, pp. 1–19, DOI: 10.2514 / 6.2019-1218, 2019.
- [16] J. T. Hwang and A. Ning, "Large-scale multidisciplinary optimization of an electric aircraft for on-demand mobility," *2018 AIAA/ASCE/AHS/ASC Structures, Structural Dynamics, and Materials Conference*, pp.1384–1403, DOI:10.2514 / 6.2018-1384, 2018.
- [17] A. Kasliwal et al., "Role of Flying Cars in Sustainable Mobility," *Nature Communications*, 10.1, article number: 1555, pp.1-10, April 9, DOI: 10.1038 / s41467-019-09426-0, 2019.
- [18] P. Pawlanda, "Cost Analysis of eVTOL Configuration Design for Air Ambulance in Japan", 2020, Master Thesis, Keio University.
- [19] T. Amago et al., "Optimization technique for first order analysis," *The Japan Society of Mechanical Engineers, The 4th Optimization Symposium*, No.00-28, pp.199-205, Oct 6-7, DOI: 10.1299 / jsmeoptis.2000.4.199, 2000.
- [20] Electrification Challenge for Aircraft (ECLAIR) Consortium, "ECLAIR", JAXA, <

---

[https://www.jaxa.jp/press/2018/07/20180702\\_eclair\\_j.html](https://www.jaxa.jp/press/2018/07/20180702_eclair_j.html)> (Accessed 2022-02-15).

[21] Development Bank of Japan, “Survey for the Use Cases of Flying Cars in Japan”, Translated by Author,

<[https://www.dbj.jp/upload/investigate/docs/fhdh\\_1.pdf](https://www.dbj.jp/upload/investigate/docs/fhdh_1.pdf)> (Accessed 2022-02-15).

[22] Flying Car Research Lab, “Flying Car System – Mobility Revolution of Technology and Service by System Design”, translated by author “”, Dec 12, 2019, The Nikkan Kogyo Shimbun.

[23] European Union Aviation Safety Agency, “Special Condition for small-category VTOL aircraft”, July 2, 2019, Issue 1, <<https://www.easa.europa.eu/sites/default/files/dfu/SC-VTOL-01.pdf>> (Accessed 2022-02-15).

[24] R. Stansbury, W. Tanis, T. Wilson, “A Technology Survey of Emergency Recovery and Flight Termination Systems for UAS”, April 6, 2009, AIAA Infotech, pp. 2038-2046.

[25] J. E. Moses, I. Jennitta, G. Wessley, “Controllable Aircraft Rescue System”, 2017, First International Conference on Recent Advances in Aerospace Engineering, pp.1-6.

[26] United States Patent, “BALLISTIC RECOVERY SYSTEM”, Patent Number: 4,607,814, Popov Date of Patent: Aug. 26, 1986, 2017.

[27] V. Prisacariu, S. Pop, I. Circiu, “Recovery System of the Multi-helicopter UAV”, 2016, Review of the Air Force Academy, No.1, 31, pp.91-98.

[28] T.Hamamoto, “Occurance Probability of the Impulsive Load”, Nov 11, 2017, Architectural Institute of Japan, pp.1-10.

- 
- [29] R. Kasai, "Relationship between impact load shape due to collision of a airplane and response of building", Nov 18, 2004, The Japan Society of Mechanical Engineers, 17th CMD, No04, pp.491-492.
- [30] S. Kano, H. Ryuzaki, etc, "Proposal of design method of buildings against impact and explosion loads: Part-1 Design method of loads", Sep 2016, the 63rd National Congress of Theoretical and Applied Mechanics, pp.1-2.
- [31] R. Kasai, T. Kurihara, "Response Characteristics of Reinforced Concrete High-Rise Buildings to Impact Loads", translated by author, Dec 2005, AIJ Journal of Technology and Design, No22, pp.211-216.
- [32] International Civil Aviation Organization, "Heliport Manual", 2020, 4th Edition.
- [33] T. Nakamura, Y. Mihara, K. Nishii, K. Ohtaki, "Parachute", Oct 25th, 2019, P2019-194172.
- [34] Tokyo Fire Department, "Emergency Heliport · Rescue Space for Emergency", Dec 2017, Core Tokyo.
- [35] A. Bacchini, and E. Cestino, "Electric VTOL Configurations Comparison," Aerospace, Vol. 6, No.26, pp. 1–19, DOI: 10.3390 / aerospace 6030026, Feb 28, 2019.
- [36] J. M. Utterback, and W. J. Abernathy, "A dynamic model of process and product innovation," Omega, Vol.3, No.6, pp. 639–656, DOI: 10.1016 / 0305-0483(75)90068-7, 1975.
- [37] T. Ha and J. T. Hwang, "Large-scale Design-economics Optimization of eVTOL Concepts for Urban Air Mobility," AIAA Scitech 2019 Forum, pp. 1–19, DOI: 10.2514 / 6.2019-1218, 2019.

- 
- [38] J. T. Hwang and A. Ning, "Large-scale multidisciplinary optimization of an electric aircraft for on-demand mobility," 2018 AIAA/ASCE/AHS/ASC Structures, Structural Dynamics, and Materials Conference, pp.1384–1403, DOI:10.2514 / 6.2018-1384, 2018.
- [39] A. Kasliwal et al., "Role of FCs in Sustainable Mobility," Nature Communications, 10.1, article number: 1555, pp.1-10, April 9, DOI: 10.1038 / s41467-019-09426-0, 2019.
- [40] T. Amago et al., "Optimization technique for first order analysis," The Japan Society of Mechanical Engineers, The 4th Optimization Symposium, No.00-28, pp.199-205, Oct 6-7, DOI: 10.1299 / jsmeoptis.2000.4.199, 2000.
- [41] R. Shishko, and R. Aster, "NASA Systems Engineering Handbook," NASA Special Publication 6105, Rev1, 1995.
- [42] German Parliament, "Closing Report of the Enquete Kommission," 13/11200, Germany, 1998.
- [43] Ogawa, Keiji, et al, "A process decision making strategy based on sustainability evaluation," International Journal of Automation Technology, Vol. 9, No. 1, pp. 51–58, DOI:10.20965/ijat. 2015.p0051, 2015.
- [44] O. Weck, "Multiobjective optimization: History and promise," Invited Keynote Paper, GL2-2, The Third China-Japan-Korea Joint Symposium on Optimization of Structural and Mechanical Systems, Kanazawa, Japan. Vol. 2, pp. 34–48, 2004.
- [45] J. Blank, and D. Kalyanmoy, "pymoo: multi-objective optimization in python," IEEE Access, Vol. 8, pp. 497–509, DOI: 10.1109 / ACCESS.2020.2990567, 2020.

---

[46] A. Kohama, “Past, present, and future of air ambulances,” *Journal of Japanese Association for Acute Medicine*, Vol.21, No. 6, pp. 271–281, DOI:10.3893 / jjaam.21.271, 2010.

[47] M. H. Sadraey, “Aircraft Design, A Systems Engineering Approach,” John Wiley & Sons, ISBN: 978-1-119-95340-1, 2013.

[48] B. Silberg, “Electric Airplanes (batteries included),” the Earth Science Communications Team, NASA’s Jet Propulsion Laboratory, Aug 22, 2016, <<https://climate.nasa.gov/news/2482/electric-airplanes-batteries-included>> (Accessed 2022-02-15).

[49] Airfoil.com, “NACA 0021 (naca0015-il) X foil prediction polar at Re=100,000 Ncrit=9,” 2020, <<http://airfoiltools.com/polar/details?polar=xf-naca0021-il-100000> > (Accessed 2022-02-15).

[50] HELIX, “Propeller Datasheets,” <<https://www.helix-propeller.de/index.php?id=57&L=1>> (Accessed 2022-02-15).

[51] G. Leishman, “Principles of Helicopter Aerodynamics,” Cambridge University Press, the second edition, ISBN: 9781107013353, 2006.

[52] K. Sumitani et al., “Development of vehicle fluid dynamics: Flow around the vehicle and aerodynamic characteristics,” *Journal of Japan Society of Fluid*, Vol. 23, No. 6, pp. 445–454, DOI:10.11426/nagare1982.23.445, 2004.

[53] J. S. Duncan, “Pilot’s Handbook of Aeronautical Knowledge,” Federal Aviation Administration, U.S. Department of Transportation, FAA-H-8083-25B, ISBN: 1602397805, 2016.

[54] E. Hendricks, R. D. Falck, “Multidisciplinary optimization of a turboelectric Tiltwing urban air mobility aircraft,” *AIAA Aviation 2019 Forum*, pp. 3551-3561, Jun 17-21, DOI:10.2514/6.2019-3551, 2019.

---

[55] C. Courtin, and J. Hansman, “Feasibility Study of Short Takeoff and Landing Urban Air Mobility Vehicles using Geometric Programming,” 18th AIAA Aviation Technology, Integration, and Operations Conference, pp. 4151–4175, DOI: 10.2514 / 6.2018-4151 June, 2018.

[56] T. O'Bryan, "An Investigation of the Effect of Downwash from a VTOL Aircraft and a Helicopter in the Ground Environment," NASA, Vol. 977, 1961.

[57] M. Nakadate, " The Aerodynamics Problems in Aircraft," Aeronautical and space sciences Japan, Vol. 45, No. 521, pp. 314–319, DOI: 10.2322 / jjsass1969.45.314, 1997.

[58 ] N. Rajaratnam, “Turbulent Jets,” Elsevier, vol. 5, ISBN: 0080869963, 1976.

[59] Z. Yongjun, Y. Shenghui, “The computational fluid dynamic modeling of downwash flow field for a six-rotor UAV,” Frontiers of Agricultural Science and Engineering, Vol.5, No.2, pp. 159–167, DOI: 10.15302 / J-FASE-2018216, 2018.

[60] Minister of Land, Infrastructure, Transport and Tourism, “Law of Aviation, Article 79, Installation Criteria 8,” 1952.

[61] Y. Koizumi, "Roles and Issues of an air ambulance," Translated by Author, Faculty of Social Sciences, Special Edition, pp. 73–85, 2011.

[62] K. Shinohara, "Investigation on the problems for developments of aviation transportation medical service," Japan Human Factors and Ergonomics Society, Vol. 49, Supplement Edition, pp. 110–111, DOI: 10.5100 / jje.49.S110, 2013.

---

[63] P. Pradeep, P. Wei, “Energy-efficient arrival with RTA constraint for multicopter eVTOL in urban air mobility,” *Journal of Aerospace Information Systems*, Vol.16, No.7, pp. 263–277, DOI: 10.2514 / 1.I010710, 2019.

[64] X. Chen, "An Overview of Lithium-ion Batteries for Electric Vehicles," 2012 10th International Power & Energy Conference (IPEC), IEEE, pp. 230–236, DOI: 10.1109/ASSCC.2012.6523269, 2012.

[65] New Energy and Industrial Technology Development Organization, “Toward Formulation of the Technology Strategy in the Field of the EV’s Battery,” Translated by author, Technology Strategy Center, October 2015, <<http://www.nedo.go.jp/content/100763660.pdf>> (Accessed 2022-02-15).

[66] The Society of Japanese Aerospace Companies, “Survey Report of the Helicopter Operation 1988,” 1988.

[67] Toyota City, “Solutions for Noise and Vibration,” translated by author, Nov 6, 2018, Environment Department, environmental Conservation Division, Toyota City Hall, <<https://www.city.toyota.aichi.jp/jigyousha/tetsuzuki/kankyohozen/1027117.html>> (Accessed 2022-02-15).

[68] MD HELICOPTERS, “MD902, Technical Description,” Department of Sales and Marketing, MD Helicopters, Inc, pp. 1–74, Feb 14, 2014, <[https://www.mdhelicopters.com/files/Models/MD902\\_Tech\\_Desc.pdf](https://www.mdhelicopters.com/files/Models/MD902_Tech_Desc.pdf)> (Accessed 2022-02-15).

[69] A. Tsuchiya, Y. Tsutsumi, and H. Yasunaga, “Outcomes after helicopter versus ground emergency medical services for major trauma—propensity score and instrumental variable analyses: a retrospective nationwide cohort study,” *Scand. J. Trauma. Rescue. Emergency*, pp. 1–11, 2016.

- 
- [70] European Union Aviation Safety Agency, “Special Condition for small-category VTOL aircraft”, July 2, 2019, Issue 1, <<https://www.easa.europa.eu/sites/default/files/dfu/SC-VTOL-01.pdf>> (Accessed 2022-02-15).
- [71] R. Stansbury, W. Tanis, T. Wilson, “A Technology Survey of Emergency Recovery and Flight Termination Systems for UAS”, April 6, 2009, AIAA Infotech, pp. 2038-2046.
- [72] J. E. Moses, I. Jennitta, G. Wessley, “Controllable Aircraft Rescue System”, 2017, First International Conference on Recent Advances in Aerospace Engineering, pp.1-6.
- [73] United States Patent, “BALLISTIC RECOVERY SYSTEM”, Patent Number: 4,607,814, Popov Date of Patent: Aug. 26, 1986, 2017.
- [74] V. Prisacariu, S. Pop, I. Circiu, “Recovery System of the Multi-helicopter UAV”, 2016, Review of the Air Force Academy, No.1, 31, pp.91-98.
- [75] T. Hamamoto, “Probability of Impulsive Load Occurrence”, Translated by author, Nov 11, 2017, Architectural Institute of Japan, Study Group on the Effects of Impact Action on Buildings and Measures to Reduce Damage, pp.1-10.
- [76] R. Kasai, “Relationship Between Impact Load Shape due to Collision of Airplane and Response of Building”, Nov 18, 2004, JSME, The 17th Conference of Computational Engineering and Science, No04, pp.491-492.
- [77] T. Kano, T. Hamamoto, etc “Proposal of design method of buildings against impact and explosion loads”, Sep 2016, The 63rd Nat. Cong. Of Theoretical & Applied Mechanics, pp.1-2.

---

[78] R. Kasai, “Response Characteristics of High Rise reinforced Concrete Building Subjected to Impact Load”, Dec 2005, AIJ journal of technology and design, No22, pp.211-216.

[79] International Civil Aviation Organization, “Helicopter Manual”, 2020, 4th Edition.

[80] Tokyo Fire Bureau, “Emergency Helicopter and Space for Emergency Rescue”, Translated by author, Dec 2017, Core Tokyo, Dec 2017.

[81] T. Hamamoto, “Introduction to Shock-Resistant Design of Buildings Chapter 3 Design Strength”, January 2015, Architectural Institute of Japan, pp.23-68, 2015.

[82] Bureau of Port and Harbor, Tokyo Metropolitan Government, “Operational Regulations for Helicopters in Tokyo”, Translated by author, July 2009, <[https://www.kouwan.metro.tokyo.lg.jp/rito/tmg-airport/tokyo\\_helicopter/kuukoukyouyoukitei.html](https://www.kouwan.metro.tokyo.lg.jp/rito/tmg-airport/tokyo_helicopter/kuukoukyouyoukitei.html)> (Accessed 2022-02-15).

[83] Opener BLACKFLY, “Parachute Test”, <<https://www.youtube.com/shorts/lcsutISR6os>> (Accessed 2022-02-15).

[84] A. Blukbasi, J. Crocco, D. Vasquez, etc, “Full Spectrum Crashworthiness Criteria for Rotorcraft”, Dec 2011, U.S. Army Research, <<https://apps.dtic.mil/dtic/tr/fulltext/u2/a556604.pdf>> (Accessed 2022-02-15).

[85] Automotive Safety Committees, “Human Tolerance to Impact Conditions as Related to Motor Vehicle Design”, Feb 2011, SAE, J885.

[86] M-LIT, “Summary of the Results of the National Survey on Road and Street Traffic Conditions: Automobile Origin-Destination Survey”, Translate

---

d by author, April 3, 2018, pp4 <<https://www.mlit.go.jp/common/001230248.pdf>> (Accessed 2022-02-15).

[87] Statistic Bureau, Ministry of Internal Affairs and Communications, “Population Estimation”, Translated by author, August 20, 2020, <<https://www.stat.go.jp/data/jinsui/new.html>>(Accessed 2022-02-15).

[88] Tokyo, “Overview of the Population in Tokyo”, Translated by author, July 2, 2020, <<https://www.metro.tokyo.lg.jp/tosei/hodohappyo/press/2020/07/02/01.html>> (Accessed 2022-02-15).

[89] Tokyo Hire-Taxi Association, “Survey Results about a Ground Taxis”, Translated by author, 2017, <<http://www.taxi-tokyo.or.jp/enquete/pdf/research2017.pdf>>(Accessed 2022-02-15).

[90] NASA, “URBAN AIR MOBILITY MARKET STUDY”, Oct 5, 2018, <[https://www.nasa.gov/sites/default/files/atoms/files/bah\\_uam\\_executive\\_briefing\\_181005\\_tagged.pdf](https://www.nasa.gov/sites/default/files/atoms/files/bah_uam_executive_briefing_181005_tagged.pdf)> (Accessed 2022-02-15).

[91] N. Iboshi, “Helicopter Accident Analysis in Japan Activities”, 2011, JASASS, Vol.59, No.690, pp.205-210.

[92] MOF, “Ministerial Ordinance on Useful Lives, etc. of Depreciable Assets”, Translated by author, 2020< [https://elaws.e-gov.go.jp/search/elawsSearch/elaws\\_search/lsg0500/detail?lawId=340M50000040015](https://elaws.e-gov.go.jp/search/elawsSearch/elaws_search/lsg0500/detail?lawId=340M50000040015) > (Accessed 2022-02-15).

[93] C. Chappelle, C. Li, P. D. Vascik, and R. J. Hansman, “Opportunities to Enhance Air Emergency Medical Service Scale through New Vehicles and Operations,” pp. 1–16, 2018.

- 
- [94] P. Pawlanda, “Cost Analysis of eVTOL Configuration Design for Air Ambulance in Japan”, 2020, Master Thesis, Keio University.
- [95] M. J. Duffy, S. R. Wakayama, and R. Hupp, “A Study in Reducing the Cost of Vertical Flight with Electric Propulsion,” pp. 1–24, 2017.
- [96] T. Zhao, “Acquisition Cost Estimating Methodology for Aircraft Conceptual Design,” *Noise Vib. Worldw.*, vol. 35, no. 11, pp. 25–26, 2004.
- [97] D. Raymer, “Aircraft Design: A Conceptual Approach,” 2012.
- [98] D. G. Ullman, V. Homer, and P. Horgan, “Comparing Electric Sky Taxi Visions,” no. June, pp. 1–31, 2017.
- [99] R. Kochhan, S. Fuchs, B. Reuter, P. Burda, S. Matz, and M. Lienkamp, “An Overview of Costs for Vehicle Components, Fuels and Greenhouse Gas Emissions,” *ResearchGate*, pp. 1–26, 2017.
- [100] S. Gudmundsson, *General Aviation Aircraft Design. Applied methods and procedures.* Butterworth-Heinemann; 1 edition, 2014.
- [101] J. Boelens, “Volocopter white paper,” pp. 1–28, 2019.
- [102] P. Pawlanda, “Cost Analysis of eVTOL Configuration Design for Air Ambulance in Japan”, 2020, Master Thesis, Keio University.

- 
- [103] Y. Mihara, "Sustainable Optimized Design of a Flying Car," Aircraft Symposium, pp. 1–4, 2019.
- [104] X. Yu and Y. Zhang, "Sense and avoid technologies with applications to unmanned aircraft systems: Review and prospects," Prog. Aerosp. Sci., vol. 74, pp. 152–166, 2015.
- [105] C. A. Haddad, "Identifying the Factors Affecting the Use and Adoption of Urban Air Mobility," Master Thesis, Technical University of Munich, Munich, 2018.
- [106] L. A. Garrow, P. L. Mokhtarian, B. J. German and J. Glodek, S-S. Bodupalli, "A Survey to Model Demand for eVTOL Urban Air Trips and Competition with Autonomous Ground Vehicles," AIAA Aviation 2019 Forum, 2019.
- [107] R. B. Binder, L. A. Garrow, B. J. German, P. L. Mokhtarian, M. J. Daskilewicz, T. H. Douthat, "If You Fly It, Will Commuters Come? A Survey to Model Demand for eVTOL Urban Air Trips," Aviation Technology, Integration, and Operations Conference, 2018.
- [108] M. Catalano, B. L. Casto, M. Migliore, "Car sharing demand estimation and urban transport demand modelling using stated preference techniques," European Transport n.40, p33-p50, 2008.
- [109] Federal Aviation Administration, "Modernization and Reform Act of 2012, Study of Operators Regulated Under Part 135," April 2016, < [https://www.nata.aero/assets/Site\\_18/files/gia/4656\\_001.pdf](https://www.nata.aero/assets/Site_18/files/gia/4656_001.pdf) > (Accessed 2022-02-15).

---

[110] Federal Aviation Administration, "General Aviation and Part 135 Activity Surveys," 21 3 2019. <[https://www.faa.gov/data\\_research/aviation\\_data\\_statistics/general\\_aviation/](https://www.faa.gov/data_research/aviation_data_statistics/general_aviation/)> (Accessed 2022-02-15).

[111] M. Sivak and B. Schoettle, "A SURVEY OF PUBLIC OPINION ABOUT FCS," Report No. SWT-2017-8, The University of Michigan, Michigan, 2017.

[112] Airchaterguider.com, "Air Charter Guide- A Definitive Resource for Online Aircraft Charter," 2017, <http://www.airchaterguide.com> (Accessed 2022-02-15).

[113] Federal Aviation Administration, "General Aviation and Part 135 Activity Surveys- CY 2019," 2020. <[https://www.faa.gov/data\\_research/aviation\\_data\\_statistics/general\\_aviation/CY2019/](https://www.faa.gov/data_research/aviation_data_statistics/general_aviation/CY2019/)> (Accessed 2022-02-15).

[114] United States Department of Transportation, "General Aviation Profile," 2021, <<https://www.bts.gov/content/general-aviation-profile>> (Accessed 2022-02-15).

[115] European Aviation Safety Agency, "Cure a Website-Cite This for Me," 2017, <<https://www.easa.europa.eu/system/files/dfu/certification-type-certificates-docs-tcdns-databases-MAdB-Rotorcraft-14-28112013.xlsx>> (Accessed 2022-02-15).

[116] J. H. Boelens, "Pioneering the Urban Air Taxi Revolution 1.0", Volocopter, 2019 <<https://press.volocopter.com/images/pdf/Volocopter-WhitePaper-1-0.pdf>> (Accessed 2022-02-15).

[117] W. H. Greene, "Econometric analysis", Fifth Edition, Pearson Education India, 2003.